Neutrinos and Dark Energy

Dissertation
zur Erlangung des Doktorgrades
des Departments Physik
der Universität Hamburg

vorgelegt von
Lily Schrempp
aus
Newcastle upon Tyne

Hamburg
2007

Gutachter der Dissertation:	Dr. A. Ringwald
	Prof. Dr. J. Louis
Gutachter der Disputation:	Dr. A. Ringwald
	Prof. Dr. J. Bartels
Datum der Disputation:	15. 01. 2008
Vorsitzender des Prüfungsausschusses:	Dr. H. D. Rüter
Vorsitzender des Promotionsausschusses:	Prof. Dr. G. Huber
Dekan der Fakultät MIN:	Prof. Dr. A. Frühwald

Abstract

From the observed late-time acceleration of cosmic expansion arises the quest for the nature of Dark Energy. As has been widely discussed, the cosmic neutrino background naturally qualifies for a connection with the Dark Energy sector and as a result could play a key role for the origin of cosmic acceleration. In this thesis we explore various theoretical aspects and phenomenological consequences arising from non-standard neutrino interactions, which dynamically link the cosmic neutrino background and a slowly-evolving scalar field of the dark sector. In the considered scenario, known as Neutrino Dark Energy, the complex interplay between the neutrinos and the scalar field not only allows to explain cosmic acceleration, but intriguingly, as a distinct signature, also gives rise to dynamical, time-dependent neutrino masses. In a first analysis, we thoroughly investigate an astrophysical high energy neutrino process which is sensitive to neutrino masses. We work out, both semi-analytically and numerically, the generic clear-cut signatures arising from a possible time variation of neutrino masses which we compare to the corresponding results for constant neutrino masses. Finally, we demonstrate that even for the lowest possible neutrino mass scale, it is feasible for the radio telescope LOFAR to reveal a variation of neutrino masses and therefore to probe the nature of Dark Energy within the next decade. A second independent analysis deals with the recently challenged stability of Neutrino Dark Energy against the strong growth of hydrodynamic perturbations, driven by the new scalar force felt between neutrinos. Within the framework of linear cosmological perturbation theory, we derive the equation of motion of the neutrino perturbations in a model-independent way. This equation allows to deduce an analytical stability condition which translates into a comfortable upper bound on the scalar-neutrino coupling which is determined by the ratio of the densities in cold dark matter and in neutrinos. We illustrate our findings by presenting numerical results for representative examples of stable as well as of unstable scenarios.

Zusammenfassung

Die beobachtete Beschleunigung der kosmischen Expansion zu späten Zeiten wirft die Frage auf nach der Natur der dunklen Energie. Wie bereits mehrfach in der Literatur erörtert wurde, eignet sich der kosmische Neutrinohintergrund auf natürliche Weise für einen Zusammenhang mit dem für die dunkle Energie verantwortlichen Sektor. Als Folge könnte er eine Schlüsselrolle spielen für die Entstehung der kosmischen Beschleunigung. In dieser Arbeit untersuchen wir verschiedene theoretische Aspekte und phänomenologische Auswirkungen von neuen Neutrinowechselwirkungen, die eine neue dynamische Kopplung zwischen dem kosmischen Neutrinohintergrund und einem leichten Skalarfeld des dunklen Sektors herstellen. In dem betrachteten Szenario, der sogannten "Neutrino Dark Energy", erlaubt das komplexe Wechselspiel zwischen den Neutrinos und dem Skalarfeld die Beschleunigung der kosmischen Expansion zu erklären. Faszinierenderweise werden darüberhinaus als eindeutiges Merkmal dynamische, zeitabhängige Neutrinomassen erzeugt. In einer ersten Analyse führen wir eine sorgfältige Untersuchung eines astrophysikalischen Neutrinoprozesses durch, der eine Abhängigkeit von den Neutrinomassen aufweist. Wir arbeiten sowohl semi-analytisch als auch numerisch die charakteristischen, klaren Signaturen der zeitlichen Neutrinomassenvariation aus und vergleichen sie mit den entsprechenden Ergebnissen für Neutrinos mit konstanten Massen. Schlussendlich zeigen wir, dass das Radioteleskop LOFAR in der Lage wäre, eine Neutrinomassenvariation zu detektieren, selbst im Falle der niedrigst möglichen Neutrinomassenskala. Auf diese Weise könnte innerhalb der nächsten Dekade das Wesen der dunklen Energie getestet werden. Eine zweite unabhängige Analyse beschäftigt sich mit der vor kurzem angezweifelten Stabilität des Szenarios. Sie wird in Frage gestellt aufgrund des möglichen starken Anwachsens von hydrodynamischen Fluktuationen, das von der neuen, zwischen Neutrinos wirkenden Kraft angetrieben wird. Im Rahmen der linearen kosmologischen Störungsrechnung leiten wir in modellunabhängiger Weise die Bewegungsgleichung für die Neutrinofluktuationen her. Die Bewegungsgleichung erlaubt, eine analytische Stabilitätsbedingung aufzustellen, die einer großzügigen oberen Schranke für die Kopplungsstärke zwischen Neutrinos und dem Skalarfeld entspricht. Sie ist bestimmt durch das Verhältnis der Dichten der kalten dunklen Materie und der Neutrinos. Wir veranschaulichen unsere Resultate mithilfe von numerischen Berechnungen für repräsentative Beispiele sowohl von stabilen als auch von instabilen Modellen.

Contents

1 Introduction

Various cosmological precision measurements provide increasingly strong evidence that the expansion of the universe has recently entered a phase of accelerated expansion [1–6]. From this observational advance arises one of the major challenges for theoretical cosmology and particle physics which, in the framework of general relativity, translates into the quest for the nature of *Dark Energy*[1]. In order to cause the observed late-time acceleration, this so far unknown source of energy has to be homogeneously distributed, can at best be slowly-varying with time and must be characterized by a negative pressure to counteract gravity.

It may be a cosmological constant identified with the energy of the vacuum [9], or a dynamical *quintessence* scalar field, slowly rolling down its self-interaction potential [10–13], or some more exotic dynamical variant [14–17]. However, in any case, so far neither fifth force searches [18] nor tests of the equivalence principle [19] could shed light on the origin of the Dark Energy sector by tracing (non-gravitational) interactions with standard model particles [20].

Recently, it has been argued that Big Bang relic neutrinos, which are the analog of the photons of the microwave background (CMB), naturally qualify for a connection with the Dark Energy sector [21–24] and as a result could play a key role for the origin of cosmic acceleration. Their existence is a fundamental prediction of Big Bang cosmology and traces its origin to the freeze-out of the weak interactions merely about 1 sec after the Big Bang at a temperature scale of 1 MeV [25]. Ever since their decoupling from the thermal bath, these relic neutrinos are assumed to permeate the universe homogeneously as *cosmic neutrino background* (CνB) with a substantial relic abundance which is only surpassed by the CMB photons.

In this thesis we explore possible realizations of non-standard neutrino interactions which dynamically link the cosmic evolution of the CνB and the sector responsible for Dark Energy. As successively described in the following, they emerge from the requirement of energy-momentum conservation of the coupled two-component system and turn out to have interesting, testable consequences for neutrino physics, cosmology as well as astro-particle physics.

The approaches are based on a scenario proposed by Fardon, Nelson and Weiner and have the following common framework [21, 22]. The authors of Ref. [21, 22] have shown that relic neutrinos are promoted to a natural Dark Energy candidate if they interact through a new force mediated by a light scalar field of the dark sector[2]. This idea has great appeal and is supported by the following line of arguments. Neutrinos are the only fermions without right-handed partners in the Standard Model. Since the discovery of neutrino oscillations we

[1] For a complementary approach in which instead of the matter sector gravity is modified in such a way as to produce cosmic acceleration see e.g. [7, 8].

[2] Implications of non-standard neutrino interactions mediated by a light scalar field have already been considered before in Refs. [26–31].

know that a deeper understanding of the neutrino sector including the origin of neutrino masses requires physics beyond the Standard Model. Provided lepton number is violated, therefore the active, left-handed neutrinos are generally assumed to mix with dark right-handed neutrinos to acquire small masses via the well-known see-saw mechanism [32–35]. Hence, if these dark fermions directly couple to the dark scalar field, the attractive possibility arises [21, 22] that neutrinos indirectly feel the scalar field mediated force by mixing with the dark fermions via the see-saw mechanism. Intriguingly, by these means they are uniquely capable of opening a window to the dark sector. Moreover, the scale relevant for neutrino mass squared differences as determined from neutrino oscillation experiments, $\delta {m_\nu}^2 \sim (10^{-2}\ \text{eV})^2$ [36], is of the order of the tiny scale associated with the Dark Energy density, $\rho_{\text{DE}} \sim (2 \times 10^{-3}\ \text{eV})^4$.

From the new interaction, in such a scenario an intricate interplay arises which links the dynamics of the relic neutrinos and the light scalar field, the mediator of the dark force. Namely, on the one hand, the vacuum expectation value ϕ of the scalar field generates neutrino masses, $m_\nu(\phi)$. Correspondingly, the ϕ dependence of the neutrino masses $m_\nu(\phi)$ is transmitted to the neutrino energy densities $\rho_\nu(m_\nu(\phi))$, since these are functions of $m_\nu(\phi)$. On the other hand, as a direct consequence, the neutrino energy densities $\rho_\nu(m_\nu, \phi)$ can stabilize the scalar field by contributing to its effective potential,

$$V(\phi, \rho_\nu(m_\nu(\phi))) = V_\phi(\phi) + \rho_\nu(m_\nu(\phi)). \tag{1.1}$$

More precisely, by these means, the competition of the self-interaction potential $V_\phi(\phi)$ of the scalar field and the neutrino source term can lead to a stabilization of ϕ in a minimum[3] exhibited by its effective potential $V(\phi, \rho_\nu)$. As a crucial consequence, ϕ cannot evolve faster than the neutrino density gets diluted by cosmic expansion. Accordingly, the characteristic time scale governing its dynamics is determined by cosmic expansion which is naturally slow. Thus, the steadily decreasing energy density of its effective potential can drive cosmic acceleration and as an intriguing side effect, its slowly evolving value generates dynamical time-dependent neutrino masses $m_\nu(\phi)$.

Accordingly, in this so-called Mass Varying Neutrino (MaVaN) Scenario, also known as Neutrino Dark Energy, the typical problems arising in slow-roll quintessence [20, 37–40] can be ameliorated. Namely, since the coupling to neutrinos impedes the scalar field from rolling down its potential, its mass can be much larger than the tiny Hubble scale sized mass $\sim 10^{-33}$ eV of a slow-roll quintessence field. As it turns out, it is allowed to be of comparable size as the milli-eV Dark Energy scale and as a consequence is more plausibly stable against radiative corrections than the Hubble scale. It should also be noted that neutrinos are ideal candidates for coupling to a light scalar field, since the arising quantum radiative corrections to its potential remain of natural size due to the smallness of neutrino masses [21, 22].[4]

From a phenomenological point of view, the Mass Varying Neutrino scenario is also appealing, since it predicts as a clear and testable signature a variation of neutrino masses with time.

The rich phenomenology of the MaVaN scenario has been explored by many authors. The cosmological effects of varying neutrino masses have been studied in Refs. [43–47] and were

[3] Since therefore in the presence of the relic neutrinos the scalar field possesses a stable (time dependent) vacuum state, in the literature both the scalar field and its vacuum expectation value are referred to as ϕ.

[4] Of course, within the framework of quintessence alternative ways out of the problems have been considered [38,41,42].

elaborated in the context of gamma ray bursts [48]. Apart from the time variation, the conjectured new scalar forces between neutrinos as well as the additional possibility of radiatively induced small scalar field couplings to matter, lead to an environment dependence of the neutrino masses governed by the local neutrino and matter densities [21, 49, 50]. The consequences for neutrino oscillations in general were exploited in Refs. [49, 51], in particular in the sun [52–54], in reactor experiments [53, 55] as well as in long-baseline experiments [56].

However, recently, it has been pointed out by Afshordi, Zaldarriaga and Kohri that the viability of the MaVaN scenario in the non-relativistic neutrino regime is threatened by a stability problem [57]. It originates from the non-standard scalar force felt between neutrinos, which can drive a strong growth of hydrodynamic perturbations in the neutrino density possibly leading to bound neutrino structure [57, 58]. We will further pursue this challenge in the second main part of this thesis.

A way of circumventing this stability problem was proposed in a follow-up publication by Fardon, Nelson and Weiner [22] implemented in a viable Supersymmetric version of the MaVaN scenario. Besides various other theoretical merits, in its framework the Dark Energy density could be expressed in terms of neutrino mass parameters. As a consequence, the origin of Dark Energy was attributed to the lightest neutrino. By naturalness arguments the authors concluded that it still has to be relativistic today as allowed by neutrino oscillation experiments. Consequently, if indeed such a low neutrino mass scale is realized in nature, the pressure support in the relativistic neutrino can stabilize the MaVaN perturbations [59]. Thereby, possible instabilities are prevented which can only occur in highly non-relativistic theories of Neutrino Dark Energy [22, 57, 59, 60].

The stage is now set for the questions to be investigated in the two main parts of this thesis:

1) Signatures of Mass Varying Neutrinos in the Sky?

In light of the possible realization of Neutrino Dark Energy in nature, an avenue will be thoroughly explored which allows for a more direct detection of the CνB [61–68]. In the framework of [22], the prospects will be analyzed for probing its interpretation as source of Neutrino Dark Energy by means of neutrino observatories largely following our Refs. [69, 70].

For this purpose, we will consider a process which is sensitive to possible variations in the relic neutrino masses with time, namely, the resonant annihilation into Z-Bosons of extremely-high energy cosmic neutrinos (EHECν's) with relic anti-neutrinos of the CνB and vice versa [61–68]. In general, this process is expected to lead to sizeable absorption dips in the diffuse cosmic neutrino fluxes to be detected on earth in the relevant energy region above 10^{13} GeV. We will work out the characteristic absorption features produced by constant and time varying neutrino masses for various cosmic neutrino sources, incorporating all thermal effects resulting from the relic neutrino motion.

As it will turn out, our results are largely independent of the details of the model, since only a few generic features of the setting enter the investigation. As a result, for the radio telescope LOFAR it will turn out to be feasible to reveal a time-dependence of neutrino masses, even for the lowest possible neutrino mass scale, given that a sufficient EHECν flux can be established. Therefore, LOFAR could provide a possible signature for Neutrino Dark Energy within the

next decade.

2) On the stability of Neutrino Dark Energy

The second main part of this thesis is devoted to an exploration of the stability issue in highly non-relativistic theories of Neutrino Dark Energy as challenged by Afshordi, Kohri and Zaldarriaga [57], largely based on our Ref. [71]. To this end, in the framework of linear cosmological perturbation theory we will thoroughly investigate the effects of the scalar-field-induced attractive force on the Mass Varying Neutrino perturbations in a model-independent way. As it will turn out, this framework naturally leads us to take into account the interplay between the scalar-neutrino fluid and other important cosmic components like cold dark matter which were not considered in Ref. [57]. As we will show, this opens up the possibility for a stabilization of the Mass Varying Neutrino perturbations even in highly non-relativistic theories of Neutrino Dark Energy.

Hence, our ultimate goal will be the derivation of the corresponding stability condition which will turn out to translate into a comfortable upper bound on the allowed scalar-neutrino coupling. We will illustrate our results by considering meaningful, representative examples both for stable and unstable scenarios of Neutrino Dark Energy.

For the convenience of the reader, each of the main sections, Sec. 3 and Sec. 4, includes an introduction as well as a summary of the results. Furthermore, in order to make the thesis as self-contained as possible, we provide an introductory chapter which briefly reviews the fundamentals and relevant concepts on which Secs. 3 – 4 rely and in addition introduces the notation. The outline of this thesis is as follows.

In the introductory section Sec. 2 we provide the tools to analyze the large scale dynamics of the universe and discuss the properties of possible sources of Dark Energy as well as of other important cosmic components. Furthermore, we include a brief excursion into the early universe to illuminate the origin of the CνB and the CMB, respectively. The second part of Sec. 2 is devoted to the basics in neutrino physics. For later reference, we introduce the see-saw mechanism as possible origin of neutrino masses and collect recent neutrino mass squared splittings, mixing parameters as well as upper bounds on the absolute neutrino mass scale.

In Sec. 3 we explore an astrophysical approach to test the realization of Neutrino Dark Energy in nature. For this purpose, in Sec. 3.1 we start by introducing the Mass Varying Neutrino Scenario focusing on its Supersymmetric version. Furthermore, it is accommodated into a generic form [22] suitable to serve as framework for our later investigation. Thereafter, in Sec. 3.2, we provide all state-of-the art tools to analyze absorption dips in the EHECν fluxes to be observed at earth extending the complete analysis to incorporate varying neutrino masses, including the full thermal effects. In addition, on the level of the survival probabilities in Sec. 3.2.3 we switch off the thermal effects, for the purpose of gaining more physical insight into the characteristic features caused by the mass variation and in order to compare to common approximations employed in the literature. Finally, in Sec. 3.2.4 we illustrate the discovery potential for neutrino observatories for the CνB and give an outlook for the testability of Neutrino Dark Energy by calculating the expected fluxes, both for astrophysical sources and for topological defect sources. In the latter case, for the first time, we employ the appropriate

fragmentation functions. Our results are summarized in Sec. 3.3.

In Sec. 4 we revisit the stability issue arising in highly non-relativistic theories of Neutrino Dark Energy. After setting the stage in Sec. 4.1 for performing a model-independent analysis, in Sec. 4.2 we briefly introduce the concept of linear cosmological perturbation theory constituting the framework for our analysis. For the purpose of developing an intuition for the main physical effects leading to instabilities, in Sec. 4.2.2 we discuss, as a simple example, gravitational instabilities in Newtonian theory. Afterwards, from linearizing Einstein's equations about an expanding background, in Sec. 4.4 we derive the equation of motion for the MaVaN perturbations. Justified approximations are applied to interpret its solutions and to arrive at the stability criterion corresponding to an upper bound on the scalar-neutrino coupling. We illustrate our results in Sec. 4.5 by the help of representative examples both for stable and unstable scenarios. In Sec. 4.7 we summarize our results and provide an outlook.

Finally, in Sec. 5 we summarize our results gained in the first and second main part of this thesis and provide an outlook on promising open issues which arose in the course of this work.

2 Cosmology and Neutrino Physics – Basics

2.1 Cosmology in a Nutshell

This subsection aims at providing an overview over the basic concepts and fundamentals of standard cosmology which our later analysis is built upon. In addition, it serves as an abstract for the introductory sections on cosmology, Secs. 2.2– 2.5.2.

The key idea of Einstein's theory of general relativity is that gravity is a distortion of space and time itself and can be described by a metric. Moreover, it responds to the matter and energy in the universe in a way described by Einstein's field equations. After this revolutionary discovery in 1916, cosmology became the task of finding solutions to Einstein's field equations consistent with the large-scale matter and energy distribution in our universe. However, owing to the inherent non-linearity of the equations, a general solution which describes the origin, the evolution and the ultimate fate of the entire Universe, turned out to be very difficult.

However, as observational cosmology has demonstrated, on the very largest scales $> 100\,\mathrm{Mpc}$ the Universe appears highly symmetric in its properties[1]. This makes the approach reasonable to study the large-scale dynamics of our universe by postulating it to be spatially homogeneous and isotropic, but evolving in time. Modeling its different matter and energy components by a fluid, this assumption allows for exact solutions of Einstein's equations. The emerging 'Friedmann models' which can be compared to observations are distinguished by their curvature, which could be positive, negative, or flat. In a universe where matter and radiation provide the only types of energy density, they would thus predict different fates of our universe, namely a collapse, an eternal expansion or something exactly in between.

However, in 1998 by the help of studies using exploding stars, Type Ia supernovae, as "standardizable candles ", for the first time solid evidence was provided that the universe recently has entered a phase of accelerated expansion [72,73]. This observation was stunning, since the gravitational attraction felt between matter in the universe on the basis of Einstein's theory of general relativity was predicted to cause a *deceleration* of cosmic expansion. Thus, if gravity does not weaken on the largest cosmological scales, this implies that our universe at present is dominated by a so far unknown exotic form of energy. This homogeneously distributed, at best slowly-varying, yet only gravitationally detected and thus *dark* energy has to be of negative pressure to act like a tension opposing gravity. It actually makes up more than 70% of the current total energy density. By now, this revolutionary observation is supported by various cosmological data (see e.g. [1–6, 74]) and has completely separated our concepts of

[1] Note that 1 Mpc corresponding to 3.3 million light years is the typical separation of two galaxies and at the same time a measure for their maximal size.

geometry and destiny. While observations strongly suggest that our universe is remarkably flat (see e.g. [6, 75]), a universe at late times dominated by Dark Energy can expand forever irrespective of the value of the spatial curvature.

However, looking back in time, an isotropic homogeneous universe governed by Einstein's equations generally must have started with a singularity of infinite density, the so-called *'Big Bang'* which initiated cosmic expansion. The most compelling evidence for its existence constituted the detection of the *'Cosmic Microwave Background'* (CMB) of photons, a blackbody spectrum of $T \sim 2.7$ K pervading the universe, interpreted as remnant heat of the Big Bang. The precisely measured, minute anisotropies in the CMB temperature over the full sky tell us that the very early Universe was indeed very smooth and isotropic.

However, according to observations, today this is only true when averaged over very large scales, while the universe appears very lumpy on scales characteristic for galaxies and clusters of galaxies (see e.g. [5]). According to the standard picture of structure formation, small primordial density perturbations in the matter density, traced by the CMB anisotropies, could slowly grow in amplitude by gravity, until they finally formed the structure we observe today. The causal mechanism which generated these primordial small fluctuations according to our current paradigm of early universe cosmology is provided by *cosmic inflation* [76] (see also [77–79]). Namely, shortly after the Big Bang the universe underwent an inflationary period where it grew exponentially. As a crucial consequence of this inflationary expansion, ordinary microscopic quantum fluctuations could become stretched up to cosmologically interesting scales [77, 80] and thus provide the seeds for structure to form.

One of the cornerstones of modern cosmology is provided by *linear cosmological perturbations theory* (for pioneering work see [81–84] and for comprehensive reviews see [85–91]). It is the right tool at hand to understand and to calculate the earliest stages of structure formation. More precisely, as long as the density perturbations are small compared to the average background values, they can be treated as small deviations from the smooth Universe. Furthermore, in its framework the angular spectrum of CMB fluctuations can be predicted (see e.g. Ref. [92] for a comprehensive review). By comparison with measurements, it provides a wealth of information about the history and geometry of our universe [6]. Combining it with the data of various other cosmological precision measurements has allowed cosmologists to establish the 'Cosmological Concordance Model' (also known as Λ Cold Dark Matter (ΛCDM) model). It rests on the theoretical basis of the Friedmann model and relies on a minimal set of parameters that fit the data impressively well, including a cosmological constant Λ as simplest realization of Dark Energy (see e.g. Refs. [5, 6, 74])[2].

From a theoretical point of view, however, Λ is not at all well understood (see Ref. [93] for a review). In fact, the zero-point energy contributions of quantum fields to the cosmological constant lead to a quartically divergent momentum integral. Thus, theorists are faced with the problem why the milli-eV momentum scale underlying Dark Energy is many orders of magnitudes smaller than any reasonable cut-off scale in an effective field theory of particle physics.

However, at the current experimental stage, dynamical alternatives are well allowed. In the

[2]Commonly, the vacuum energy is referred to as cosmological constant and vice versa.

course of this work examples of such scenarios will be explored in which neutrinos turn out to play a key role for the apparently non-trivial acceleration history of our universe. As a nice feature, opposed to scenarios involving no dynamics, such approaches imply the possibility of testing the scenarios within the near future as we will discuss in Sec. 3.

2.2 Einstein's Equation

In the framework of general relativity Einstein's field equations describe the fundamental forces of gravitation as a curved spacetime responding to the energy and momentum within the spacetime,

$$G_{\mu\nu} = 8\pi G T_{\mu\nu}. \tag{2.1}$$

The Einstein tensor $G_{\mu\nu}$, constructed from the metric $g_{\mu\nu}$ and its first and second derivatives, and the energy momentum tensor $T_{\mu\nu}$ are symmetric, conserved tensors. The constant of proportionality that links them is the square of the inverse, reduced Planck mass $M_{\rm Pl}^{-2} = 8\pi G$, with G being Newton's constant. Here and throughout this work natural units are used in which the speed of light, the reduced Planck constant and Boltzmann's constant are unity, $c = \hbar = k_B = 1$. Furthermore, we take the signature of the metric to be $(-+++)$ and Greek indices run from 0 to 3, while Latin indices denote only the spatial degrees of freedom.

It should be noted that in contrast to e.g. Maxwell's equations of electrodynamics the set of six independent second-order differential equations for $g_{\mu\nu}$ resulting from Einstein's equations are non-linear. The reason is that the universality of gravity implies a coupling of the gravitational field to itself which, however, is absent for the electromagnetic field. Accordingly, the electromagnetic field does not carry charge, while the gravitational field both carries energy and momentum and therefore must contribute to its own source.

However, owing to the non-linearity of Einstein's equations, it is very difficult to solve them in full generality. The most popular sort of simplifying assumptions is to ascribe a significant degree of symmetries to the metric. We will follow this approach in Sec. 2.4 with the aim of describing the large-scale dynamics of our universe.

2.3 Redshifts and Scales

Let us in this section briefly introduce the cosmic redshift and the cosmic scale factor $a(t)$ which play an essential role for the description of the dynamics of the expanding universe and the interpretation of cosmological measurements.

In the beginning of the 20th century Hubble found the spectral redshifts of relatively nearby galaxies to increase in proportion to their distance from the observer [94] implying that they appear to be moving away from us. Interpreted as stretching of the wavelengths of photons propagating through the expanding space, it provided the first evidence for the expansion of the Universe, a key feature of the 'Big Bang Theory'.

The cosmic redshift is usually described in terms of the 'redshift parameter' z (abbreviated as

'redshift'), defined as fractional increase in wavelength,

$$z \equiv \frac{\lambda_0 - \lambda_{\rm em}}{\lambda_{\rm em}} = \frac{a(t_0)}{a(t_{\rm em})} - 1, \tag{2.2}$$

where $\lambda_{\rm em}$ and λ_0 denote respectively, the wavelength of the photon at the time of emission, $t_{\rm em}$, and at the time of detection, t_0. Furthermore, $a(t)$ is the cosmic scale factor which represents the relative expansion of the universe and can measure how much bigger or smaller the universe is today than it was at some other instant of time. For example, if the wavelength of a photon is stretched by a factor of two on its way from a distant galaxy to us, the Universe must have been half its current size when the corresponding photon was emitted. Note also, that in cosmology, the redshift is commonly used as a time equivalent[3] $dz = dt(1+z)\dot{a}(t)/a(t)$, where in natural units $t = r$ is the time in which a photon travels the distance r.

Due to the last equality in Eq. (2.2), our most important information about the cosmic scale factor $a(t)$ is gained through the observation of the redshift of light emitted by distant sources like galaxies, quasars, and intergalactic gas clouds.

It should be noted that since photons travel at a finite speed of $\sim 3 \times 10^5\,$km/s, we are looking into the past when we are observing distant objects. For example, a visible star in the sky is typically 10 or 100 light years away, which means that we can see it as it was 10 or 100 years ago. Accordingly, the CMB (cf. the discussion in Sec. 2.5.2) – tracing its origin to about $\sim 3 \times 10^5$ years after the Big Bang – gives us a glimpse on the very early universe. Thus from studying its properties we can learn about conditions on the very largest cosmological scales.

In the next section we will provide the tools to study the large-scale dynamics of our universe from Einstein's equations and we will thus see how the scale factor $a(t)$ evolves with time. Furthermore, we will make contact with the energy components of the universe and their time evolution relevant for our later analysis in the main part of the thesis.

2.4 The Homogeneous Expanding Universe

In the framework of the 'Standard Cosmological Model' in this section we briefly discuss the evolution of the so-called *cosmological background*, defined as idealized homogeneous and isotropic space-time. This approach allows to model the behavior of the universe as a whole, when averaged over large scales (for very nice reviews and books on this subject see e.g. Refs. [95–99] and Refs. [25, 100], respectively).

Requiring the background to be homogeneous and isotropic implies that no point in space should be distinguished. The metric which exhibits this maximal spatial symmetry is called *'Friedmann-Lematre-Robertson-Walker metric'*. In its most general form it reads,

$$ds^2 = g_{\mu\nu} dx^\mu dx^\nu = -dt^2 + a^2(t) \left[\frac{dr^2}{1 - \mathcal{K} r^2} + r^2 (d\theta^2 + \sin^2\theta d\phi^2) \right] \tag{2.3}$$

[3] In this thesis, we will likewise parameterize cosmic time in terms of the cosmic redshift and the cosmic scale factor.

with $a(t)$ denoting the scale factor characterizing the relative size of spatial sections as a function of time and $\mathcal{K} \in \{-1, 0, 1\}$ referring to constant negative curvature ('open Universe'), no curvature ('flat Universe') and positive curvature ('closed universe'), respectively. It is often convenient to express the metric in terms of the 'conformal time' τ, defined by $d\tau = dt/a(t)$ such that the line element takes the form[4]

$$\begin{aligned} ds^2 = g_{\mu\nu} dx^\mu dx^\nu &= a^2(\tau) \left[-d\tau^2 + \frac{dr^2}{1 - \mathcal{K} r^2} + r^2 (d\theta^2 + \sin^2\theta d\phi^2) \right], \text{where} \\ g_{\mu\nu} &= a^2(\tau)\, \mathrm{diag}(-1, 1, 1, 1) \text{ for } \mathcal{K} = 0. \end{aligned} \tag{2.4}$$

In order to determine from Einstein's field equations how the scale factor a evolves with time, we have to specify the stress-energy tensor T^μ_ν of the large-scale energy and matter distribution of the universe. In accordance with the symmetries of the metric, it is diagonal and in order to comply with isotropy its spatial components are equal. As simplest realization, the universe's matter content is conventionally modeled by a perfect fluid with time-dependent density $\rho(t)$ and pressure $p(t)$ and a stress-energy tensor T^μ_ν of the form,

$$T^\mu_\nu = p g^\mu_\nu + (\rho + p) U^\mu U_\nu, \tag{2.5}$$

where $U^\mu = dx^\mu / \sqrt{-ds^2}$ is the 4-velocity of a comoving observer at rest with the fluid at the instant of the measurement. The nature of the fluid is completely specified, once the relation between $\rho(t)$ and $p(t)$ is given in the form of an equation of state $\omega(t)$, where

$$w(t) = \frac{p(t)}{\rho(t)}. \tag{2.6}$$

Finally, by plugging Eq. (2.3) and Eq. (2.5) into Einstein's equations, we arrive at the time-evolution of the scale factor a which is described by two independent equations, the 'Friedmann equation' and the 'acceleration equation', respectively,

$$H^2 \equiv \left(\frac{\dot{a}}{a} \right)^2 = \frac{8\pi G}{3} \rho - \frac{\mathcal{K}}{a^2}, \tag{2.7}$$

$$\frac{\ddot{a}}{a} = -\frac{4\pi}{3} (1 + 3\,\omega) \rho, \tag{2.8}$$

where dots denote time derivatives and $H = d \log a / dt = \dot{a}/a$ is the Hubble parameter. Its value today, $H_0 \equiv H(t_0)$ is often expressed in terms of the dimensionless quantity h [6] [5],

$$h = H_0 / (100\,\mathrm{km\,s^{-1}\,Mpc^{-1}}) = 0.710 \pm 0.026, \tag{2.9}$$

where here and in the following the subscript 0 denotes present day quantities. Furthermore, in this work we will adhere to the convention of normalizing a such that $a_0 = 1$.

Moreover, Einstein's equations imply that the stress-energy tensor is locally conserved such that its covariant derivative vanishes, $T^\mu_{\nu;\mu} = 0$. Thus, the $\mu = 0$ component yields the following

[4] Note that conformal time is the natural choice for the time variable to calculate the perturbation evolution in Sec. 4.
[5] This value is taken from combined data of WMAP3 and the Sloan Digital Sky Survey (SDSS).

energy-conservation equation,

$$\dot{\rho} + 3H(1+\omega)\rho = 0, \tag{2.10}$$

with ω as defined in Eq. (2.6). Accordingly, the energy density gets diluted as the Universe expands,

$$\rho \propto e^{-3\int da \frac{1+\omega(a)}{a}}. \tag{2.11}$$

At present, the universe appears to be well described by a fluid which contains five independent contributions,

$$T^{\mu}_{\nu} = \sum_i T^{\mu}_{\nu\, i} \tag{2.12}$$

where the summation index i comprises photons (γ), baryons (b), neutrinos (ν), Dark Matter (DM) and Dark Energy (DE) whose properties we will briefly describe in the following.

For this purpose it is useful to realize that as long as a component $T^{\mu}_{\nu\, i}$ of the total stress-energy tensor negligibly exchanges energy and momentum with the other components[6], we have $T^{\mu}_{\nu\, i;\, \mu} = 0$ for the component i. This turns out to be a fairly good approximation in the present universe and thus we can assume Eq. (2.10) to be satisfied separately by each of the components i. Consequently, inserting the respective equations of state ω_i into Eq. (2.11), we arrive at different evolutions of the energy densities with the scale factor a,

$$\omega_{\text{radiation}} = \frac{1}{3} \quad \rightarrow \quad \rho_{\text{radiation}} \propto a^{-4} \propto (1+z)^4, \tag{2.13}$$

$$\omega_{\text{matter}} = 0 \quad \rightarrow \quad \rho_{\text{matter}} \propto a^{-3} \propto (1+z)^3, \tag{2.14}$$

$$\omega_{\Lambda} = -1 \quad \rightarrow \quad \rho_{\Lambda} = const., \tag{2.15}$$

$$\omega_{\text{DE}}(a) < -\frac{1}{3} \neq const. \quad \rightarrow \quad \rho_{\text{DE}} \propto e^{-3\int da \frac{1+\omega_{\text{DE}}(a)}{a}} \propto e^{3\int dz \frac{1+\omega_{\text{DE}}(z)}{1+z}}. \tag{2.16}$$

Let us in the following discuss which of the universe's components contribute to the radiation and matter, respectively.

The universe around us is filled with photons, whose energy density is dominated by the photons of the CMB which have always contributed to the radiation content of the universe. Note however, that the nature and thus the equation of state of particles can change with time in an evolving universe as we will see in the following.

According to Big Bang theory, there is almost an equal number of relic neutrinos composing the cosmic neutrino background (CνB) (cf. Secs. 2.5.1 – 2.5.2 for a discussion of the origin of the CνB and CMB, respectively). In contrast to other particles of the standard model of particle physics, the masses of neutrinos are sufficiently small in order for neutrinos to have been relativistic at least up to very recent epoches of the universe (cf. Ref. [101]). Therefore, the neutrinos have also contributed to the universe's radiation content for most of its history with an equation of state according to Eq. (2.13). However, after the non-relativistic transition, the pressure p_ν in the neutrino gas drops (and thus also the kinetic energy) until $p_\nu \simeq 0$. As a consequence, weakly interacting non-relativistic neutrinos contribute together with electrons,

[6] Note that in the early universe this is not fulfilled for radiation and matter which where tightly coupled by Thompson scattering.

nucleons and atoms to the ordinary matter content of the universe characterized by an equation of state according to Eq. (2.14) (cf. Secs. 3 – 4, where neutrinos are assumed to exchange energy with the dark sector and as a consequence Eq. (2.10) gets modified for neutrinos).

In addition, consistent evidence for the existence of a large amount of so far unknown, non-relativistic matter in the universe is provided by observations.[7] This non-relativistic matter gravitates just as ordinary matter does with an equation of state according to Eq. (2.14), however, it does not emit or reflect enough electromagnetic radiation to be observed directly and thus is dubbed *dark matter*.

Finally, let us comment on the cosmological constant and another possible form of dynamical Dark Energy relevant for this thesis.

As can be read off Eq. (2.8), in order to obtain an accelerated universe with $\ddot{a} > 0$, its dominant energy component has to exhibit sufficiently negative pressure such that $\omega < -\frac{1}{3}$.

According to recent observations, the equation of state of Dark Energy is $\omega_{\mathrm{DE}} < -0.8$ at 1σ [102]. Thus, as we will see in the following, it is consistent with a cosmological constant Λ identified with the energy density of the vacuum. It can be thought of as a perfect fluid as defined in Eq. (2.5) with,

$$\rho_\Lambda = -p_\Lambda, \tag{2.17}$$

where p_Λ denotes its negative pressure and ρ_Λ its time-independent energy density,

$$\rho_\Lambda \simeq (2.3 \times 10^{-3}\,\mathrm{eV})^4. \tag{2.18}$$

Accordingly, this corresponds to an equation of state $w_\Lambda = -1$ (cf. Eq. (2.13)).

However, as another observationally allowed possibility, the Dark Energy could be some component whose energy density has dynamically evolved to the value stated in Eq. (2.18). Accordingly, its equation of state can be slowly varying with time, but has to be close to -1 today.

As a good candidate which plays a key role in the first and second main part of this thesis, in the following we consider a spatially homogeneous scalar field ϕ [10–13]. Scalar matter fields are special in the sense that they allow for the presence of a potential energy term $V(\phi)$. Their stress-energy tensor reads,

$$T^\mu_\nu = \dot{\phi}^2 - \delta^\mu_\nu \left(\frac{1}{2}\dot{\phi}^2 + V(\phi) \right). \tag{2.19}$$

Accordingly, the energy density ρ_ϕ and pressure p_ϕ are given by,

$$\rho_\phi = \frac{1}{2}\dot{\phi}^2 + V(\phi), \quad p_\phi = \frac{1}{2}\dot{\phi}^2 - V(\phi). \tag{2.20}$$

[7] It should be noted that at sufficiently early times even particles constituting the non-relativistic matter today were relativistic and thus contributed to radiation.

Thereby, an in general time-dependent equation of state is implied,

$$\omega_\phi = \frac{\frac{1}{2}\dot{\phi}^2 - V(\phi)}{\frac{1}{2}\dot{\phi}^2 + V(\phi)}, \tag{2.21}$$

which apparently can take values $-1 \leq \omega_\phi \leq 1$.

Consequently, as long as the scalar field is slowly-varying such that, $\frac{1}{2}\dot{\phi}^2 \ll V(\phi)$, it has a dynamical, but slowly-evolving equation of state whose value is close to -1.

After having described the matter and radiation content of our universe, let us briefly turn to its geometry. For later reference, it is convenient to define the *critical density* $\rho_{\rm cr} \equiv 3H^2/8\pi G$ corresponding to a flat universe today as well as $\Omega_i \equiv \rho_i(t_0)/\rho_{\rm cr}$, where i again labels the various components of the total stress-energy tensor. Recasting 'Friedmann's equation' as,

$$1 - \sum_i \Omega_i = -\frac{\mathcal{K}}{a^2 H^2} \equiv \Omega_\mathcal{K}, \tag{2.22}$$

it becomes apparent that the universe is open if $\sum_i \Omega_i < 1$, flat if $\sum_i \Omega_i = 1$, closed if $\sum_i \Omega_i > 1$.

For later reference, it is furthermore instructive to express the evolution of the Hubble parameter in terms of its value today as well as the universe's present energy fraction provided by radiation ($\Omega_{\rm R}$), ordinary and Dark Matter ($\Omega_{\rm M}$), curvature ($\Omega_\mathcal{K}$) and Dark Energy ($\Omega_{\rm DE}$), respectively,

$$H^2(z) = H_0^2 \left[\Omega_R(1+z)^4 + \Omega_M(1+z)^3 + \Omega_\mathcal{K}(1+z)^2 + \Omega_{\rm DE} f(z)\right], \tag{2.23}$$

where in general $f(z) = e^{3\int dz \frac{1+\omega_{\rm DE}(z)}{1+z}}$, which for a cosmological constant with $\Omega_{\rm DE} = \Omega_\Lambda$ and $\omega_{\rm DE} \equiv \omega_\Lambda = -1$ reduces to $f(z) = f = 1$.

According to the best fit values for the minimal cosmological model based on Friedmann cosmology as well as a cosmological constant Λ as simplest realization of Dark Energy, the universe is currently composed of [6][8],

$$\begin{aligned} \Omega_{\rm M} &= 0.265 \pm 0.030, \\ \Omega_{\rm b} &= 0.0442 \pm 0.001, \\ \Omega_\mathcal{K} &= -0.0053 \pm 0.006, \\ \Omega_\Lambda &= 0.707 \pm 0.041, \end{aligned} \tag{2.24}$$

where $\Omega_{\rm M}$ denotes the total matter density which includes the baryon density Ω_b. It should be noted that this minimal ΛCDM model appears to fit all currently available cosmological data from various independent sources with remarkably small discrepancies. Note also that the curvature of space is very close to 0 and thus the universe appears to be flat and the contribution of radiation to the current total energy density is negligible, $\Omega_R \simeq 0$. Therefore, according to Eq. (2.22) and Eq. (2.24) the remaining energy densities approximately sum up

[8] These values result from combining WMAP3 and SDSS data.

to one.

According to Eq. (2.24), we see that the Universe today is dominated by Dark Energy which implies $H(z) \sim const.$ for an equation of state close to -1 as suggested by recent observations [6]. However, taking a closer look at Eq. (2.23), we observe that due to the different scaling laws of the various energy components with redshift this has not always been the case. For redshifts $z \gtrsim 0.5$ [103], however smaller than $z \simeq 4 \times 10^3$, the universe was in a matter-dominated phase and thus $H(0.5 \lesssim z \lesssim 4 \times 10^3) \propto (1+z)^{3/2}$. Finally, for $z \gtrsim 4 \times 10^3$, the universe was radiation-dominated and accordingly $H(z \gtrsim 4 \times 10^3) \propto (1+z)^2$.

After having defined the Hubble expansion rate, for later reference it is also very important to mention its inverse, the *Hubble radius*, $H^{-1}(z)$. It defines a length scale which constitutes the maximal distance that microphysics can act coherently over a Hubble expansion time. In particular, it is the maximal distance on which any causal process could create fluctuations.

2.5 A Brief Thermal History of the Universe

In the last sections the tools were set up to analyze the kinematics and dynamics of the idealized homogeneous and isotropic universe. In addition we have made contact with the situation in our real, current Universe. This section will set the stage for an appropriate description of the cosmic neutrino background CνB, the analog of the CMB of photons, which is of essential relevance in the main part of this work. For this purpose, we have to turn back in time and briefly discuss the physics of the very early Universe. Since it was characterized by very high temperatures and densities, many particle species were kept in (approximate) thermal equilibrium by rapid interactions. Thus we are led to extend the simple treatment of matter and radiation as non-interacting fluids to a thermodynamical description in the expanding universe.

In order to be in equilibrium with the surrounding thermal plasma in the very early universe, the interaction rate Γ of a particle had to be faster than the expansion rate H. By this means, the products of reactions involving this particle had the opportunity to recombine in the reverse reaction. Conversely, a particle would fall out of equilibrium (*freeze out* or *decouple*) as soon as

$$\begin{aligned} \Gamma &> H, \text{ where typically} \\ \Gamma &= \langle \sigma v \rangle \, n, \end{aligned} \tag{2.25}$$

with σ denoting the cross-section, v the particle velocity and n the number density. Accordingly, as long as the universe was inhabited by ultra-relativistic particles of extremely high densities, most of them (apart from very weakly coupled species) were in thermal equilibrium with the thermal bath of temperature T. However, its temperature was continously cooled by the expansion of the universe, $T \propto a^{-1}$, and the number density of the particles was diluted, $n \propto a^{-3}$. As a consequence, today no particles are in thermal equilibrium anymore with the background plasma (represented by the CMB).

Let us in the following briefly discuss how the appropriate thermodynamical description of the

various particles occupying the universe depends on whether they are in thermal equilibrium or decoupled, bosons or fermions or relativistic or non-relativistic. We will start by considering particles in equilibrium.

In thermal equilibrium the density of a weakly-interacting gas of particles in a given momentum bin can be characterized by a phase-space distribution function $f(P)$ with P denoting the momentum. The number density n, energy density ρ and pressure p in terms of $f(P)$ read,

$$\begin{aligned} n &= \frac{g}{(2\pi)^3}\int d^3P f(P), \\ \rho &= \frac{g}{(2\pi)^3}\int d^3P E(P) f(P), \\ p &= \frac{g}{(2\pi)^3}\int d^3P \frac{P^2}{3E(P)} f(P), \end{aligned} \tag{2.26}$$

$$\tag{2.27}$$

where g is the number of spin states. For fermions and bosons in thermal equilibrium at temperature T the distribution function $f(P)$ is of Fermi-Dirac $(+)$ or Bose-Einstein $(-)$ form, respectively,

$$f(P) = \frac{1}{e^{(E(P)-\mu)/T} \pm 1}, \tag{2.28}$$

with $E(P) = \sqrt{P^2 + m^2}$ denoting the particle energy and μ the chemical potential which arises in the presence of an asymmetry between the particle and its anti-particle.

If a particle species according to Eq. (2.25) is no longer maintained in thermal equilibrium by its interactions, the subsequent evolution of its distribution function can be approximated in the limit that the particle is either highly relativistic ($T \gg m$) or highly non-relativistic ($T \ll m$) at decoupling. In the ultra-relativistic case it is,

$$f^{\rm Rel}(P) = \frac{1}{e^{P/T^{\rm Rel}} \pm 1}, \tag{2.29}$$

where the plus sign applies to fermions and the minus sign to bosons and $T^{\rm Rel}$ can be regarded as an effective temperature of the distribution function. It depends on the temperature T_d at the decoupling time t_d,

$$T^{\rm Rel}(a) = T_d \left(\frac{a_d}{a}\right), \tag{2.30}$$

where $a_d = a(t_d)$. Note that $P, T^{\rm Rel} \propto a^{-1}$ and thus $P/T^{\rm Rel}$ is a non-redshifting quantity. Therefore, as long as the particle stays ultra-relativistic after decoupling, the form of $f(P)$ is preserved even though the particle is not in equilibrium anymore.

In case the particle decoupled while being highly non-relativistic, its distribution function reads,

$$f^{\rm NR}(P) = e^{-\frac{m-\mu}{T_d}} e^{-\frac{P^2}{2mT^{\rm NR}}}, \tag{2.31}$$

	Relativistic Bosons	Relativistic Fermions	Non-relativistic (Either)
n	$\frac{\zeta(3)}{\pi^2} g T^3$	$\left(\frac{3}{4}\right) \frac{\zeta(3)}{\pi^2} g T^3$	$g \left(\frac{mT}{2\pi}\right)^{3/2} e^{-(m-\mu)/T}$
ρ	$\frac{\pi^2}{30} g T^4$	$\left(\frac{7}{8}\right) \frac{\pi^2}{30} g T^4$	mn
p	$\frac{1}{3}\rho$	$\frac{1}{3}\rho$	$nT \ll \rho$

Table 2.1: Number density n, energy density ρ, and pressure p, for species in thermal equilibrium.

while the effective temperature $T^{\rm NR}$ scales as the kinetic energy $\propto a^{-2}$ of the particle,

$$T^{\rm NR}(a) = T_d \left(\frac{a_d}{a}\right)^2 . \tag{2.32}$$

In table 2.1 the resulting time evolution of n, ρ and p is summarized in the relativistic and non-relativistic limit, respectively, in which ζ is the Riemann zeta function, and $\zeta(3) \approx 1.202$. Note that in case a particle has frozen out while being relativistic, but subsequently turns non-relativistic, its distribution function is distorted away from a thermal spectrum.

2.5.1 The Cosmic Neutrino Background

Having now at hand the appropriate thermodynamics to describe particles in the early universe, let us in the following briefly turn to the part of its thermal history relevant to understand the origin of the *cosmic neutrino background* (CνB) and its characteristic temperature T_ν in comparison to the CMB temperature T_γ.

- $\boldsymbol{T > 1\,\mathrm{MeV},\ t > 1\,\mathrm{sec}}$ **:** Neutrinos with interaction rate $\Gamma_\nu \propto G_F^2 T^5$, where G_F denotes the Fermi constant, were kept in thermal equilibrium by weak interaction processes of the sort

$$\bar{\nu}\nu \to e^+ e^-,\ \nu e \to \nu e, \text{ etc. with}$$

$$\frac{\Gamma_\nu}{H} \simeq \frac{G_F^2 T^5}{T^2/M_{\rm Pl}} \simeq \left(\frac{T}{1\mathrm{MeV}}\right)^3 > 1$$

- $\boldsymbol{T \simeq 1\,\mathrm{MeV},\ t \simeq 1\,\mathrm{sec}}$ **:** The number density of the weakly-coupled neutrinos had been diluted sufficiently by the expansion of the universe to allow for Γ_ν to drop below H. Thus, the ultra-relativistic neutrinos and anti-neutrinos froze out, leaving electrons, positrons and photons (and a few nucleons) in thermal equilibrium. Subsequently, assuming the absence of neutrino interactions, the neutrinos began a free expansion, distributed according to Eq. (2.29) with effective temperature T_ν as in Eq. (2.30) cooled by

the expansion[9],

$$f_\nu(P) = \frac{1}{e^{P_\nu/T_\nu} + 1}. \tag{2.33}$$

Note that we have neglected the contribution of a relic neutrino asymmetry μ_ν to $f_\nu(P)$ in Eq. (2.33), which is justified, since current bounds on the common value of the degeneracy parameter $\xi_\nu = \mu_\nu/T_\nu$ are as small as $-0.05 < \xi_\nu < 0.07$ at 2σ [101].

Thus, as a generic prediction of the hot Big Bang model, the *cosmic neutrino background* (CνB) (or equivalently the *relic neutrino background*) is assumed to permeate our universe ever since neutrino decoupling.

- $\boldsymbol{T \simeq 511\,\mathrm{keV},\ t \simeq 1\,\mathrm{sec}}$ **:** Shortly after neutrinos had decoupled, T dropped below the electron mass m_e. Thus, electron-positron pairs annihilated into photons, while the reverse reaction of $e^\pm$-pair production was energetically disfavored. The $e^\pm$-entropy release was transferred to the thermal plasma, but not to the decoupled neutrinos (in the limit of instantaneous freeze-out[10]). Consequently, only the temperature $T_\gamma = T$ of photons (still being in equilibrium) was raised by a factor $(11/4)^{1/3}$,

$$\left(\frac{T_\gamma}{T_\nu}\right)_{T<m_e} = \left(\frac{11}{4}\right)^{1/3} \simeq 1.401, \tag{2.34}$$

which according to precise measurements of the CMB temperature by the FIRAS instrument on the COBE satellite [105] implies today,

$$T_{\nu 0} \equiv T_\nu(a=1) = \left(\frac{11}{4}\right)^{1/3} T_\gamma(a=1) = 1.697 \times 10^{-4}\,\mathrm{eV}. \tag{2.35}$$

Since after $e^\pm$ decoupling the remaining protons, neutrons and few electrons were no longer moving relativistically, subsequently, the energy density of the universe was dominated by photons with a contribution from neutrinos.

Since the content of this section is of central relevance for this thesis, let us summarize the most important facts. Since (anti-)neutrinos were ultra-relativistic at the time of their freeze-out, their distribution still assumes the relativistic Fermi-Dirac form as stated in Eq. (2.33) [101] on large cosmological scales[11]. Unaffected by the process of decoupling, Big Bang theory predicts the CνB to have expanded freely ever since on these scales, only subject to the expansion which cools its characteristic temperature $T_\nu \propto a^{-1}$. As neutrinos did not share the entropy release of $e^\pm$ in opposition to photons, T_ν is slightly smaller than the CMB temperature (cf. the next section for a brief discussion of the origin of the CMB).

[9] Strictly speaking, the neutrino distribution is not an equilibrium one, since more precisely the Fermi factor in Eq. (2.33) reads $[\exp(\sqrt{(P/T_\nu)^2 + (m_\nu(T_{\nu_d})/T_{\nu_d})^2}) + 1]^{-1}$ [104] with T_d the temperature at decoupling. However, since $T_{\nu_d} \sim 1$ MeV and accordingly $\frac{m_\nu(T_d)}{T_d} < 10^{-6}$ for $m_\nu(T_d) < 1$ eV, the bulk of the neutrino distribution with $\frac{P}{T_\nu} > \frac{m_\nu(T_d)}{T_d}$ is not affected by the strongly suppressed mass correction and can thus well be characterized by an effective equilibrium temperature T_ν.

[10] See Ref. [101] for a recent review on this subject.

[11] Note that on small cosmological scales the relic neutrino spectrum is distorted as a result of the relic neutrino clustering into the potential wells formed by cold dark matter [106, 107].

2.5.2 The Cosmic Microwave Background

As long as photons were sufficiently energetic to ionize hydrogen atoms, the universe was filled with a charged plasma – photons where tightly coupled to matter through Thomson scattering. However, roughly 3×10^5 years after the Big Bang, the photons where cooled sufficiently by cosmic expansion to allow for protons and electrons to combine and to form neutral atoms such that the universe was not opaque to photons anymore. Afterwards, the photons could travel essentially freely to us, however, being subject to cosmic expansion. As we have learnt in the last section, as a result, the form of their equilibrium Bose-Einstein distribution is retained, but its effective temperature is cooled. Accordingly, today these relic photons permeate the universe as Cosmic Microwave Background (CMB). It constitutes the exact analog of the CνB predicted by Big Bang theory, however, with a slightly higher temperature and thus slightly higher abundance today.

The minute anisotropies in the CMB spectrum allow to extract cosmological parameters with high precision [6].

2.6 Neutrinos

The historic discovery of neutrino flavor oscillations provided one of the most important signatures for new physics beyond the Standard Model (SM). Namely, it implied that neutrinos exhibit distinct, non-zero masses and that the propagating mass eigenstates in general are different from the flavor eigenstates produced and detected in experiments. While by now solar and atmospheric oscillation experiments have provided us with a fairly good knowledge of both neutrino mass squared differences and mixing angles (for a recent review see [36]), they are insensitive to one crucial, still outstanding input – the absolute neutrino mass scale. So far, only upper limits exist which are derived from the non-observation of neutrinoless beta-decay $0\nu\beta\beta$ and endpoint spectrum studies of (e.g. tritium) beta decay as well as from cosmological measurements sensitive to neutrino masses.

This chapter provides the theoretical basics of neutrino physics. Furthermore, up-to-date neutrino data – to be employed in the phenomenological parts of Secs. 3 – 4 – is presented, including a summary of recent upper bounds on the absolute neutrino mass scale.

2.6.1 Neutrino Masses – The See-Saw Mechanism

In the framework of the SM of particle physics, right-handed neutrinos are not required by electroweak theory and thus the left-handed chiral neutrinos, ν (with $\nu^T = (\nu_{eL}^T, \nu_{\mu L}^T, \nu_{\tau L}^T)$), are the only fermions without right-handed partners in the SM. Accordingly, since Dirac mass terms (generated by the Higgs-mechanism, see e.g. [108]) necessitate fields of opposite chirality, neutrinos are massless in the SM as opposed to quarks and charged leptons.

However, experiments not only suggest that neutrinos are massive, but also that their masses are in the (sub-) eV range and thus orders of magnitude smaller than any other SM masses.

Probably the most elegant and natural explanation beyond the SM description is provided by the so-called *see-saw mechanism* [32–35]. In the following, it will be introduced in some detail because it plays a central role in Sec. 3 (cf. also Sec. 4)[12].

In the framework of the see-saw mechanism, the SM Lagrangian is augmented to include three fermions which play the role of 'right-handed neutrinos' N (with $N^T = (\nu_{eR}^T, \nu_{\mu R}^T, \nu_{\tau R}^T)$), and are singlets under the SM gauge group. Consequently, for them, unlike for their left-handed partners, a lepton-number violating Majorana mass term is not protected by symmetries and is thus permitted. In addition, they can have a Yukawa interaction λ allowing for a Dirac mass term, possibly generated by the standard Higgs-mechanism [36],

$$\mathcal{L} = \mathcal{L}_{\rm SM} + \bar{N}_i i\partial\!\!\!/ N_i + (\lambda_{ij} N_i L_j H - \frac{1}{2} M_{ij} N_i N_j + h.c.) \tag{2.36}$$

where $i, j = \{1-3\}$ denote the family-number indices, L_i are the $SU(2)$ lepton doublets, and H is the ordinary Higgs doublet and the Majorana mass matrix M and the Yukawa matrix λ

[12] For alternative approaches which, however, mostly lack a natural explanation for the relative smallness of neutrino masses and thus appear less attractive, see e.g. Ref. [36] for a recent review.

are 3×3 flavor matrices[13].

The new scale introduced by the elements of M in Eq. (2.36) is assumed to be related to some 'fundamental' physics at ultra-high energies beyond the low-energy description of the SM, e.g. to some symmetry breaking in the framework of grand unified theories. It thus seems natural to expect the eigenvalues of M to be much larger than those of the Dirac mass matrix $M_D \propto \lambda$, since it is not protected by the SM gauge symmetries. Under this assumption, after integrating out the heavy right-handed neutrinos, one arrives at the effective Lagrangian [109],

$$\mathcal{L} = \mathcal{L}_{\rm SM} + \frac{1}{2}\sum_k (\lambda_{ik}^T M_k^{-1} \lambda_{kj})(L_i H)(L_j H) + h.c. \tag{2.37}$$

which only contains observable low-energy fields. Furthermore, it exhibits a (non-renormalizable) dimension-five operator suppressed by a small matrix factor which violates lepton number by two units $\Delta L = 2$.[14] At spontaneous electroweak symmetry breaking [108], the Higgs field acquires a vacuum expectation value, $\langle H \rangle = v \sim 246\,\text{GeV}$, which generates the following 3×3 Majorana mass matrix for light neutrinos,

$$(m_\nu)_{ij} \simeq -(M_D^T M^{-1} M_D)_{ij} \text{ with } M_{Dij} = v\lambda_{ij}. \tag{2.38}$$

From naturalness arguments it should be expected that the Dirac mass for each generation of neutrinos is of the same order of magnitude as the mass of the corresponding quark or charged fermion. Accordingly, the see-saw mechanism naturally ascribes the relative smallness of neutrino masses to the suppression of the Dirac mass matrix M_D by the small matrix factor $M_D^T (M)^{-1}$. In addition, the neutrinos ν_i with definite masses $m_{\nu i}$ (cf. the next section) are predicted to be Majorana particles. This implies that they possess only half of the four independent components of Dirac particles and are their own charge conjugates[15],

$$\nu_i = \mathcal{C}\bar{\nu}_i^T \equiv \nu_i^c, \tag{2.39}$$

with $\mathcal{C}$ denoting the charge conjugation matrix. Importantly, the predicted Majorana nature of neutrino masses is a clear signature for the see-saw mechanism and implies the existence of a new fundamental scale in nature $\Lambda \simeq \frac{v^2}{m_\nu} \simeq 10^{14} - 10^{15}\,\text{GeV}$ for $m_\nu \sim O(10^{-2}) - O(10^{-1})\,\text{eV}$. It is mainly searched for by neutrinoless double β decay experiments to be discussed in Sec. 2.6.4.

2.6.2 Neutrino Mixing and Flavor Oscillations

Since the neutrino mass matrix is not diagonal when expressed in terms of the flavor eigenstates, one is led to the concept of neutrino flavor oscillations. In other words, the flavor eigenstates ν_α participating in weak interactions are superpositions of the propagating neu-

[13] Without loss of generality we adopt a basis in which the matrix M_{ij} is diagonal [109].

[14] Such an effective non-renormalizable operator can be regarded as low-energy manifestation of a renormalizable new theory beyond the SM.

[15] It should be noted that a Majorana mass is unique for neutrinos, since for quarks and charged leptons it is forbidden by electric charge conservation.

trino states ν_i of definite mass m_i,

$$\nu_\alpha = \sum_{i=1}^{3} U_{\alpha i}\nu_i, \tag{2.40}$$

where $\alpha = e, \mu, \tau$ and the 3×3 neutrino mixing matrix U [110] is determined by the condition

$$U^T m_\nu U = \mathrm{diag}(m_1, m_2, m_3). \tag{2.41}$$

The most common parameterization of the mixing matrix in components, $U_{\alpha i}$, is given by

$$\begin{array}{c} \\ \nu_e \\ \nu_\mu \\ \nu_\tau \end{array} \begin{array}{c} \begin{array}{ccc} \nu_1 & \nu_2 & \nu_3 \end{array} \\ \begin{pmatrix} c_{12}c_{13} & c_{13}s_{12} & s_{13}e^{-i\varphi_{13}} \\ -c_{23}s_{12} - c_{12}s_{13}s_{23}e^{i\varphi_{13}} & c_{12}c_{23} - s_{12}s_{13}s_{23}e^{i\varphi_{13}} & c_{13}s_{23} \\ s_{23}s_{12} - c_{12}c_{23}s_{13} & -c_{12}s_{23}e^{i\varphi_{13}} - c_{23}s_{12}s_{13}e^{i\varphi_{13}} & c_{13}c_{23} \end{pmatrix} \end{array}$$

$$\times\, \mathrm{diag}(1, e^{i\lambda_{21}}, e^{i\lambda_{31}}) \tag{2.42}$$

with $c_{ij} \equiv \cos\vartheta_{ij}$, $s_{ij} \equiv \sin\vartheta_{ij}$, where ϑ_{12}, ϑ_{23},ϑ_{13} are the three mixing angles, φ_{13} is the Dirac phase and λ_{21} and λ_{13} are the Majorana phases. The Dirac phase is the analog of the phase in the quark mixing matrix. In case neutrinos are Dirac particles, the Majorana phases can be eliminated by a rephrasing of the massive neutrino fields. All of the three complex phases in the mixing matrix generate violations of the CP symmetry.

Let us in the following consider a neutrino produced and detected with definite flavor in weak charged-current interactions after propagating a time T and a distance L in vacuum. The normalized neutrino state at the production point,

$$|\nu_\alpha\rangle = \sum_{i=1}^{3} U^*_{\alpha i}|\nu_i\rangle, \tag{2.43}$$

is related to the state $|\nu_\alpha(L,T)\rangle$ at the detection point by the Schroedinger equation. Accordingly, one arrives at,

$$|\nu_\alpha(L,T)\rangle = \sum_{\beta=e,\mu,\tau} \left[\sum_{i=1}^{3} U^*_{\alpha i} e^{-iE_iT+ip_iL} U_{\beta i}\right] |\nu_\beta\rangle, \tag{2.44}$$

where E_i and p_i, respectively, are the energy and momentum of the massive neutrino ν_i. Consequently, at detection the state describes a superposition of different neutrino flavors

giving rise to the possibility of flavor change $P_{\nu\alpha\to\nu\beta}$,

$$\begin{aligned} P_{\nu\alpha\to\nu\beta}(L) &= |\langle\nu_\beta|\nu_\alpha(L)|^2 = \left|\sum_{i=1}^{3} U^*_{\alpha i} e^{-i\frac{\Delta m^2_{ij} L}{2E}} U_{\beta i}\right| \\ &= \sum_{i=1}^{3} |U_{\alpha i}|^2 |U_{\beta i}|^2 + 2Re \sum_{i>j} U^*_{\alpha i} U_{\beta i} U_{\alpha j} U^*_{\beta j} e^{-i\frac{\Delta m^2_{ij} L}{2E}}, \end{aligned} \tag{2.45}$$

where $\Delta m^2_{ij} = m^2_i - m^2_j$ and the dependence on T has been expressed in terms of the neutrino masses and energy. Accordingly, the neutrino mass squared differences as well as the mixing matrix are the fundamental inputs which determine neutrino oscillations. Neutrino oscillation experiments are characterized by a different neutrino energy E and propagation distance L.

It should be noted that the vacuum transition probability $P_{\nu\alpha\to\nu\beta}$ in Eq. (2.45) gets modified by neutrino interactions resulting from the propagation through matter. While neutral current interactions are common to all neutrino flavors, only electron neutrinos can additionally have charged current interactions with electrons composing the matter besides nucleons (or quarks). As a result, with respect to the other flavors, the time development of electron neutrinos is altered by a phase which is determined by the electron density of the medium of propagation. Under favorable conditions, a resonant amplification of oscillations may occur known as the Mikheyev-Smirnov-Wolfenstein (MSW) effect (see e.g. Ref. [36] for a recent review).

Neutrino Mixing Parameters

In this section we state the results of a global analysis of recent experimental data on the neutrino mixing parameters gained from neutrino oscillation experiments [36,111] to be employed in Sec. 3.2.3. The central values are

- $\sin^2\vartheta_{12} = 0.314(1^{+0.18}_{-0.15})$
- $\sin^2\vartheta_{23} = 0.44(1^{+0.41}_{-0.22})$
- $\sin^2\vartheta_{13} = 0.9^{+2.3}_{-0.9} \times 10^{-2}$.

Note that the leptonic mixing matrix U has a different texture than the quark mixing matrix. While the latter only exhibits small mixing angles, two of the mixing angles of the leptonic mixing matrix are large.

2.6.3 Neutrino Mass Splittings

One of the key achievements of neutrino oscillation experiments is the provided knowledge on the neutrino mass squared differences $\Delta m^2_{ij} = m^2_i - m^2_j$. Solar neutrino and reactor-antineutrino experiments as well as atmospheric and long-baseline accelerator neutrino experiments nicely allow to interpret the oscillation data in terms of three-neutrino mixing with, respectively (see Ref. [36] for a recent review),

- $\Delta m^2_{\rm SOL} = \Delta m^2_{21} = (8.0 \pm 0.3) \times 10^{-5}\,{\rm eV}^2$ from ν_e disappearance
- $\Delta m^2_{\rm ATM} \simeq |\Delta m^2_{31}| \simeq |\Delta m^2_{32}| = (2.5 \pm 0.2) \times 10^{-3}\,{\rm eV}^2$ from ν_μ disappearance.

So far both the sign of Δm^2_{31} and the absolute neutrino mass scale are not known, thus leaving undetermined which of the following three possible neutrino mass schemes are realized in nature:

- **Degenerate spectrum:**[16] $m_1 \sim m_2 \sim m_3 \gg |m_i - m_j|$
- **Normal hierarchy:** $m_3 \gg m_{2,1}$ ($\Delta m^2_{31} > 0$) in analogy to quarks and charged leptons
- **Inverted hierarchy:** $m_1 \sim m_2 \gg m_3$ ($\Delta m^2_{31} < 0$)

LSND Anomaly

The LSND experiment [112, 113] claims an unconfirmed 3.8σ $\bar\nu_\mu \to \bar\nu_e$ anomaly at the $\Delta m^2 \sim 1{\rm eV}^2$ scale which cannot be accommodated in an extension of the SM allowing for three neutrinos only (without adding extra sterile neutrino states). While MINIBOONE [114] measures a presently unexplained discrepancy with data lying above background at low energy, it excludes two neutrino appearance-only oscillations as an explanation for the LSND anomaly at 98% confidence level. In case the LSND and MINIBOONE anomalies are caused by new physics, some exotic explanation is needed. In the following, we will thus ignore their data.

2.6.4 Bounds on the Absolute Neutrino Mass Scale

Since neutrino oscillation experiments are only sensitive to neutrino mass squared differences but not to the absolute neutrino mass scale, they can only provide lower limits, $\sqrt{\Delta m^2_{\rm ATM}} \simeq 0.05$ eV and $\sqrt{\Delta m^2_{\rm SOL}} \simeq 0.01$, for two of the neutrino masses. In the following we will summarize bounds on the absolute neutrino mass scale gained from beta decay and neutrinoless double β decay ($0\nu2\beta$) experiments as well as from cosmological measurements.

- **β decay:**

  The neutrino mass $m_{\nu e}$ distorts the energy spectrum of electrons emitted in the β decay of a nucleus (the most sensitive choice being tritium). The analysis of the electron spectrum near the end-point thus allows a robust kinematical measurement of

  $$m^2_{\nu e} = \sum_i |U_{ei}|^2 m_i^2. \tag{2.46}$$

  The most stringent upper bound on the electron neutrino mass derived from tritium beta decay is $m_{\nu_e} < 2.0$ eV [115–117] at 95% confidence level. Assuming CPT-invariance,

[16] This possibility is excluded by the most stringent cosmological bounds on $\sum_i m_{\nu i}$ which, however, rely on possible systematics and model assumptions, cf. the discussion in Sec. 2.6.4.

combined with the observed oscillation frequencies this mass bound applies to all active neutrinos.The approved experiment KATRIN will improve the sensitivity to m_{ν_e} by one order of magnitude down to about 0.2 eV [118–120].

- **Neutrinoless Double β decay:**

  Less direct information on the absolute neutrino mass scale can be inferred from neutrinoless double β decay which is, however, only allowed if neutrinos are Majorana particles. Thus, the importance of its discovery would mainly lie in the establishment of lepton number violation as well as the Majorana nature of neutrino masses.

  The measured decay amplitude not only depends on $|m_{ee}|^2$ with,

  $$m_{ee} = \sum_i U_{ei}^2 m_i, \tag{2.47}$$

  but also on the $0\nu2\beta$ nuclear matrix elements, which are affected by sizeable theoretical uncertainties.

  Present limits on the effective electron neutrino mass are $|m_{ee}| < (0.105 - 0.840)$ eV [Heidelberg-Moscow(^{76}Ge)] [121–123], $|m_{ee}| < (0.114 - 0.912)$ eV [IGEX(^{76}Ge)] [121, 122, 124] and $|m_{ee}| < (0.168 - 1.134)$ eV [Cuoricino(^{130}Te)] [121, 125, 126].

  The controversial claim of part of the Heidelberg Moscow collaboration of a 4.2σ evidence for $0\nu2\beta$ (see [127] and Refs. therein) is still to be verified by the GERDA-experiment [128] currently under construction. If confirmed, the signal would be interpreted in terms of quasi-degenerate neutrino masses of $0.1 - 0.9$ eV ($\sum m_\nu > 1.2$ eV at 2σ).

- **Cosmology:**

  Various cosmological and astrophysical measurements are also sensitive to the absolute neutrino mass scale. More precisely, to first order, they are influenced by the sum of neutrino masses $\sum m_\nu$, which controls the present day energy fraction in neutrinos Ω_ν. Let us quote one of the current most stringent bounds,

  $$\sum_i m_\nu < 0.17\,\text{eV at } 95\% \text{ confidence level.} \tag{2.48}$$

  It was derived by combining various cosmological data sets [74] and already excludes a degenerate neutrino mass spectrum (however, the latter is still allowed by more conservative bounds which constrain the sum of neutrino masses to be smaller than about 1 eV depending on the data sets taken into account, see e.g. [6, 74, 129–136]). However, in general, one should be aware of possible systematic errors inherent in cosmological measurements and of the strong dependence on the underlying theoretical assumptions on the cosmological model. For the purposes of this work, in particular for the latter reason the bound on $\sum m_\nu$ in Eq. (2.48) has to be taken with care. It can be considerably relaxed, when non-standard neutrino interactions are taken into account, which modify both the neutrino properties and the cosmological model (see e.g. our Ref. [137] or Refs. [46, 101, 138]).

Part I

3 Probing Neutrino Dark Energy with Extremely-High Energy Cosmic Neutrinos

As argued in the introduction, relic neutrinos of the cosmic neutrinos background (CνB) are promoted to a natural Dark Energy candidate, if they interact through a new non-standard force mediated by a light scalar field of the dark sector [21, 22]. Intriguingly, as a further consequence of this new interaction, time dependent, dynamical neutrino masses are predicted to arise, providing a clear and testable signature for the Mass Varying Neutrino (MaVaN) scenario, also known as Neutrino Dark Energy [21, 22]. How could the variation of relic neutrino masses and thus the interpretation of the CνB as source of Neutrino Dark Energy be tested?

The weakness of neutrino interactions so far has spoilt all attempts to directly probe the 1.95 K cosmic neutrino background (CνB), the analog of the 2.73 K cosmic microwave background (CMB) of photons, in a laboratory setting [107, 139–142]. At present, the only evidence for its existence comes from other cosmological measurements, such as the light element abundance, large scale structure (LSS) and the CMB anisotropies, being sensitive to the presence of the CνB (see e.g. Ref. [143] for a review). However, according to Big Bang theory, in turn, the feebleness of the weak interaction has caused an early decoupling of cosmic neutrinos and thus guarantees a substantial relic abundance as we have learned in Sec. 2.5. An impressive number of 10^{87} neutrinos per flavor are predicted to permeate the visible universe, corresponding to an average number density $n_{\nu_{0,i}} = n_{\bar{\nu}_{0,i}} = 56\,\mathrm{cm}^{-3}$ per neutrino species $i = 1, 2, 3$ at present.

This turns out to open up the possibility to get a glimpse of the CνB by studying an astrophysical high energy scattering process for which the neutrinos of the CνB serve as targets. Accordingly, as we will see in the following, its characteristic fingerprints are sensitive to their masses and if detected could trace a variation of neutrino masses and thus reveal the nature of Dark Energy. In addition, the general importance of a (more) direct evidence for the existence of the CνB lies in a confirmation of standard cosmology back to the first second after the Big Bang.

Let us in the following set the stage for our later analysis which largely follows our Refs. [69,70].

While the current generation of man-made accelerators reaches center of mass energies of $O(10)$ TeV [144], these energies are easily surpassed by the cosmic laboratory from which the existence of extremely high-energy cosmic neutrinos (EHECν's) is predicted (see e.g. Refs. [145,146] for a review). Such EHECν's can annihilate with relic anti-neutrinos (and vice versa) into Z bosons, if their energies coincide with the respective resonance energies E_i^{res} of the corresponding

process $\nu\bar{\nu} \to Z$ [61–68]. These energies,

$$E_i^{\mathrm{res}} = \frac{M_Z^2}{2m_{\nu_i}} = 4.2 \times 10^{12} \left(\frac{\mathrm{eV}}{m_{\nu_i}}\right) \mathrm{GeV}, \tag{3.1}$$

in the rest system of the relic neutrinos, are entirely determined by the Z boson mass M_Z as well as the respective neutrino masses m_{ν_i}. An exceptional loss of transparency of the CνB for cosmic neutrinos results from the fact that the corresponding annihilation cross-section on resonance is enhanced by several orders of magnitude with respect to non-resonant scattering. As a consequence, the diffuse EHECν flux arriving at earth is expected to exhibit sizeable absorption dips whose locations in the spectrum are determined by the respective resonance energies of the annihilation processes. Provided that the dips can be resolved on earth, they could produce the most direct evidence for the existence of the CνB so far and possibly reveal the nature of Dark Energy.

The goal of the following Secs. 3.2.2 – 3.2.4 is to carefully work out the characteristic differences in the EHECν absorption features which result from treating the neutrino masses as time varying dynamical quantities in comparison to constants.

This section is organized as follows. In Sec. 3.1 we introduce the MaVaN scenario focusing on a viable, Supersymmetric version which we promote into a generic form and determine the resulting neutrino mass variation with time. After discussing the current status and next decade prospects for EHECν's physics, in Sec. 3.2 we provide the tools for interpreting absorption dips in the diffuse neutrino fluxes to be observed at earth extending the complete analysis to also incorporate varying neutrino masses. Furthermore, we take account of the Fermi motion arising from the thermal distribution of the relic-neutrino gas. In Sec. 3.2.2 we make contact to treatments in the literature [61, 62, 64, 66–68], by discussing common approximations [64, 66, 67] which neglect part or all of the dependence of the damping on the relic neutrino momenta. In order to gain more physical insight, the latter approximation is employed on the level of the survival probabilities of EHECν's which encode the physical information on all possible annihilation processes in Sec. 3.2.3. This allows to disentangle the characteristic features of the absorption dips caused by the neutrino mass variation. In Sec. 3.2.4, both for astrophysical sources and for a topological defect scenario, we calculate the expected observable EHECν flux arriving at earth which results from folding the survival probabilities with the corresponding EHECν source emissivity distribution and interpret our results, which are summarized in Sec. 3.3.

3.1 Neutrino Dark Energy – The Mass Varying Neutrino Scenario

In Ref. [21] a new non-Standard Model interaction between neutrinos and a light 'dark' scalar field was introduced. In essence, it serves as possible origin of the apparent accelerated expansion of the universe and promotes the CνB to a natural Dark Energy candidate. Furthermore, as a very interesting and intriguing secondary effect, it causes a time evolution of neutrino masses.

A follow-up publication [22] takes care of a possible stability problem of the model [57,59,60,71]

(cf. Sec. 4) and furnishes a viable model of the whole scenario.

Largely following Refs. [21, 22], in this section we discuss the details of the complex interplay between the scalar field and the neutrinos which arises from a coupling between them. Thereby, we will mainly focus on the determination of the resulting time variation of neutrino masses to be implemented later on in our analysis on relic neutrino absorption in Sec. 3.2. For the latter it will turn out that the results are largely independent of the details of the model, since only a few generic features of the setting enter the investigation which are determined from the effective Lagrangian in Eq. (3.6) to be discussed later on.

The new scalar-neutrino interaction has a twofold effect. On the one hand, as a direct consequence, the neutrino masses m_{ν_i} are generated from the vacuum expectation value (VEV) ϕ of the scalar field and become functions of ϕ, $m_{\nu_i}(\phi)$, $i = 1, 2, 3$. On the other hand, the dependence of m_{ν_i} on ϕ turns the neutrino energy densities ρ_{ν_i} into implicit functions of ϕ, since the energy densities $\rho_{\nu_i}\left(m_{\nu_i}(\phi)\right)$ depend on the masses $m_{\nu_i}(\phi)$, $i = 1, 2, 3$. In this way, the energy density contained in a homogeneous background of neutrinos can stabilize the scalar field by contributing to its effective potential $V(\phi)$. In other words, the dependence of the free energy on the value of ϕ gets a contribution from the rest energy in neutrinos in addition to the self-interaction scalar potential $V_\phi(\phi)$. The total energy density of the system parameterized by the effective scalar field potential $V(\phi)$ takes the following form[1],

$$V(\phi) = \sum_{i=1}^{3} \rho_{\nu_i}(m_{\nu_i}(\phi), z) + V_\phi(\phi). \tag{3.2}$$

This is to be contrasted with the situation in empty space: if $V_\phi(\phi)$ is a 'run-away potential', the scalar field does not possess a stable vacuum state but unimpededly rolls to its state of lowest energy given by the minimum of its pure potential $V_\phi(\phi)$.

Taking now the expansion of the universe into account, the dilution of the neutrino energy densities $\rho_{\nu_i}(z)$ introduces a time dependence (here parameterized in terms of the cosmic redshift z, introduced in Sec. 2.3) into the effective scalar field potential V.

Thus, importantly, due to the stabilizing effect on the scalar field achieved by the coupling to the neutrinos, to accomplish late-time acceleration, the scalar field mass does not have to be as small as the tiny Hubble scale sized mass of a quintessence field $\sim H \sim 10^{-33}$ eV [10–13]. Note that a larger scalar field mass $m_\phi^2 \gg H^2$ is more plausibly stable against radiative corrections than the Hubble scale and as it turns out later on, can be of comparable size as the energy scale associated with the Dark Energy density [21].

Accordingly, taking the curvature scale of the potential to be much larger than the expansion rate, $\partial^2 V(\phi)/\partial\phi^2 = m_\phi^2 \gg H^2$, the adiabatic solution to the equations of motion of the scalar field applies. In this case for $|\phi| < M_{\rm Pl} \simeq 3 \times 10^{18}$ GeV the effects of the kinetic energy terms can be safely ignored [21] (cf. Sec. 4.1, where the scalar field evolution is discussed in some more detail). Correspondingly, by choosing the two terms in Eq. (3.2) to compete with a minimum at an intermediate value of ϕ with non-zero value for V_ϕ, the equilibrium

[1] As discussed in the following, the contribution of the kinetic energy of the scalar field to the total energy density is negligible at late times.

value ϕ instantaneously tracks this minimum[2]. As a crucial consequence, the scalar field is slowly varying. More precisely, it cannot evolve faster than the neutrino density gets diluted. Accordingly, the characteristic time scale governing its dynamics is determined by the cosmic expansion which is naturally slow.

Finally, since the neutrino masses $m_{\nu_i}(\phi)$ are directly affected by changes in the ϕ condensate, as an intriguing consequence, they are promoted to dynamical, time dependent quantities $m_{\nu_i}(z)$.

Note that Eq. (3.2) takes the neutrino energy density ρ_{ν_i} to be spatially constant. To justify this assumption, the ϕ condensate is not allowed to vary significantly on distances of the order of the inter-neutrino spacing r of the relic neutrinos, with currently $1/r \simeq 336^{1/3}\text{cm}^{-1}$, where we have assumed a neutrino and anti-neutrino number density of $n_{\nu_{0,i}} = n_{\bar{\nu}_{0,i}} \simeq 56\,\text{cm}^{-3}$ per species $i = 1, 2, 3$. Consequently, remembering that the range of the force mediated by a scalar field is equal to its inverse mass, one arrives at an upper bound on the ϕ mass m_ϕ given by $m_\phi < 1/r \sim O(10^{-4}\,\text{eV})$ at the present time. Accordingly, this mean-field approach allows for a scalar field mass of about the same order of magnitude as the scale underlying the present Dark Energy density as mentioned above.

Let us now determine the time evolution of the physical neutrino masses $m_{\nu_i}(z)$. Since the neutrino masses arise from the instantaneous equilibrium value ϕ, we have to analyze the minimum of the total energy density $V(\phi)$. In the left panel of fig. 3.1, schematically, the time evolution of the self-interaction potential V_ϕ, the neutrino energy density ρ as well as the effective potential V and its minimum are plotted as a function of the neutrino mass m_ν. Assuming $\frac{\partial m_{\nu_i}(\phi)}{\partial \phi}$ to be non-vanishing, one arrives at,

$$\frac{\partial V(\phi)}{\partial \phi} = \sum_{i=1}^{3} \left.\frac{\partial \rho_{\nu_i}(m_{\nu_i}, z)}{\partial m_{\nu_i}}\right|_{m_{\nu_i}=m_{\nu_i}(\phi)} \frac{\partial m_{\nu_i}(\phi)}{\partial \phi} + \frac{\partial V_\phi(\phi)}{\partial \phi} = 0, \tag{3.3}$$

where according to our discussion in Sec. 2.5.1,

$$\begin{aligned} \rho_{\nu_i}(m_{\nu_i}, z) &= \frac{T_{\nu_0}^4}{\pi^2}\,(1+z)^4 \int_0^\infty \frac{dy\, y^2 \sqrt{y^2 + x_i^2}}{e^y + 1}, \qquad \text{where} \qquad y = \frac{P}{T_\nu} \\ \text{and} \quad x_i &= \frac{m_{\nu_i}}{T_{\nu_0}\,(1+z)}, \end{aligned} \tag{3.4}$$

with P being the modulus of the neutrino momentum and T_ν denoting the neutrino temperature which takes the value $T_{\nu_0} = 1.697 \times 10^{-4}$ eV today (as discussed in Sec. 2.5.1). Note that the condition for the minimal energy density leads to a dependence of the neutrino masses on the neutrino energy densities which evolve with z on cosmological time scales.

The smallness of the active neutrino masses m_{ν_i} can be explained by letting the neutrinos only indirectly feel the scalar field mediated force through the see-saw mechanism [32–35] which we discussed in Sec. 2.6.1. Therefore, following Refs. [21, 22], we introduce three 'right-

[2]Since therefore in the presence of the relic neutrinos the scalar field possesses a stable (time dependent) vacuum state, in the literature both the scalar field and its VEV are referred to as ϕ.

handed' or 'sterile' neutrino N_i fields with no Standard Model charges, whose masses M_{N_i} are constructed to vary with ϕ due to a direct interaction. In the see-saw mechanism the active neutrino masses m_{ν_i} are functions of the sterile neutrino masses $M_{N_i}(\phi)$ as we discussed in Sec 2.6.1. Consequently, the ϕ dependence of the $M_{N_i}(\phi)$ is transmitted to the active neutrino masses $m_{\nu_i}(\phi)$ and causes them to change accordingly. Let us consider the interaction [21, 22] (cf. Eq. (2.37) in Sec. 2.6.1):

$$\mathcal{L} \supset m_{D_{ij}} N_i \nu_{l_j} + \kappa_{ij} N_i N_j \phi + h.c. + V_\phi(\phi). \tag{3.5}$$

where $i, j = 1, 2, 3$ are the family-number indices and ν_{l_i} correspond to the left-handed active neutrino fields. Furthermore, $\kappa\phi$ corresponds to the ϕ dependent mass matrix of the sterile neutrinos and m_D is the Dirac type matrix originating from electroweak symmetry breaking as discussed in Sec. 2.6.1. Assuming the eigenvalues of $\kappa\phi$ to be much larger than the eigenvalues of m_D one can integrate out the sterile neutrinos N_i, arriving at the following effective low energy Lagrangian [21, 22] (cf. Eq. (2.38) in Sec. 2.6.1),

$$\mathcal{L} \supset M_{ij}(\phi)\, \nu_{l_i} \nu_{l_j} + h.c. + V_\phi(\phi), \text{ where} \tag{3.6}$$

$$M_{ij}(\phi) = \frac{(m_D^T \kappa^{-1} m_D)_{ij}}{\phi} \tag{3.7}$$

represents the mass matrix of the active neutrinos.

In order to solve Eq. (3.3) for $m_{\nu_i}(z)$ and to explore the MaVaN phenomenology, the fundamental scalar potential $V_\phi(\phi)$ has to be specified in an appropriate way. Namely, the coupled scalar neutrino fluid has to act as a form of Dark Energy which is stable against the growth of inhomogeneities [57] and, as suggested by observations, must redshift with an equation of state $\omega \sim -1$ today.

An appealing possibility arises in the framework of so-called hybrid models [147]. Those models were introduced to explain accelerated expansion in the context of inflation [76] (see also [77–79]). In essence, two scalar fields interact in such a way that one of them stabilizes the other one in a metastable minimum. The energy density stored in the potential associated with the false minimum can drive accelerated expansion.

It turns out, that a straightforward supersymmetrization [22] of the MaVaN model naturally sets the stage to apply the idea of the acceleration mechanism to Dark Energy. For the reader not familiar with Supersymmetry, let us in the following briefly summarize the very basics relevant for this work. Supersymmetric theories [148] predict a fundamental symmetry between fermions and bosons. For example, within these theories, this implies the existence of scalar *sneutrinos* of spin 0 which are the superpartners of the spin 1/2 neutrinos. Since in accelerator searches we have not observed any superpartners of the standard model fermions yet, Supersymmetry has to be broken at a scale > 1 TeV.

Identifying ϕ with the former of the two scalar fields, the hybrid model provides a microscopic origin for a quadratic self-interaction potential $V_\phi(\phi) \sim \phi^2$. The role of the residual scalar field coupled to ϕ is attributed to the scalar partner $\mathcal{N}$ of a sterile neutrino naturally present in a Supersymmetric theory. The scalar field is stabilized by the presence of the fermionic

neutrino background which drives its VEV to larger values (cf. Eq. (3.2)). Accordingly, acceleration lasts so long as the VEV of the ϕ field is sufficiently high to keep the sterile sneutrino $\mathcal{N}$ in a false metastable minimum. As long as the energy density stored in the ϕ condensate is sufficiently small, the combined scalar potential $V(\mathcal{N}, \phi)$ will appear as Dark Energy redshifting with an equation of state $\omega \sim -1$ [22]. Consequently, the neutrino Dark Energy density $\Omega_X \sim$ const. cosmologically behaves very much like a cosmological constant.

According to Ref. [22] naturalness arguments require $\mathcal{N} \equiv \mathcal{N}_1$, assigning the lightest sterile sneutrino $\mathcal{N}_1$ to be responsible for Dark Energy. Furthermore, one can conclude that $\mathcal{N}_1$ has to be at least moderately relativistic today, $m_{\nu_{0,1}} \lesssim T_{\nu_0}$. Accordingly, in this Supersymmetric MaVaN model probable instabilities [57, 59, 60] of highly non-relativistic MaVaN theories do not occur (cf. the discussion in Sec. 4).

In the past, the heavier two sterile sneutrinos $\mathcal{N}_2, \mathcal{N}_3$ of the theory were stabilized by the scalar field ϕ just as the lightest $\mathcal{N}_1$. However, by today they are assumed to have already reached their state of lowest energy having acquired vacuum expectation values.[3]

The relevant contribution [22] to the superpotential is given in terms of couplings of the superfield containing the scalar field ϕ to two superfields with generation indices i and j, with $i, j = 1, 2, 3$, which comprise the sterile neutrinos N_i,N_j and their respective scalar partners $\mathcal{N}_i$ and $\mathcal{N}_j$. The coupling constant matrix has elements κ_{ij}. This superfield interaction provides the necessary couplings mentioned above, namely of the scalar field to the sterile sneutrino fields as well as the coupling of scalar field to the sterile neutrinos in terms of κ_{ij}. In Ref. [22] the one loop radiative corrections were estimated and taken to give a lower bound on the natural size for the magnitudes of the soft susy breaking masses squared of the ϕ and the $\mathcal{N}_i$.

Given the exploratory nature of this investigation and following largely Ref. [22] it is reasonable to exploit the rough proportionality $\delta m^2_{\mathcal{N}_i} \sim -m^2_{D_i}$ to get an estimate of the ϕ mass squared m^2_ϕ; here $\delta m^2_{\mathcal{N}_i}$ represent the one loop radiative corrections to the mass of a sterile sneutrino $\mathcal{N}_i$ and m_{D_i} label the respective eigenvalues of the Dirac type matrix m_D. For simplicity, we assume no off-diagonal elements for the coupling constant matrix κ and denote the diagonal matrix elements by κ_i. Finally, one arrives at an estimate for the square of the scalar field mass m^2_ϕ [22],

$$m^2_\phi \sim \sum_{i=1}^{3} \kappa_i^2 m^2_{\mathrm{D_i}}, \tag{3.8}$$

such that the quadratic self-interaction potential can be expressed in terms of neutrino mass parameters according to

$$V_\phi(\phi) \sim m^2_\phi \phi^2 = \sum_{i=1}^{3} \kappa_i^2 m^2_{D_i} \phi^2. \tag{3.9}$$

Now we are in a position to determine the respective mass-redshift relations $m_{\nu_i}(z)$ of the active MaVaNs whose mass squared differences today have to be compatible with neutrino oscillation experiments. Taking the matrix κ as well as the Dirac type mass matrix m_D in

[3] We refer to the mechanism proposed in [22] to evade large $\mathcal{N}_{2,3}$ VEV contributions to the ϕ mass conflicting with the upper mass bound set by the current inter-neutrino spacing $O(10^{-4})$ eV.

Eq. (3.7) to be diagonal, one arrives at the approximate see-saw formula for the physical neutrino masses:

$$m_{\nu_i}(\phi) = \frac{m_{D_i}^2}{\kappa_i \phi}, \text{ where } i = 1, 2, 3. \tag{3.10}$$

Accordingly, the instantaneous minimum of V in Eq. (3.3) is determined by

$$\frac{\partial V(\phi)}{\partial \phi} = \sum_{i=1}^{3} \frac{\partial \rho_{\nu_i}(m_{\nu_i}, z)}{\partial m_{\nu_i}}\bigg|_{m_{\nu_i}=\frac{m_{D_i}^2}{\kappa_i \phi}} \left(\frac{-m_{D_i}^2}{\kappa_i \phi^2}\right) + 2\sum_{i=1}^{3} \kappa_i^2 m_{D_i}^2 \phi = 0. \tag{3.11}$$

Since this equation has to hold for all z, the scalar field VEV becomes a function of z. As a direct consequence, it generates redshift dependent neutrino masses $m_{\nu_i}(z)$,

$$m_{\nu_i}(z) = \frac{m_{D_i}^2}{\kappa_i \phi(z)} \text{ with } m_{\nu_i}(0) = m_{\nu_{i_0}} = \frac{m_{D_i}^2}{\kappa_i \phi(0)}, \tag{3.12}$$

which implies

$$m_{\nu_i}(z) = m_{\nu_{0,i}} \frac{\phi(0)}{\phi(z)}. \tag{3.13}$$

Note that in general a MaVaN mass with subscript 0 has to be identified with the present day neutrino mass. Consequently, the $m_{\nu_{0,i}}$ have to be consistent with the mass squared differences measured in neutrino oscillation experiments which we discussed in Sec. 2.6.3.

Accordingly, inserting Eq. (3.13) and Eq. (3.9) into Eq. (3.3) yields,

$$\sum_{i=1}^{3} m_{\nu_{0,i}} \frac{\partial \rho_{\nu_i}(m_{\nu_i}, z)}{\partial m_{\nu_i}}\bigg|_{m_{\nu_i}=m_{\nu_{0,i}}\frac{\phi(0)}{\phi(z)}} - \left(\frac{\phi(z)}{\phi(0)}\right)^3 2\sum_{i=1}^{3} \frac{m_{D_i}^6}{m_{\nu_{0,i}}^2} = 0. \tag{3.14}$$

Evaluating Eq. (3.14) at $z = 0$,

$$2\sum_{i=1}^{3} \frac{m_{D_i}^6}{m_{\nu_{0,i}}^2} = \sum_{i=1}^{3} m_{\nu_{0,i}} \frac{\partial \rho_{\nu_i}(m_\nu 0, i)}{\partial m_{\nu_i}}\bigg|_{m_{\nu_i}=m_{\nu_{0,i}}}, \tag{3.15}$$

allows to eliminate $2\sum_{i=1}^{3} \frac{m_{D_i}^6}{m_{\nu_{0,i}}^2}$ from Eq. (3.14) leading to

$$\sum_{i=1}^{3} m_{\nu_{0,i}} \left(\frac{\partial \rho_{\nu_i}(m_{\nu_i}, z)}{\partial m_{\nu_i}}\bigg|_{m_{\nu_i}=m_{\nu_{0,i}}\frac{\phi(0)}{\phi(z)}} - \left(\frac{\phi(z)}{\phi(0)}\right)^3 \frac{\partial \rho_{\nu_i}(m_{\nu_i}, 0)}{\partial m_{\nu_i}}\bigg|_{m_{\nu_i}=m_{\nu_{0,i}}} \right) = 0. \tag{3.16}$$

Finally, the solution for $\left(\frac{\phi(z)}{\phi(0)}\right)^3$, which can only be determined numerically, fixes the neutrino mass evolution according to Eq. (3.13) in terms of the present day neutrino masses $m_{\nu_{0,i}}$.

However, the mass behavior in the low as well as in the high redshift regime can be approximated analytically by using the respective limits for $\frac{\partial \rho_{\nu_i}}{\partial m_{\nu_i}}$. As mentioned before, in the

Supersymmetric MaVaN model [22] the lightest neutrino is at least moderately relativistic today such that its mass is required to be small, $m_{\nu_{0,1}} \lesssim T_{\nu_0} = 1.697 \times 10^{-4}$ eV. Furthermore, it can be deduced from the mass squared differences measured at neutrino oscillation experiments (see [36] for a recent review) that the heavier two neutrinos are non-relativistic today ($m_{\nu_{0,i}} \gg T_{\nu_0}$ for $i = 2, 3$).

Accordingly, in the low redshift regime it is a good approximation to neglect the contribution of the lightest neutrino species to V and solely employ the non-relativistic limit of $\frac{\partial \rho_{\nu_i}}{\partial m_{\nu_i}}$ with $i = 2, 3$ and $x_i = \frac{m_{\nu_i}}{T_{\nu_0}(1+z)} \gg 1$,

$$\frac{\partial \rho_{\nu_i}(m_{\nu_i}, z)}{\partial m_{\nu_i}} \approx \frac{T_{\nu_0}^3}{\pi^2}(1+z)^3 \int_0^\infty \frac{y^2}{e^y + 1} dy. \tag{3.17}$$

where Eq. (3.4) has been used. Accordingly, in the low redshift regime Eq. (3.16) is solved by

$$\begin{aligned} \phi_{\text{low}}(z) &= \phi(0)\,(1+z) && (3.18)\\ \rightarrow m_{\nu_{i,\text{low}}}(z) &= m_{\nu_{0,i}}(1+z)^{-1},\ \text{i=1,2,3}, && (3.19) \end{aligned}$$

where Eq. (3.13) was used.

Once in the past all neutrinos were relativistic. In this regime, $x_i \ll 1$, such that according to Eq. (3.4) $\frac{\partial \rho_{\nu_i}}{\partial m_{\nu_i}}$ can be approximated by,

$$\frac{\partial \rho_{\nu_i}(m_{\nu_i}, z)}{\partial m_{\nu_i}} \approx \frac{T_{\nu_0}^2}{\pi^2}(1+z)^2 m_{\nu_i} \int_0^\infty \frac{y}{e^y + 1} dy. \tag{3.20}$$

By taking the appropriate approximations Eq. (3.17) and Eq. (3.20) for the two terms in Eq. (3.16), V is minimized for,

$$\begin{aligned} \phi_{\text{high}}(z) &\propto (1+z)^{1/2} && (3.21)\\ \rightarrow m_{\nu_{i,\text{high}}}(z) &\propto (1+z)^{-1/2},\ \text{i=1,2,3}, && (3.22) \end{aligned}$$

where the factor of proportionality is a function of the present day neutrino masses and the integrals in Eq. (3.17) and Eq. (3.20).

In our analysis on cosmic neutrino absorption later on, these approximations will help towards a better understanding of the numerical calculations since the corresponding results agree very well in the respective regimes.

As becomes apparent from the approximations in Eq. (3.19) and Eq. (3.22) the MaVaN masses $m_{\nu_i}(z)$ are decreasing functions of redshift. Correspondingly, in the standard scenario [21, 22, 57, 59, 104], MaVaNs can be regarded as practically massless in the past whereas in the present epoch they have reached their maximal mass values $m_{\nu_{0,i}}$. In the following we will assume a normal neutrino mass hierarchy and take the mass of the lightest neutrino to be

$$m_{\nu_{0,1}} = 10^{-5}\,\text{eV}, \tag{3.23}$$

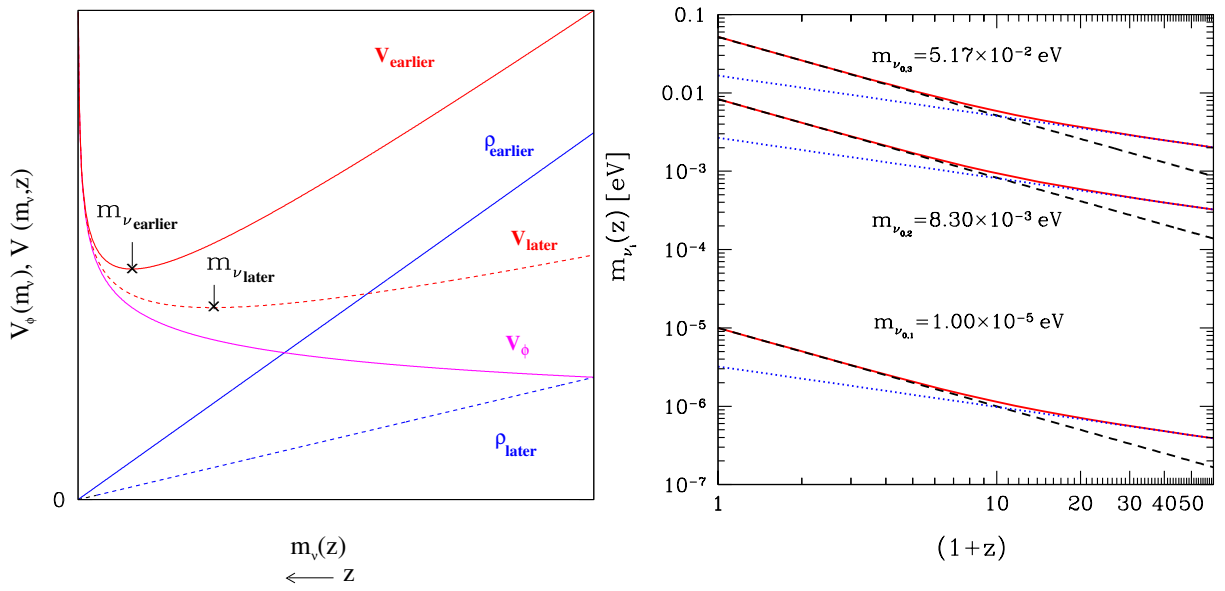

Figure 3.1: *Left:* Schematic time evolution of the effective potential $V(m_\nu, z)$ and the neutrino mass $m_\nu(z)$ due to changes in the neutrino energy density $\rho_\nu(z)$. *Right:* In this log-log plot the exact mass-redshift relations $m_{\nu_i}(z)$ are plotted as solid lines. In the low as well as in the high redshift regime they are well approximated by simple power laws, $m_{\nu_i}(z) \propto (1+z)^{-1}$ and $m_{\nu_i}(z) \propto (1+z)^{-1/2}$, respectively (dashed and dotted lines). The lightest MaVaN is assumed to have a mass of $m_{\nu_{0,1}} = 10^{-5}\,\mathrm{eV}$ today. Consequently, for a normal neutrino mass hierarchy, solar and atmospheric mass splittings fix the present time neutrino masses of the heavier neutrinos to be $m_{\nu_{0,2}} = 8.3 \times 10^{-3}\,\mathrm{eV}$ and $m_{\nu_{0,3}} = 5.17 \times 10^{-2}\,\mathrm{eV}$.

such that it is still relativistic today (i.e. $m_{\nu_{0,1}} \leq T_{\nu_0}$). According to the solar and atmospheric neutrino mass splittings the corresponding present time masses of the heavier non-relativistic neutrinos are fixed to be (according to the mass splittings stated in Sec. 2.6.3),

$$m_{\nu_{0,2}} = 8.30 \times 10^{-3}\,\mathrm{eV} \gg T_{\nu_0}, \tag{3.24}$$

$$m_{\nu_{0,3}} = 5.17 \times 10^{-2}\,\mathrm{eV} \gg T_{\nu_0}. \tag{3.25}$$

Figure 3.1 shows that the exact mass-redshift relations $m_{\nu_i}(z)$, $i = 1, 2, 3$, as numerically determined from Eq. (3.16) in combination with Eq. (3.13), are very well approximated in the low as well as in the high redshift regime by simple power laws stated in Eq. (3.19) and in Eq. (3.22), respectively. These results have to be contrasted with the standard time-independent neutrino masses $m_{\nu_{0,i}}$ for $i = 1, 2, 3$. Let us summarize the essential features of the presented viable MaVaN model which will enter the analysis on relic neutrino absorption later on. Firstly, the lightest neutrino is required to be still moderately relativistic today ($m_{\nu_{0,1}} \leq T_{\nu_0} = 1.697 \times 10^{-4}\,\mathrm{eV}$) and therefore fixes the neutrino mass scale to be low. Secondly, the specific mass-redshift evolution $m_{\nu_i}(z)$ is determined by the model dependent quadratic form of the potential $V_\phi \sim \phi^2$ in Eq. (3.9) which enters Eq. (3.15). In this case, we found the masses to behave like $\propto (1+z)^{-1}$ and $\propto (1+z)^{-1/2}$ in the low and in the high redshift regime, respectively (cf. Eq. (3.19) and Eq. (3.22)). However, the generically important feature (of any standard MaVaN model) is that the MaVaN masses $m_{\nu_i}(z)$ are decreasing functions of

redshift which is easily achieved within the framework of the see-saw mechanism (see above). As will turn out in our investigation later on, for decreasing $m_{\nu_i}(z)$ the results do not strongly dependent on the actual functional dependence $m_{\nu_i}(z)$. Furthermore, since the considered mass scale essentially corresponds to the minimal neutrino mass hierarchy[4], our results for the discovery potential of Neutrino Dark Energy will be independent of the actual neutrino mass scale realized in nature. Note also that the characteristic differences in the absorption features of MaVaNs with respect to constant mass neutrinos (cf. Sec.3.2.3 and Sec.3.2.4) are independent of the supersymmetrization of the MaVaN scenario.

3.2 Signatures of Ultra-Energetic Mass Varying Neutrinos in the Sky?

3.2.1 Extremely High-Energy Cosmic Neutrinos

Before we discuss in detail in the following sections the diagnostic potential of extremely high-energy cosmic neutrinos (EHECν's) by means of relic neutrino absorption spectroscopy, let us in this section comment on the current status and next generation prospects for EHECν physics and let us add some general remarks on EHECν's.

As a start, the existence of EHECν's is theoretically well motivated and is substantiated by numerous works on possible EHECν sources of astrophysical nature (bottom-up) (see e.g. [145] for a review) or so-called top-down sources (see e.g. Ref. [146] for a review). In the latter case, EHECν's with energies well above 10^{11} GeV are assumed to be produced in the decomposition of topological defects (TD's) which originate from symmetry breaking phase transitions in the very early universe. In Sec. 3.2.4 we will discuss these plausible sources in some more detail.

As demonstrated by Fig. 3.2, we are actually living in exciting times for EHECν's. Depending on the underlying EHECν sources, the EHECν fluxes could be close to the current observational bounds set by existing EHECν observatories such as AMANDA [149] (see also Ref. [150, 151]), ANITA-lite [152], BAIKAL [165], FORTE [153], GLUE [154] and RICE [155] which cover an energy range of 10^7 GeV $< E_0 < 10^{17}$ GeV (cf. Fig. 3.2). Promisingly, the sensitivity in this energy range will be improved by orders of magnitude (cf. Fig. 3.2) by larger EHECν detectors such as ANITA, EUSO [156], IceCube [157], LOFAR [158], OWL [159], SalSA [161] and WRST [158] which are planned to start operating within the next decade (cf. Fig. 3.2). Accordingly, the prospects of confirming the existence of the CνB by tracking its interaction with EHECν's have substantially improved since the original proposal in 1982 [61]. Moreover, in the likely case of appreciable event samples the valuable information encoded in the absorption features of the EHECν spectra could be revealed within the next decade (cf. Fig. 3.2), rendering the theoretical exploration of relic neutrino absorption spectroscopy a timely enterprise.

Note that the scenario introduced in the beginning of Sec. 3 has also attracted attention for another reason than the possible detection of the CνB– namely for the controversial possibility

[4] In principle, in the minimally allowed neutrino mass scheme, according to oscillation experiments the lightest neutrino could be massless, while in this case the masses of the heavier neutrinos, compared to the values employed in this analysis, would hardly be smaller. Since it turns out that due to thermal wash out only the heavier neutrinos produce characteristic signatures, our analysis is representative for the testability of the MaVaN scenario.

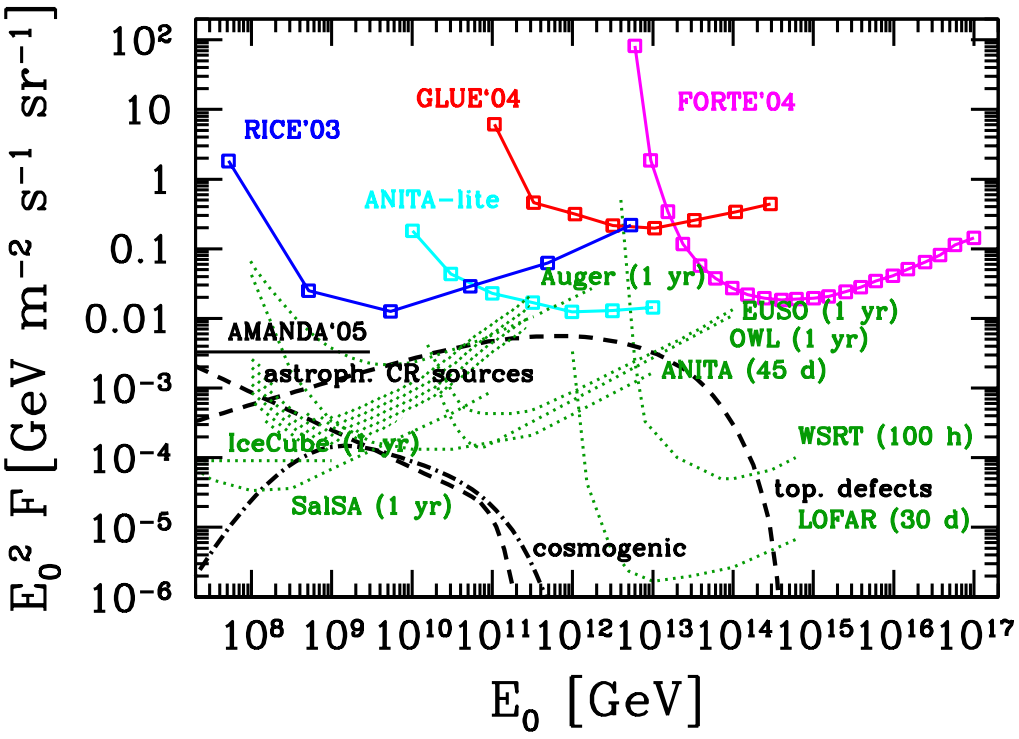

Figure 3.2: Current status and next decade prospects for EHECν physics, expressed in terms of diffuse neutrino fluxes per flavor, $F = F_{\nu_\alpha} + F_{\bar{\nu}_\alpha}$, $\alpha = e, \mu, \tau$. The upper limits from AMANDA [149], see also Ref. [150, 151], ANITA-lite [152], FORTE [153], GLUE [154], and RICE [155] are plotted. Also shown are projected sensitivities of ANITA [152], EUSO [156], IceCube [157], LOFAR [158], OWL [159], the Pierre Auger Observatory in ν_e, ν_μ modes and in ν_τ mode (bottom swath) [160], SalSA [161], and WSRT [158], corresponding to one event per energy decade and indicated duration. Also shown are predictions from astrophysical Cosmic Ray (CR) sources [162], from inelastic interactions of CR's with the cosmic microwave background (CMB) photons (cosmogenic neutrinos) [162, 163], and from topological defects [164].

of solving the so-called GZK-puzzle to be discussed briefly in the following. Beyond the Greisen-Zatsepin-Kuzmin (GZK) energy, $E_{\rm GZK} = 4 \times 10^{10}$ GeV, ultra-high energy nucleons rapidly lose energy due to the effective interaction with CMB photons (predominantly through resonant photo-pion production) [166, 167]. In the so-called Z-burst scenario, the observed mysterious cosmic rays above $E_{\rm GZK}$ were associated with the secondary cosmic ray particles produced in the decays of Z bosons. The latter were assumed to originate from the neutrino annihilation process outlined above [168–173].

However, recently, ANITA-lite [152] appears to have entirely excluded the Z-burst explanation for the GZK-puzzle at a level required to account for the observed fluxes of the highest energy cosmic rays. Moreover, recent data by the Pierre Auger Collaboration indicates that there is no GZK-puzzle after all [174]. However, in any case, this neither restricts the possible success of producing evidence for the CνB by means of detecting absorption dips in the EHECν

spectra nor does it spoil the possibility of gaining valuable information from performing relic neutrino absorption spectroscopy.

In the next section we will discuss in detail the propagation of EHECν's through the thermal bath of relic neutrinos and the resulting damping of EHECν's which governs their survival probability on their way from their source to us. We will incorporate the full thermal background effects on the absorption process whose impact grows for smaller neutrino masses [67, 68]. This means, in general relic neutrinos have to be treated as moving targets with a momentum distribution, if their mean momenta turn out to be of the order of the relic neutrino masses.

3.2.2 The Damping Factor

Due to the feebleness of the weak interaction cosmic neutrinos can propagate cosmological distances through the cosmic microwave and neutrino background (CMB and CνB) without a significant probability of interacting.

As outlined in the beginning of Sec. 3, an interesting exception arises under the assumption that EHECν's with energies of order $E_i^{\rm res} = M_Z^2/2m_{\nu_i} = 4.2 \times 10^{14}\,{\rm GeV}\,(0.01{\rm eV}/m_{\nu_i})$ in the rest system of the target $\bar{\nu}$ exist, where M_Z is the Z mass and m_{ν_i} the respective neutrino mass. The Z resonance in the s channel for the process $\nu\bar{\nu} \to X$, characterized by the energy $E_i^{\rm res}$, enhances the cross-section for the annihilation of such an EHECν on a big-bang relic anti-neutrino (and vice versa) by orders of magnitude. As a consequence, the corresponding interaction probability significantly increases with respect to non-resonant scattering. Accordingly, the annihilation processes would reduce the survival probability of EHECν's traveling through the CνB to us and could therefore be detectable as sizeable absorption dips in the EHECν spectra.

In this section we consider EHECν's (on whose plausible sources we will comment in Sec. 3.2.4) propagating through a thermal bath of relic neutrinos in the expanding universe. Following Ref. [68], we discuss the corresponding damping rate of the EHECν's which governs their survival probability (cf. Sec. 3.2.3). Furthermore, we will summarize common approximations for the damping which result from averaging over the neutrino momenta [67] or from completely neglecting the relic neutrino motion [61, 62, 64, 66].

The investigation applies to both constant mass neutrinos as well as to MaVaNs. In the latter case, the neutrino masses m_{ν_i} are not constant but – as discussed in Sec. 3.1 – complicated functions of the neutrino densities and thus functions of z (cf. Eq. (3.16) in combination with Eq. (3.13) in Sec. 3.1).

For simplicity, throughout this section we drop the indices $i = 1, 2, 3$ labeling the mass, energy or momentum of the neutrino mass eigenstates, since the discussion applies to all three neutrinos likewise (m_ν corresponds to m_{ν_i}, E to E_i etc.).

The crucial quantity which describes the attenuation of an ultra-relativistic EHECν neutrino

traversing the CνB is the damping rate $\gamma_{\nu\bar{\nu}}$. It can be expressed in the following form,[5]

$$\gamma_{\nu\bar{\nu}}(E) = \int_0^\infty \frac{dP}{2\pi^2}\ P^2\ f_{\bar{\nu}}(P, T_\nu)\ \sigma_{\nu\bar{\nu}}(P, E), \tag{3.26}$$

and is governed by the Z-formation cross-section $\sigma_{\nu\bar{\nu}}(P, E)$ weighted by the momentum distribution $f_{\bar{\nu}}(P, T_\nu)$ of the relic anti-neutrinos, both to be discussed in the following. Here, P denotes the modulus of the relic anti-neutrino momentum, whereas E represents the EHECν energy and T_ν is the CνB temperature. Note that in the expanding universe these quantities are subject to cosmic redshift. They can be expressed in terms of their present day values, labeled by a subscript 0, in the following way,

$$P = P_0(1+z),\ E = E_0(1+z),\ T_\nu = T_{\nu_0}(1+z), \tag{3.27}$$

where the second equality assumes $E \simeq \sqrt{E^2 - m_\nu^2}$ for an ultra-relativistic EHECν. Furthermore, throughout this paper we take the CνB temperature at present to be $T_{\nu_0} = 1.697 \times 10^{-4}$ eV as discussed in Sec. 2.5.1.

Let us first recall from Sec. 2.5, that according to Big Bang theory, ever since neutrino decoupling the momentum distribution of the relic neutrinos is frozen into a freely expanding, ultra-relativistic Fermi Dirac form [101].

In order to express the cross-section $\sigma_{\nu\bar{\nu}}(P, E)$ of the $\nu\bar{\nu}$ annihilation process it is convenient to introduce the parameter $\xi = \Gamma_Z^2/M_Z^2 \ll 1$. It describes the square of the quotient of the total width for Z decaying to fermion pairs, $\Gamma_Z = 2.4952$ GeV [175], and the mass of the Z, $M_Z = 91.1876$ GeV [175]. Accordingly, $\sigma_{\nu\bar{\nu}}(P, E)$ can be written in the following form [68],

$$\sigma_{\nu\bar{\nu}}(P, E) = \frac{G_F}{\sqrt{2}} \frac{\Gamma_Z M_Z}{2E^2} \frac{1}{P E_P} \int_{s_-}^{s_+} ds\ \frac{s(s - 2m_\nu^2)}{(s - M_Z^2)^2 + \xi s^2}, \tag{3.28}$$

where $G_F = 1.166\,37 \times 10^{-5}\,\mathrm{GeV}^{-2}$ is the Fermi coupling constant and $E_p = \sqrt{P^2 + m_\nu^2}$ is the energy of the relic neutrino. Furthermore, s is the square of the center-of-mass energy of the neutrino-anti-neutrino system. Using $\sqrt{E^2 + m_\nu^2} \simeq E$ for an ultra-relativistic EHECν one arrives at the following expression for s,

$$s = 2m_\nu^2 + 2E(E_p - P\cos\theta), \tag{3.29}$$

where θ characterizes the direction of the relic anti-neutrino with respect to the line of flight of the incident EHECν in the center-of-mass system. Accordingly, for fixed P and E the integration over s corresponds to the angular integration. As a consequence, the limits of the integral in Eq. (3.28) take the values,

$$s_\pm = 2m_\nu^2 + 2E(E_p \pm P), \tag{3.30}$$

corresponding to $\cos\theta = \mp 1$.

[5] The formula for the cross-section as well as the damping rate in Eq. (3.26) apply likewise if both of the interacting particles are replaced by their anti-particles.

Note that, following Ref. [68], in Eq. (3.28) the energy dependence of the Z boson width $\Gamma(s)$ in the Z propagator due to higher order corrections [176, 177] has been taken into account. In the region of the resonance where the s dependence is crucial, $\Gamma(s)$ can well be approximated by the linear relation [176, 177]

$$\Gamma(s) = \frac{\Gamma_Z}{M_Z^2} s = \sqrt{\xi}\frac{s}{M_Z}, \text{ where } \Gamma_Z = \text{const.}. \tag{3.31}$$

The integral in Eq. (3.28) for the cross-section can be solved analytically. Since the MaVaN mass $m_\nu(z)$ is a decreasing function of redshift, it has its maximal value today which corresponds to the mass of a constant mass neutrino. Accordingly, for both constant mass neutrinos and MaVaNs one can exploit that $m_\nu \ll M_z, E$ for all redshifts such that one finally gets the following expression for the cross-section [68][6]

$$\begin{aligned}
\sigma_{\nu\bar{\nu}}(P,E) &= \frac{2\sqrt{2}G_F\Gamma_Z M_Z}{2EE_p}\left\{\frac{1}{1+\xi}\right. \\
&+ \frac{M_Z^2}{4EP(1+\xi)^2}\ln\left(\frac{(1+\xi)4E^2(E_p+P)^2 - 4M_Z^2E(E_p+P)+M_Z^4}{(1+\xi)4E^2(E_p-P)^2 - 4M_Z^2E(E_p-P)+M_Z^4}\right) \\
&+ \frac{1-\xi}{(1+\xi)^2}\frac{M_Z^3}{4EP\Gamma_Z}\left[\arctan\left(\frac{2E(1+\xi)(E_p+P)-M_Z^2}{\Gamma_Z M_Z}\right)\right. \\
&\left.\left. - \arctan\left(\frac{2E(1+\xi)(E_p-P)-M_Z^2}{\Gamma_Z M_Z}\right)\right]\right\}.
\end{aligned} \tag{3.32}$$

The calculation of the damping defined by Eq. (3.26) in combination with Eq. (3.32) includes the full thermal background effects. To allow for a comparison of our findings to published results, in the following, we will summarize two common approximations used in the literature. They result from averaging over the neutrino momenta [67] or from completely neglecting the relic neutrino motion [61, 62, 64, 66]. As will become apparent in the next section, in the neutrino mass range favored by the supersymmetric MaVaN model (cf. Sec. 3.1) their applicability is quite limited. However, the assumption of relic neutrinos at rest will later on remove the thermal distortion of the absorption dips and thus allow a deeper insight into the characteristic features caused by the mass variation $m_{\nu_i}(z)$ described in Sec. 3.1.

The weaker approximation for $\sigma_{\nu\bar{\nu}}(P,E)$ commonly used in the literature is obtained by approximating the mean value theorem. The factor $(s-2m_\nu^2)$ in the integrand of Eq. (3.28) takes the role of the weight function and is integrated over, whereas the residual part of the integrand is – as an approximation – evaluated at the midpoint of the integration interval

[6] The neglect of the neutrino mass in Eq. (3.32) leads to a spurious singularity in the integrand of Eq. (3.26) in a region of the relic neutrino momenta where the integral is supposed to be negligible. This can be cured by an appropriate limitation of the integration interval.

$\bar{s} \simeq 2EE_p = 2E\sqrt{P^2 + m_\nu^2}$. Accordingly, the cross-section takes the following form

$$\bar{\sigma}_{\nu\bar{\nu}}(E, P) = \bar{\sigma}_{\nu\bar{\nu}}(\bar{s}) = 2\sqrt{2}G_F\Gamma_Z M_Z \ \frac{\bar{s}}{(\bar{s} - M_Z^2)^2 + \xi\bar{s}^2}, \tag{3.33}$$

with $\xi = \Gamma_Z^2/M_Z^2$. Let us point out again that due to higher order corrections a precise handling of the Z propagator near the resonance [176, 177] leads to an energy dependence of the Z boson width $\Gamma(\bar{s})$ (cf. Eq. (3.31)). Note that in earlier work on neutrino-absorption (e.g. [61, 62, 64, 66]) this correction has not been made but the lowest order (simple Breit-Wigner) form for the cross-section $\bar{\sigma}_{\nu\bar{\nu}}(E, P)$ has been used. We would like to stress that by the averaging procedure, which leads to the approximation for $\sigma_{\nu\bar{\nu}}$ in Eq. (3.33), part of the angular information gets lost. This results in an underestimation of the thermal spread of the absorption dips [68].

Let us now come to the second, more radical approximation: In earlier work on cosmic neutrino absorption (e.g. [64, 66]) it was assumed that the relic neutrinos are at rest [64, 66], thereby switching off all thermal background effects. The corresponding cross-section can be recovered from the full expression in Eq. (3.28) by taking the limit $P \to 0$ or from Eq. (3.33) by setting $P = 0$ such that $\bar{s} = s_0 = 2Em_\nu$. In this case, the remaining integral over P in Eq. (3.26) reduces to the neutrino number density $n_\nu(z) = n_{\bar{\nu}}(z) = n_{\nu 0}(1+z)^3$. Accordingly, the damping $\gamma_{\nu\bar{\nu}}$ takes the following form

$$\gamma^0_{\nu\bar{\nu}}(E) = \bar{\sigma}_{\nu\bar{\nu}}(s_0)\ n_\nu(z) = 2\sqrt{2}G_F\Gamma_Z M_Z \ \frac{2Em_\nu}{4(1+\xi)E^2m_\nu^2 - 4M_Z^2Em_\nu + M_Z^4}\ n_\nu. \tag{3.34}$$

As will become apparent in the next section, by assuming the neutrinos to be at rest one neglects two conspiring effects on the damping which become more important with decreasing ratio m_ν/T_ν [68]:

On the one hand, the full cross-section $\sigma_{\nu\bar{\nu}}(P, E)$ in Eq. (3.32), which governs the damping, depends on $E_p = \sqrt{P^2 + m_\nu^2}$. As a consequence, the peak of the cross-section for a thermal bath of relic anti-neutrinos at $E_i^{\rm res}$ [67],

$$E_i^{\rm res} = \frac{M_Z^2}{2(\sqrt{P_i^2 + m_{\nu_i}^2} - P_i\cos\theta)}, \tag{3.35}$$

actually lies at lower energies than the one of $\bar{\sigma}_{\nu\bar{\nu}}(s_0)$ for relic anti-neutrinos at rest: the energy $E_{0,i}$ reduces to

$$E_i^{\rm res} = \frac{M_Z^2}{2m_{\nu_i}}. \tag{3.36}$$

Note that in the case of MaVaNs the masses m_{ν_i} are functions of redshift, $m_{\nu_i}(z)$, and therefore introduce a z dependence into the resonance energies. Thus, they only coincide with the respective constant mass ones for $z = 0$ and $m_\nu(0) = m_{\nu 0}$. We will discuss the consequences for the absorption features in detail in the next section.

As indicated by Eq. (3.35), the effect of the relic neutrino momenta P becomes significant for small neutrino masses, according to Ref. [68] for $m_\nu \leq 0.01$ eV. Furthermore, $\bar{\sigma}_{\nu\bar{\nu}}(s_0)$

overestimates the peak height of the full expression and cannot account for the broadening of $\sigma_{\nu\bar{\nu}}(P, E)$ for increasing relic neutrino momentum P.

On the other hand, the thermal distribution of the relic neutrinos which gives rise to a Fermi momentum smearing of the cross-section is totally neglected. In the full expression the damping $\gamma_{\nu\bar{\nu}}$ results from the integration over all neutrino momenta, where the weight factor $P^2 f_{\bar{\nu}}(P, T_\nu)$ selects relic neutrino momenta P of the order of T_ν. Accordingly, Eq. (3.34) overestimates the damping efficiency with respect to the full expression defined by Eq. (3.32) and Eq. (3.26). As we will see in the next section the realistic description of neutrino-absorption leads to less well defined absorption features spread over a larger range of EHECν energies than in the idealized scenario which neglects any thermal effects. These discrepancies increase with decreasing neutrino mass.

3.2.3 The Survival Probability

The relevant quantity to be discussed in this section is the survival probability P_{ν_α} of extremely high-energy cosmic neutrinos ν_α of flavor $\alpha = e, \mu, \tau$ traveling through the CνB to us. It is governed by the damping rate $\gamma_{\nu\bar{\nu}}$ introduced in the last section and it determines, folded with the respective EHECν source emissivity distribution $\mathcal{L}_{\nu_i}$, the resulting neutrino spectra to be observed on earth, which are treated in Sec. 3.2.4.

The main goal of this section is to work out the characteristic differences in the shape of the absorption dips in the EHECν survival probabilities which arise from considering the neutrino masses to be dynamical quantities $m_{\nu_i}(z)$ instead of constant parameters. After presenting our results and pointing out the generic differences, we will have a closer look at the MaVaN absorption features. As motivated in the last section, for the purpose of gaining more physical insight, we will disentangle the different influences which define their shape. First of all, we will study the impact of the mass variation $m_{\nu_i}(z)$ as well as of the cosmic redshift caused by the expansion of the universe. To this end, we will initially switch off any thermal background effects by assuming the relic neutrinos to be at rest and compare the results for MaVaNs to those of constant mass neutrinos.

Nonetheless, we would like to stress again that due to the low neutrino mass scale required in the MaVaN model under consideration (cf. Sec. 3.1) only the full treatment of the background effects can serve as a test for Neutrino Dark Energy.

In our calculation we make the standard simplifying assumption that the EHECν source switched on at a distinct redshift z_s in the past. As concerns plausible EHECν sources, in the following we would like to mention the most relevant classes as well as the corresponding typical EHECν emission redshifts z_s.

As a first possibility, EHECν are assumed to originate from pion decays, where the latter either are produced in inelastic pp or $p\gamma$ interactions. Those astrophysical acceleration sites (bottom-up mechanism), notably active galactic nuclei (AGN) and gamma-ray bursts, have source positions z_s of a few (e.g. [145, 178]). The conjectured energies of cosmic neutrinos produced by these astrophysical acceleration sites in the case of shock acceleration are $E_{\max} \lesssim 10^{11} - 10^{12}$ GeV [145,178]. However, even higher energies are possible in proposed non-shock acceleration

mechanisms, such as unipolar induction, acceleration in strong magnetic waves in plasma (wakefields) [179], or by magnetic recombination in the vicinity of massive black holes [180,181] (see [178] for a recent review).

As a second possibility, extremely energetic cosmic neutrinos with energies above 10^{12} GeV may be generated in the decomposition of so-called topological defects (top-down scenarios) into their constituent particles. Topological defects are predicted to originate from symmetry breaking phase transitions immediately after (hybrid) inflation (see [182] for a recent review). In particular, cosmic string formation is highly generic in Supersymmetric Grand Unified Theories (SUSY GUTs) (see [183] and references therein). Those topological defects produce super-heavy quanta generically denoted as X particles (often heavy Higgs or gauge bosons) with masses $m_X \sim 10^{12} - 10^{16}$ GeV. Those X particles rapidly decay into stable Standard Model (SM) particles, also releasing extremely energetic neutrinos [146, 184] with energies up to $\sim 0.5\, m_X$ [185]. For those exotic, non-accelerator sources, z_s can be as high as the epoch of light neutrino decoupling, $z_s \sim \mathcal{O}(10^{10})$ [63].

In our analysis we take resonant Z-production caused by the interaction with the CνB as the only source of attenuation of the propagating EHECν. This approximation is well justified in the energy regions of the absorption dips which we are focusing on in our investigation [66]. Accordingly, the survival probability of an extremely high-energy cosmic neutrino ν_i with $i = 1, 2, 3$ injected at redshift z_s is given by,

$$P_{\nu_i}(E_0, z_s) = \exp\left[-\int_0^{z_s} \frac{dz}{H(z)(1+z)} \gamma_{\nu\bar{\nu}}\big(E_0(1+z)\big)\right],\ i = 1, 2, 3, \tag{3.37}$$

where the integral in the exponential, which governs the survival probability, is called the optical depth (or the opacity). It contains the product of the propagation distance $dr = dz/[(1+z)H(z)]$ and the damping rate $\gamma_{\nu\bar{\nu}}(E)$ defined in Eq. (3.26) with $E = E_0\,(1+z)$, which is integrated over all redshifts from the present time up to the emission redshift z_s. Moreover, the evolving Hubble factor is given by Eq. (2.23) in Sec. 2.4, as corresponds to a Λ Cold Dark Matter (ΛCDM) universe (for numerical values see Eq. (2.9) and Eq. (2.24)).

Note that this specific form for $H(z)$ also applies to the MaVaN scenario under consideration: according to Sec. 3.1, the Neutrino Dark Energy density $\Omega_{\rm DE}$ redshifts with an equation of state $\omega \sim -1$ [22] and therefore behaves very much like a cosmological constant Λ, $\Omega_{\rm DE} \sim \Omega_\Lambda \sim$ const..

We will express our results for the survival probabilities in terms of the propagating neutrino flavors ν_α according to,

$$\begin{aligned} P_{\nu_\alpha} &= \sum_i |U_{\alpha i}|^2 P_{\nu_i},\ \text{with} \\ i &= 1, 2, 3 \text{ and } \alpha = e, \mu, \tau, \end{aligned} \tag{3.38}$$

where the absolute square of the leptonic mixing matrix elements $U_{\alpha i}$ relates the neutrino flavor components ν_α to the mass eigenstates ν_i. Note that since the mixing matrix element $|U_{e3}| \ll 1$, the absorption dip produced by the heaviest mass eigenstate will not be visible in the case of P_{ν_e}. However, apart from this exception, the flavor survival probabilities to be

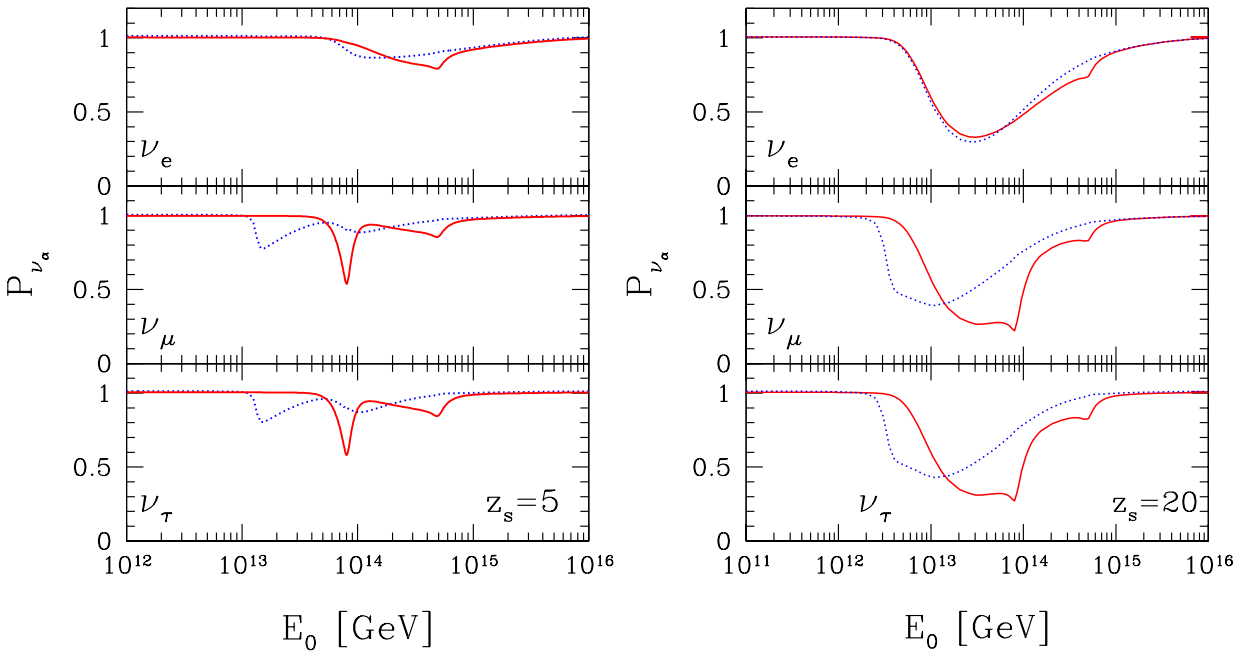

Figure 3.3: Flavor survival probability P_{ν_α}, $\alpha = e, \mu, \tau$ with all thermal background effects included and integrated back to $z_s = 5$ (left panel) and $z_s = 20$ (right panel), respectively, for a normal neutrino mass hierarchy with $m_{\nu_{0,1}} = 10^{-5}$ eV and varying neutrino masses (solid lines) as well as constant neutrino masses (dotted lines).

discussed in the following exhibit absorption dips at the respective resonance energies of the mass eigenstates ν_i, for $i = 1, 2, 3$.

Let us begin our analysis by comparing our results for the flavor survival probabilities defined in Eq. (3.37) and Eq. (3.38), each with varying and constant mass, including all thermal background effects according to Eq. (3.26) and Eq. (3.32). Throughout this section we assume a normal neutrino mass hierarchy, where the masses take values according to Eq. (3.23) – Eq. (3.25) and the mass variation is given in Fig. 3.1 (cf. Sec. 3.1). Furthermore, the best fit values for the mixing angles which determine the mixing matrix $|U_{\alpha i}|$ in Eq. (2.42) in Sec. 2.6.2 are stated in Sec. 2.6.2.

Let us start by considering the flavor survival probabilities P_{ν_α} for an emission redshift of $z_s = 5$ which are plotted in Fig. 3.3 on the left hand side. Apparently, both in the case of varying and constant neutrino masses, the absorption features produced by the lighter two neutrino mass eigenstates are merged together. However, for MaVaNs, the absorption dips produced by the heavier two neutrino mass eigenstates exhibit sharp spikes at the respective resonance energies $E_{0,i}^{res} = \frac{M_Z^2}{2m_{\nu_{0,i}}}$ with $i = 2, 3$ instead of being washed out and distorted to lower energies as in the constant mass case. In principle, by this means, the neutrino masses $m_{\nu_{0,i}}$ for $i = 2, 3$ could be directly inferred from the respective spike positions of the MaVaNs dips in the low redshift regime.

Altogether, the MaVaN absorption dips are much deeper and narrower in comparison to the constant mass features. In addition, the respective minimum positions are shifted to higher

energies by almost an order of magnitude with respect to the corresponding constant mass dips.

As demonstrated by Fig. 3.3 on the right hand side, for an increased emission redshift $z_s = 20$, the absorption features are considerably deeper than for $z_s = 5$. In addition, for each neutrino flavor the dips have merged, both in the case of varying and constant neutrino mass. As we learned in the last section, this effect of the thermal motion has increased with z, since the thermal bath of relic neutrinos was hotter at earlier times.

For MaVaNs, the characteristic narrow spikes at the resonance energies $E_{0,i}^{\mathrm{res}}$ with $i = 2, 3$ are less pronounced than for $z_s = 5$ and also suffer a distortion towards lower energies. Nevertheless, for ν_μ and ν_τ, they remain well distinguishable from the respective constant mass dips. As in the case of $z_s = 5$ the absorption features are clearly shifted to higher energies and exhibit substantially deeper dips.

The characteristic absorption features produced by the mass variation can be worked out by separating the different influences on the MaVaN absorption dips. Let us for this purpose assume the relic neutrinos to be at rest, in order to eliminate any thermal background effects on the MaVaN survival probabilities. By doing so, we are left with the combined effects of the cosmic redshift and the mass variation. Let us first of all consider the former effect which is present both for MaVaNs as well as for constant mass neutrinos. It originates in the expansion of the universe and manifests itself in an energy loss of EHECν's of energy E according to $E_0 = E/(1 + z)$, where E_0 is the EHECν energy to be measured at earth. Accordingly, the survival probability P_{ν_i} of an EHECν is reduced, as long as somewhere on its way to us ($z_s \geq z \geq 0$) it has the right amount of energy,

$$\frac{E_{0,i}^{\mathrm{res}}}{(1 + z_s)} \leq E_0 \leq E_{0,i}^{\mathrm{res}}, \tag{3.39}$$

to annihilate resonantly with a relic anti-neutrino (whereas for all other energies the CνB is transparent for the EHECν such that $P_{\nu_\alpha} = 1$). As a consequence, the effect of cosmic redshift is observable in a broadening of the EHECν absorption dips.

Let us stress that in addition to this cosmological effect in the case of MaVaNs, the variation of the neutrino masses $m_{\nu_i}(z)$ causes a redshift dependence of the respective resonance energies $E_i^{\mathrm{res}}(z)$ as already mentioned in the last section. To be more concrete, the masses $m_{\nu_i}(z)$ at redshift z determine the corresponding resonance energies to be $E_i^{\mathrm{res}}(z) = M_Z^2/2m_{\nu_i}(z)$ in the rest system of the relic neutrinos which only coincide with $E_{0,i}^{\mathrm{res}} = M_Z^2/2m_{\nu_{0,i}}$ for $z = 0$.

In Fig. 3.4 we plot the respective survival probabilities of the neutrino flavors with varying and constant masses, neglecting the relic neutrino momenta and integrating back to $z_s = 5$. As expected from the discussion in the last section, the thermal spread of the absorption features provoked by the relic neutrino motion is removed such that the dips do not merge. Instead, for constant mass neutrinos, the absorption features in Fig. 3.4 are only subject to the broadening caused by the cosmic redshift and span the energy interval specified in Eq. (3.39).

In striking contrast, the absorption dips produced by the MaVaN mass eigenstates exhibit sharp minima at the resonance energies $E_{0,i}^{\mathrm{res}} = \frac{M_Z^2}{2m_{\nu_{0,i}}}$ with $i = 1, 2, 3$ showing no spread

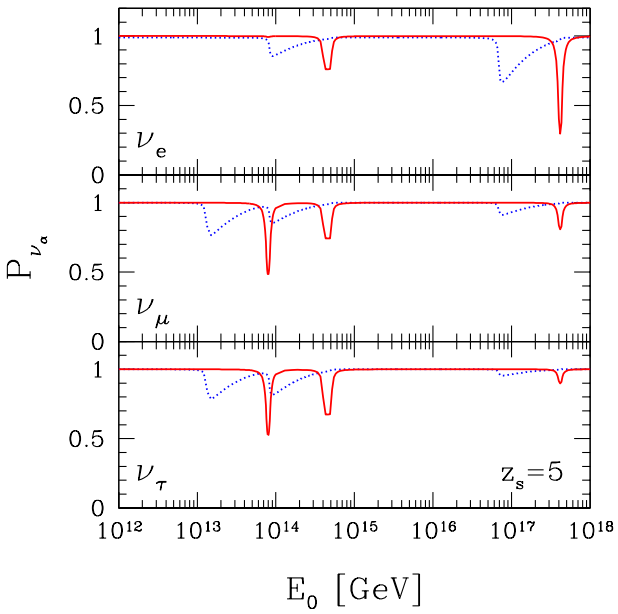

Figure 3.4: Approximated flavor survival probability for P_{ν_α}, $\alpha = e, \mu, \tau$, which assumes the target relic-neutrinos to be at rest, $P = 0$, after an integration back to $z_s = 5$, for a normal neutrino mass hierarchy with $m_{\nu_{0,1}} = 10^{-5}$ eV and varying neutrino masses (solid lines) as well as constant neutrino masses (dotted lines) plotted as a function of their energy E_0 at earth.

towards lower energies. Thus, interestingly, these MaVaN dips look like those of constant mass neutrinos in a non-expanding universe. Actually, it turns out that the mass induced redshift dependence of the resonance energies $E_i^{\rm res}(z) = \frac{M_Z^2}{2m_{\nu_i}(z)}$, $i = 1, 2, 3$, compensates for the energy loss of the EHECν due to cosmic redshift in the limit of low redshifts. This can be understood by remembering that the approximation in Eq. (3.19) gives a good estimate for the redshift dependence of the neutrino masses $m_{\nu_i}(z)$ in the low redshift regime (cf. Fig. 3.1). In this limit one arrives at the following functional dependence of the resonance energies on z,

$$E_i^{\rm res}(z) = \frac{M_Z^2}{2m_{\nu_i}(z)} = E_{0,i}^{\rm res}(1+z). \tag{3.40}$$

In turn, the resonance energy $E_i^{\rm res}(z) = E_{0,i}^{\rm res}(1+z)$ of an EHECν at redshift z corresponds to the redshifted energy measured at earth,

$$\frac{E_i^{\rm res}(z)}{(1+z)} = E_{0,i}^{\rm res}, \text{ with } i = 2, 3, \tag{3.41}$$

Accordingly, the annihilation of an EHECν on the CνB at any given redshift $z_s \geq z \geq 0$ always leads to an absorption peak at $E_{0,i}^{\rm res}$. In other words, in this approximation the square of the center-of-mass energy, $s_{0,i} = 2m_{\nu_i}(z)E_0(1+z) = 2m_{\nu_{0,i}}E_0$, $i = 1, 2, 3$, becomes redshift independent. Correspondingly, the undistorted shape of the annihilation cross-section $\bar{\sigma}_{\nu\bar{\nu}}(s_{0,i})$ (weighted with the neutrino density per unit redshift and integrated over z) gets projected on the sky.

Note that even for higher redshifts the appropriate mass-redshift approximation from Eq. (3.22) leads to the following redshift dependence of $E_i^{\rm res}(z)$,

$$E_i^{\rm res}(z) = \frac{M_Z^2}{2m_{\nu_i}(z)} \propto (1+z)^{1/2} \text{ with } i = 1,2,3. \tag{3.42}$$

Apparently, the neutrino mass variation still partially counterbalances the effect of the cosmic redshift at high redshifts.

In summary, all of the respective MaVaN absorption lines can be distinguished from those of constant mass neutrinos, since the redshift distortion is much less pronounced in any case. We would like to point out that this is a generic feature of any standard MaVaN scenario where the neutrino mass is a decreasing function of redshift.

We are now in a position to complete the interpretation of the MaVaN features in Fig. 3.3 which result from combining all effects on the absorption features including the thermal ones. As already mentioned in the last section, the Fermi-weight factor $P^2 f_{\bar{\nu}}(P,T)$ entering the damping integral in Eq. (3.26) selects momenta P of the order of the CνB temperature $T_\nu(z)$. Accordingly, the ratio $m_{\nu_i}/T_\nu(z)$ is a measure for the relevance of the mass and its probable evolution with respect to the temperature effects. Let us in the following discuss the absorption features which are completely determined by the thermal effects. In these cases the absorption lines were produced by relativistic neutrinos, since $m_{\nu_i}(z)/T_\nu(z) \ll 1$. Firstly, for ν_e the absorption lines of MaVaNs and constant mass neutrinos are similar (cf. Fig. 3.3). This can be understood by recalling that ν_e is mostly composed of the lightest mass eigenstate for which mass effects neither today nor in the past have played any role, since $(m_{\nu_{0,1}}/T_{\nu_0} \ll 1)$. Secondly, as opposed to the case of $z_s = 5$, the MaVaN absorption features for $z_s = 20$ are distorted to much lower energies (cf. Fig. 3.3). In addition, for MaVaNs, the low energy ends of the dips for ν_μ and ν_τ have the same shape as the one of ν_e. The reason is, that the absorption lines in this energy region stem from absorptions at high $z < z_s$ (as indicated by Eq. (3.39) in absence of any thermal effects), where all neutrino masses still were negligible with respect to the temperature. As a consequence, they are clearly distinguishable from the corresponding ones of constant mass neutrinos, which apparently are already non-relativistic in the same energy region. This is due to the fact that while the temperature rises with increasing z, only the MaVaN masses $m_{\nu_i}(z)$ evolve and become lighter. Thus, MaVaNs generically turn non-relativistic much later than constant mass neutrinos. At energies above this transition from the non-relativistic to the relativistic regime, the variation of the heavier two neutrino masses is not washed out by the temperature effects. Therefore, it leads to sharp and thus deep absorption minima at the respective resonance energies according to Eq. (3.41) (cf. Fig. 3.3), without and with transition of the regimes, respectively).

As a conclusion we have learned that the characteristic effects of the neutrino mass variations in the case of the heavier two MaVaNs become apparent in the higher energy regions of the absorption dips, where the MaVaNs are still non-relativistic. However, also the low energy end of the absorption dips differs as long as the MaVaNs are relativistic and the constant mass neutrinos have already turned non-relativistic.

The next section will deal with realistic neutrino fluxes to be measured by neutrino observatories. In general, a flavor tagging at extremely high energies seems unlikely apart from

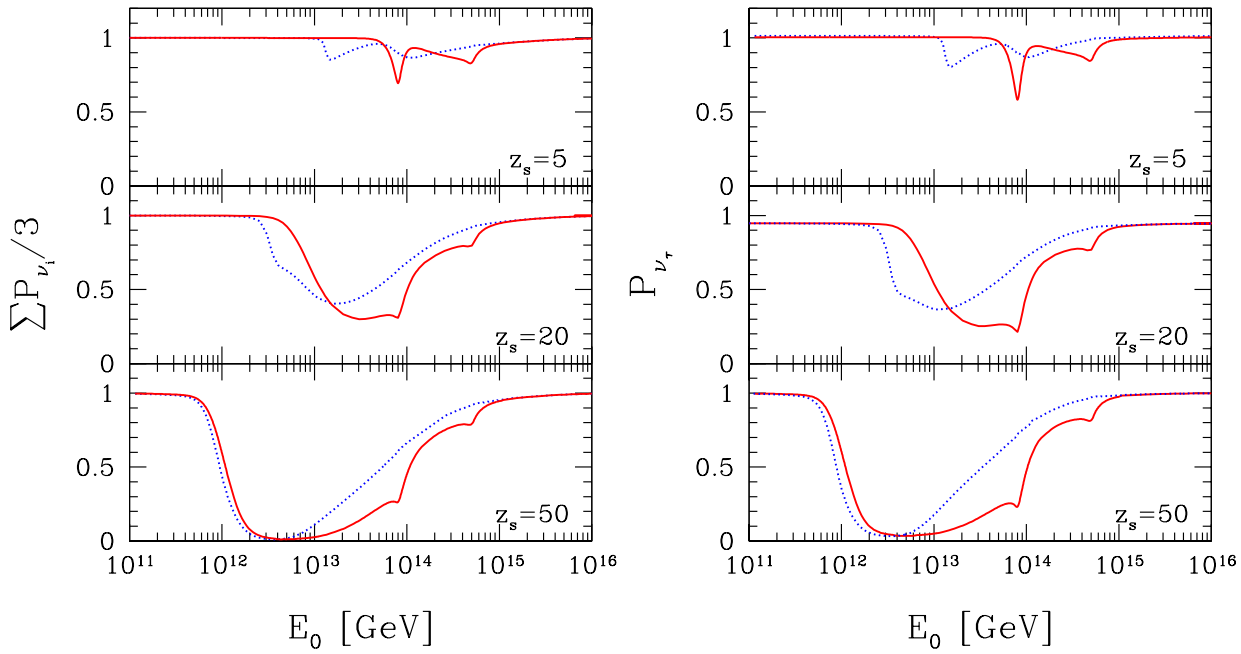

Figure 3.5: The normalized sum of the survival probabilities, $\frac{1}{3}\sum P_{\nu_i}$, and the flavor survival probability P_{ν_τ}, respectively, including all thermal background effects, for a normal neutrino mass hierarchy with $m_{\nu_{0,1}} = 10^{-5}$ eV and varying neutrino masses (solid lines) as well as constant neutrino masses (dotted lines) plotted as a function of their energy E_0 at earth for $z_s = 5$, $z_s = 20$ and $z_s = 50$.

exceptions (e.g. for particular flavors), whereas all observatories will be sensitive to the flavor summed EHECν fluxes $\sum F_{\nu_\alpha}$ with $\alpha = e, \mu, \tau$. Accordingly, we will base our final discussion on the totalized fluxes $\sum F_{\nu_\alpha}$. In addition, we will include our results for the ν_τ whose identification will at best be feasible by the LOFAR radio telescope [186]. For this purpose, for emission redshifts $z_s = 5$, $z_s = 20$ and $z_s = 50$ in Fig. 3.5 we collect both the resulting normalized sum of the survival probabilities, $\frac{1}{3}\sum P_{\nu_i}$ which governs the $\sum F_{\nu_\alpha}$ as well as the respective P_{ν_τ}. Note that emission redshifts of $z_s = 50$ (and much higher) will contribute to the EHECν fluxes which result from the decomposition of super-heavy particles produced by topological defects (top-down sources). Apparently, also for emission redshifts of this order, the characteristic differences between the respective absorption features of varying and constant mass neutrinos, which we have discussed above, are still visible. Furthermore, the absorption dips get considerably deeper with increasing emission redshift z_s.

3.2.4 Absorption Dips in Realistic Neutrino Spectra

So far, in our analysis we have concentrated on the determination and the comparison of the survival probabilities P_{ν_α} of mass varying and constant mass EHECν's traversing the CνB, where the P_{ν_α} contain the physical information on the annihilation process $\nu_\alpha\bar{\nu}_\alpha \to Z$. In the following we will outline how our results can be employed to perform relic neutrino absorption spectroscopy and to what extend the latter can serve as a test for the MaVaN scenario. For this purpose, we will firstly consider astrophysical EHECν acceleration sites and, secondly,

topological defect sources both introduced in the last section. In the latter case, we will not approximate the EHECν injection spectrum by a standard power-law, but go through the appropriate calculation involving fragmentation functions as discussed below.

As a starting point, we require both the detection of EHECν fluxes in the energy region of interest as well as the observation of absorption lines in these spectra. The EHECν flux $F_{\nu_\alpha}(E_0)$ for a neutrino of flavor $\alpha = e, \mu, \tau$ to be measured at earth is given by [66]

$$F_{\nu_\alpha}(E_0) = \frac{1}{4\pi} \int_0^\infty \frac{dz_s}{H(z_s)} \times \sum_{\beta,j} |U_{\alpha j}|^2 P_{\nu_j}(E_0\,(1+z_s), z_s)\, |U_{\beta j}|^2 \mathcal{L}_{\nu_\beta}(E_0\,(1+z_s), z_s). \tag{3.43}$$

The flux integral is governed by the survival probability P_{ν_j} defined in Eq. (3.37) weighted by the EHECν source emissivity distribution $\mathcal{L}_{\nu_\beta}$, which depends on the properties of the source as described in the following. On the one hand, the diffuse source emissivity $\mathcal{L}_{\nu_\beta}(E_0\,(1+z), z_s)$ takes into account the distribution of the sources in the universe (the activity η) and on the other hand it considers the number of neutrinos of flavor $\beta = e, \mu, \tau$ emitted by each of the sources (the injection spectrum J_{ν_β}). Under the standard assumption of identical injection spectra for all sources, one can factorize the z and E dependence,

$$\mathcal{L}_{\nu_\beta}(z_s, E) = \eta(z_s) J_{\nu_\beta}(E), \text{ with } E = E_0(1+z_s). \tag{3.44}$$

As already stated in the last section, a flavor tagging at extremely high-energies cannot be expected at all neutrino observatories. However, we can hope for the identification of the ν_τ absorption lines at LOFAR [186], which we will therefore consider according to Eq. (3.43). Furthermore, in our analysis, we will consider the total flux of all neutrino flavors $\sum F_{\nu_\alpha}$ which can well be approximated by [66],

$$\sum F_{\nu_\alpha}(E_0) \simeq \frac{1}{4\pi} \int_0^\infty \frac{dz_s}{H(z_s)} \frac{1}{3} \mathcal{L}_\nu^{\text{tot}}(E_0\,(1+z_s), z_s) \sum_{j=1}^{3} P_{\nu_j}(E_0\,(1+z_s), z_s), \tag{3.45}$$

where $\mathcal{L}_\nu^{\text{tot}}$ denotes the total, flavor-summed neutrino emissivity at the source and the formula holds as long as $\mathcal{L}_{\nu_\mu} + \mathcal{L}_{\nu_\tau} = 2\mathcal{L}_{\nu_e}$. The latter is fulfilled for hadronic sources like astrophysical accelerator bottom-up sources or non-accelerator top-down sources, since in both cases the neutrinos emerge from charged pion decays such that

$$\mathcal{L}_{\nu_e} : \mathcal{L}_{\nu_\mu} : \mathcal{L}_{\nu_\tau} = 1 : 2 : 0. \tag{3.46}$$

However, Eq. (3.45) also holds in the case of equal flavor source emissivities,

$$\mathcal{L}_{\nu_e} : \mathcal{L}_{\nu_\mu} : \mathcal{L}_{\nu_\tau} = 1 : 1 : 1, \tag{3.47}$$

as could arise in the decays of topological defects not directly coupled to matter (e.g. mirror-matter 'necklaces') [187, 188].

Note that the dependence on the leptonic mixing matric elements $|U_{\alpha j}|$, present in Eq. (3.43),

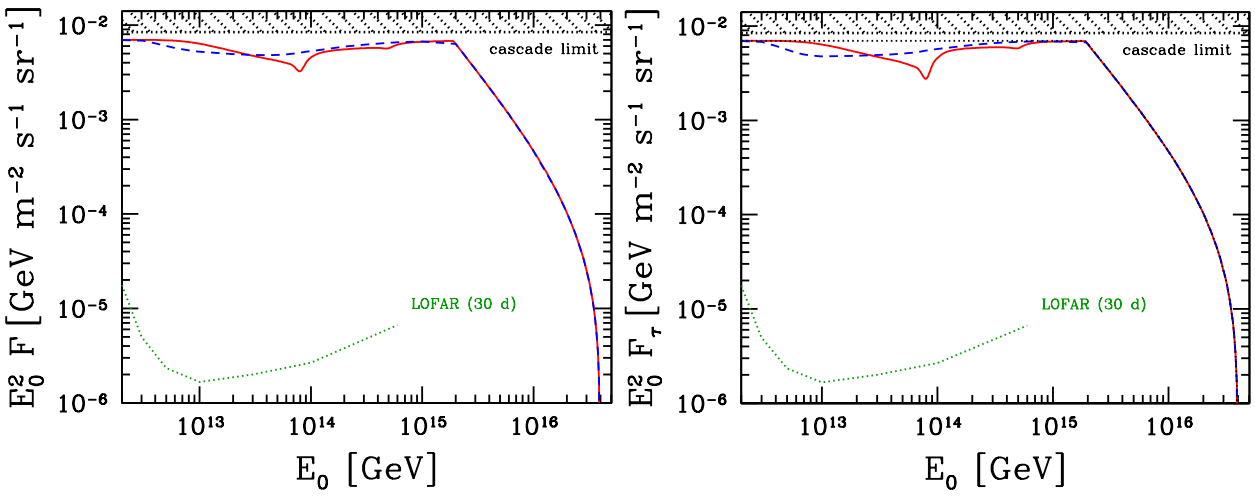

Figure 3.6: Projected sensitivity of LOFAR [158] expressed in terms of the diffuse neutrino flux per flavor, corresponding to one event per energy decade and indicated duration, together with $E_0^2 F$ with $F = \sum F_{\nu_\alpha} + \sum F_{\bar{\nu}_\alpha}$ (left column) and $E_0^2 F_\tau$ with $F_\tau = F_{\nu_\tau} + F_{\bar{\nu}_\tau}$ (right column) for varying (solid lines) and constant (dashed lines) neutrino masses and for $z_{\max} = 20$, assuming a normal neutrino mass hierarchy with $m_{\nu_{0,1}} = 10^{-5}$ eV, $n = 4$ and $\alpha = 2$ as well as $E_{\max} = 4 \times 10^{16}$ GeV.

has dropped out in the expression for $\sum F_{\nu_\alpha}$ in Eq. (3.45) due to unitarity[7].

In the next section we start our investigation by considering astrophysical (bottom-up) EHECν sources. In the subsequent section we continue our analysis for the case of topological defect (top-down) EHECν sources.

Astrophysical Neutrino Sources

In the following we will discuss EHECν fluxes which are assumed to originate from astrophysical EHECν sources. In order to parameterize their source emissivity distribution $\mathcal{L}_{\nu_\beta}$ we employ the following standard ansatz (e.g. [66, 189, 190]) in combination with Eq. (3.44),

$$\eta(z_s) = \eta_0 (1 + z_s)^n \theta(z_s - z_{\min}) \theta(z_{\max} - z_s), \tag{3.48}$$

$$J_{\nu_\beta}(E) = j_{\nu_\beta} E^{-\alpha} \theta(E - E_{\min}) \theta(E_{\max} - E). \tag{3.49}$$

Throughout our analysis, we will take $z_{\min} = 0$ and $E_{\min} = 0$ as default values and suppose that $E_{\max} > E_{0,i}^{\text{res}}(1 + z_{\max})$ for $i = 2, 3$. Furthermore, we will not examine the possibility of broken power-law injection spectra, but assume the spectral index α to be constant in the whole energy region of interest.

[7] The factor of 1/3 in Eq. (3.45) guarantees that the flavor summed flux in the case $\sum_{j=1}^{3} P_{\nu_j} = 3$ reduces to the total flux for no absorption; for its derivation see the appendix of Ref. [66].

For the purpose of illustrating our results, we consider Eq. (3.48) and Eq. (3.49) for $n = 4$ and $\alpha = 2$ as often used in the literature to mimic astrophysical sources and take $E_{\max} = 4 \times 10^{16}$ GeV. As in the last sections, we assume a normal neutrino mass hierarchy according to Eq. (3.23) – Eq. (3.25) and for the MaVaNs a neutrino mass variation according to Fig. 3.1. We present our results in Fig. 3.6, on the left hand side we plot the EHECν energy squared times the flavor summed flux $E_0^2 F$ with $F = \sum F_{\nu_\alpha} + \sum F_{\bar{\nu}_\alpha}$ according to Eq. (3.45) and on the right hand side $E_0^2 F_\tau$ with $F_\tau = F_{\nu_\tau} + F_{\bar{\nu}_\tau}$ as defined in Eq. (3.43). In Fig. 3.6 we plot our results both for varying (solid lines) and constant (dotted lines) neutrino masses for $z_{\max} = 20$, together with the projected sensitivity of LOFAR [158] to be in operation by 2008 expressed in terms of diffuse fluxes per neutrino flavor, respectively. We would like to point out that Monte Carlo simulations promise even better sensitivities in the relevant energy region for a proposed Moon-orbiting satellite using radio methods [191, 192].

In our calculation we have assumed the EHECν flux to be close to the so-called cascade limit [193, 194]. It applies to sources where the neutrinos emerge from pion decays or even from electroweak jets [195] and are thus accompanied by photons and electrons which escape the source. Consequently, the measurements of diffuse gamma-ray fluxes, which are of the same origin but have cascaded down in energy during the propagation through the universe, restrict the neutrino flux to lie below the cascade limit. Apparently, the predicted sensitivity of LOFAR [158], corresponding to one event per neutrino flavor per energy decade, lies below the cascade limit by several orders of magnitude. Accordingly, at best 3500 neutrinos (plus anti-neutrinos) in the energy interval $10^{12} - 10^{13}$ GeV can be expected to be detected by the radio telescope.

The large event numbers N result in tiny error bars ($\sigma = \sqrt{3N}/3N$). In a blow-up of the absorption features in Fig. 3.7, we have adjusted them to the curves with no absorption for emission redshifts $z_{\max} = 20$, $z_{\max} = 10$ and $z_{\max} = 5$ from top to bottom. Thereby, we have assumed a conservative and therefore rather poor energy resolution corresponding to one energy bin per energy decade, whereas at best LOFAR is predicted to achieve an energy resolution of $\Delta E/E \sim 30\%$ [186]. The latter would correspond to ~ 4 energy bins per energy decade. Apparently, the dips become considerably deeper with increasing $z_{\max}$. Despite the underlying low neutrino mass scale, both for varying and constant neutrino masses, LOFAR can be expected to produce significant evidence for absorption dips in the EHECν spectra for emission redshifts $z_{\max} = 20$ and $z_{\max} = 10$ – even for a bad energy resolution. In the case of $z_{\max} = 5$, in the interval $10^{14} - 10^{15}$ GeV, the considerably higher dip depth for MaVaNs leads to a more than 5σ deviation from the curve with no absorption whereas for constant mass neutrinos the departure is not significant (both for the flavor summed flux F and for F_τ). Even if the underlying EHECν fluxes are much lower, at least for EHECν sources at $z_{\max} = 20$, a detection of absorption features produced by varying, light neutrino masses could well be feasible. Correspondingly, if such EHECν fluxes of astrophysical origin exist, the most direct detection of the CνB so far seems to be in reach within the next decade. From the experimental point of view, the prospects are even better for scenarios with time varying neutrino masses, which in general produce deeper absorption dips in the regime of astrophysical emission redshifts.

Let us now turn in more detail to the prospects of probing scenarios of Neutrino Dark Energy by identifying the characteristic absorption signatures of a possible neutrino mass evolution.

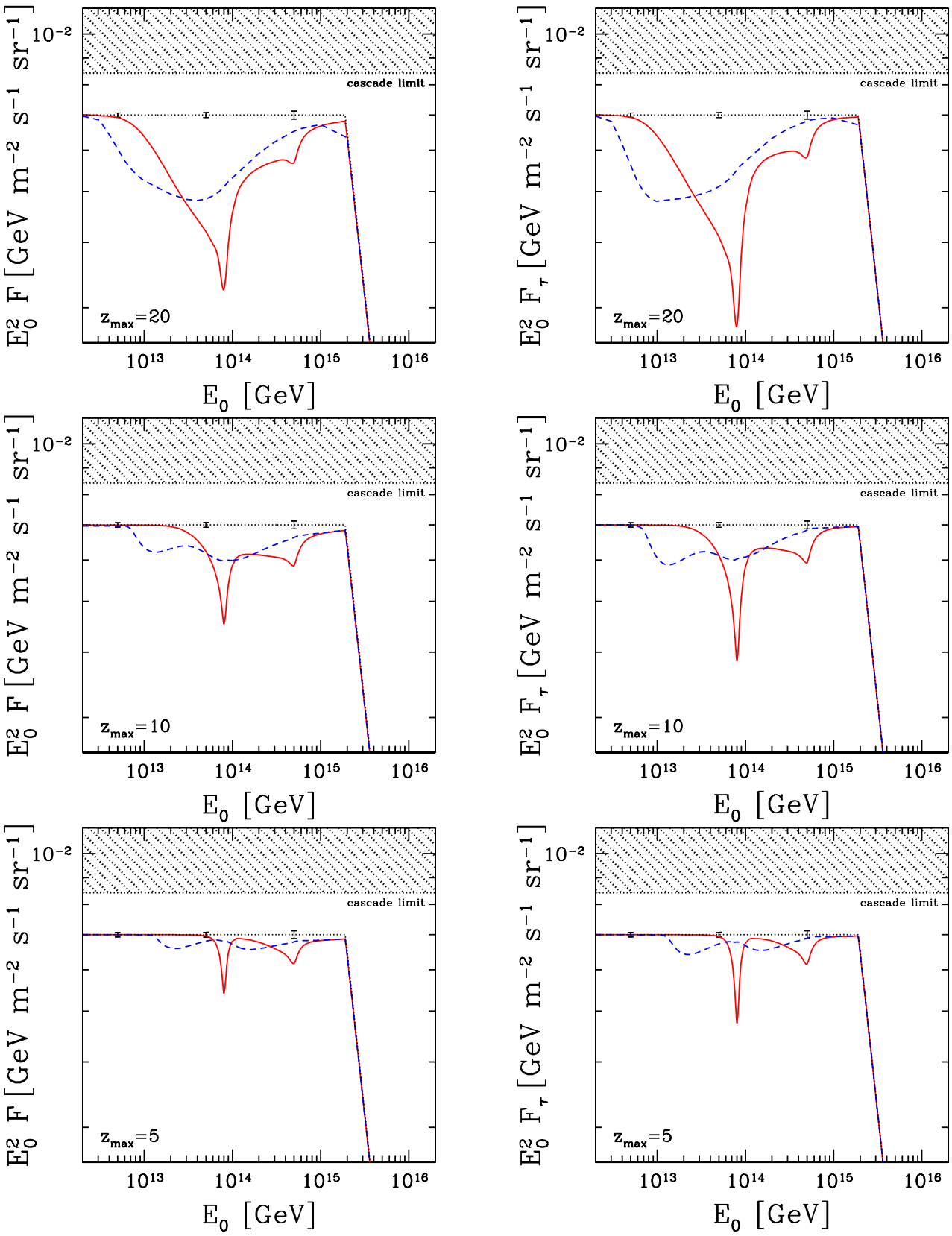

Figure 3.7: The energy squared times the flavor summed neutrino flux $E_0^2 F$ with $F = \sum F_{\nu_\alpha} + \sum F_{\bar{\nu}_\alpha}$ (left column) and $E_0^2 F_\tau$ with $F_\tau = F_{\nu_\tau} + F_{\bar{\nu}_\tau}$ (right column) for varying (solid lines) and constant (dotted lines) neutrino masses for $z_{\max} = 20$, $z_{\max} = 10$ and $z_{\max} = 5$ from top to bottom, respectively. All curves assume a normal neutrino mass hierarchy with $m_{\nu_{0,1}} = 10^{-5}$ eV, $n = 4$ and $\alpha = 2$ as well as $E_{\max} = 4 \times 10^{16}$ GeV.

Since the EHECν fluxes are governed by the respective survival probabilities discussed in the last section, the characteristic differences in the absorption features for varying instead of constant neutrino masses are maintained. Namely, for MaVaNs one observes a clear shift of the dips to higher energies as well as considerably deeper absorption minima with respect to constant mass neutrinos. Accordingly, given a decent energy resolution of $\Delta E/E \sim 30\%$ [186] for LOFAR, relic neutrino absorption spectroscopy could serve as a test for the nature of neutrino masses and therefore for Neutrino Dark Energy. However, certainly, the feasibility strongly depends on the energy resolution achieved by the EHECν observatory.

Topological Defect Neutrino Sources

In the following we will discuss neutrino fluxes expected to result from exotic top-down EHECν sources like topological defects. As already mentioned, EHECν's might be produced among other Standard Model particles in the decays of super-heavy X quanta which constitute the topological defects. Accordingly, the corresponding EHECν injection spectra J in Eq. (3.44) are fragmentation functions which can reliably be predicted by the help of Monte Carlo generators [196, 197] or via the Dokshitzer-Gribov-Lipatov-Altarelli-Parisi (DGLAP) evolution [198–200] from experimentally determined initial distributions at a scale M_Z to the ones at m_X. The corresponding injection rate (the activity η in Eq. (3.44)), which in particular determines the overall normalization of the neutrino flux, in terms of cosmic time t is given by,

$$\frac{\partial n_X}{\partial t} = \frac{Q_0}{m_X}\left(\frac{t}{t_0}\right)^{-4+b}, \tag{3.50}$$

where Q_0 is the energy emitted per unit volume per unit time at present and b is a dimensionless constant. Both Q_0 and b depend on the specific topological defect scenario [184].

In the following, we will illustrate the prospects for performing relic neutrino absorption spectroscopy for top-down sources considering as example superconducting strings whose evolution is characterized by $b = 0$ in Eq. (3.50). In our analysis, we calculate the absorption features in the EHECν spectra by the help of fragmentation functions as well as by Eq. (3.50) according to Eq. (3.44).[8] Note that in the energy region of the absorption dips the Standard Model and SUSY fragmentation functions (which we have taken from [199]) have practically the same shape. Accordingly, all our results on relic neutrino absorption are independent of the supersymmetrization of the MaVaN scenario (cf. Sec. 3.1). In Fig. 3.8 we plot the expected absorption features for varying (dashed lines) and constant (dotted lines) neutrino masses as defined in Eq. (3.23) – Eq. (3.25), where for the MaVaNs we assume a mass variation according to Fig.3.1. Again, we present our results for the energy squared times the flavor summed flux $E_0^2 F$ according to Eq. (3.45) in the left column of Fig. 3.8 and $E_0^2 F_\tau$ as defined in Eq. (3.43) in the right column of Fig. 3.8. As in the case of astrophysical sources, in the first panel of each column we have plotted the projected sensitivities of ANITA and LOFAR as well as the predicted EHECν flux for $m_X = 10^{16}$ GeV with and without absorption (where the latter by design scratches the cascade limit). In the second panel of Fig. 3.8, we again show a blow-up

[8] In the literature on absorption dips so far the injection spectra of top-down sources had been approximated by Eq. (3.48) and Eq. (3.49). Cf. e.g. Refs. [66, 68] for the appropriate values for n and α.

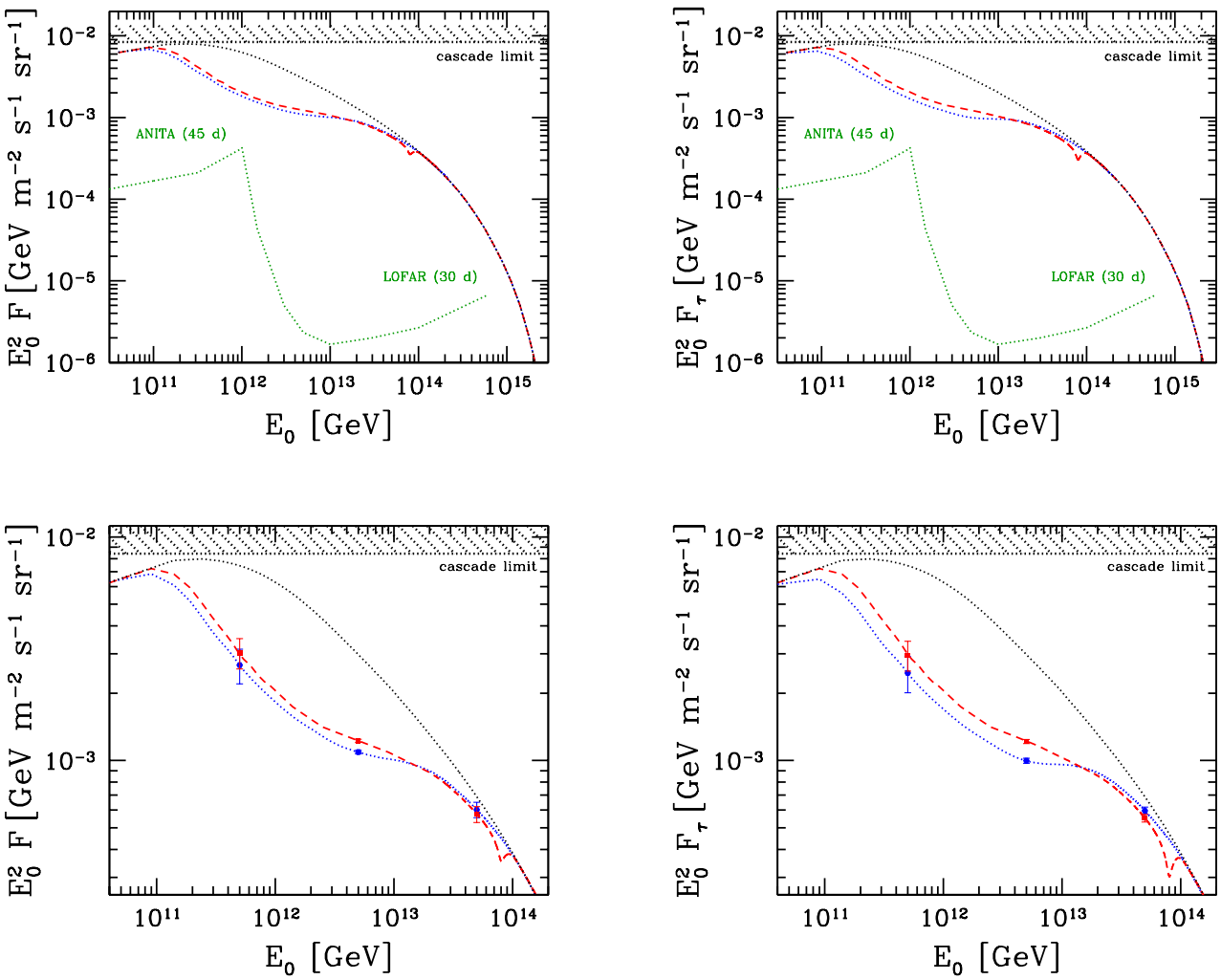

Figure 3.8: The energy squared times the neutrino flux $E_0^2 F$ with $F = \sum F_{\nu_\alpha} + \sum F_{\bar{\nu}_\alpha}$ (left column) and $E_0^2 F_\tau$ with $F_\tau = F_{\nu_\tau} + F_{\bar{\nu}_\tau}$ (right column) for varying (dashed lines) and constant (dotted lines) neutrino masses expected from the decomposition of a superconducting string with $b = 0$ and $m_X = 10^{16}$ GeV, in the first panel together with the projected sensitivities for ANITA [152] and LOFAR [158], which correspond to one event per flavor, energy decade and indicated duration, respectively.

of the absorption features. Apparently, with respect to the astrophysical sources (cf. Fig. 3.7), the dips are broader by almost an order of magnitude in energy. This is due to the fact that the constituents of topological defects have started to decay and therefore to release neutrinos at $z \gg 1$. As a further consequence, the dips for top-down sources are much deeper than for bottom-up sources, since the survival probability of a neutrino traveling to us is much lower (as discussed in the last section and as illustrated by the comparison of the flavor summed survival probability for $z_s = 50$ and $z_s = 20$ in Fig. 3.5). Consequently, both of these features facilitate a detection of the absorption dips in the EHECν spectra. Accordingly, top-down sources with the same underlying fluxes as astrophysical sources are even better suited to provide evidence

for the existence of the CνB. By this means valuable information on the topological defect scenario, on cosmological parameters as well as the neutrino mass scale could be gained both for varying and constant neutrino masses. Furthermore, for the first time in cosmic particle physics, the GUT energy scale $\mathcal{O}(m_X) \sim 10^{16}$ GeV could be probed.

In the second panel of Fig. 3.8, we have also included the expected error bars, again assuming one energy bin per energy decade, both for the MaVaN and constant mass neutrino absorption lines. Clearly, the discrepancy between the two curves is larger for $E_0^2 F_\tau$ than for $E_0^2 F$, whereby in contrast to EHECν's of astrophysical origin, constant neutrino masses produce somewhat deeper dips than time dependent masses. These features can be understood by realizing that ν_τ is dominantly composed of the heaviest mass eigenstate m_{ν_3}, whereas $E_0^2 F$ by definition gets equal contributions from all mass eigenstates. Furthermore, for constant mass neutrinos, m_{ν_3} is the only mass eigenstate for which the ratio $m_{\nu_3}/T_\nu(z) \sim (1+z) \gg 1$ up to $z \sim 1000$. In other words, it produces much deeper absorption dips than the lighter mass eigenstates (even when integrating back to $z \gg 1$) and their characteristic shape is not dominated by the temperature effects (cf. the discussion in the last section). In contrast, for MaVaNs, the ratio $m_{\nu_i}(z)/T_\nu(z)$ with $i = 1, 2, 3$ for all mass eigenstates drops much faster with increasing z and takes values $m_{\nu_i}(z)/T_\nu(z) \ll 1$ for $z \gg 1$. As a result, the low energy end of the dip (which corresponds to higher annihilation redshifts z) has the same shape both for all MaVaN mass eigenstates and the lighter two constant ones and is totally determined by the thermal background effects.

In summary, promisingly, we found that a resolution of absorption features for either mass behavior seems to be possible both for ANITA and for LOFAR. Yet, a differentiation of the MaVaN and constant mass neutrino absorption features seems only feasible, if tau flavor tagging and a good energy resolution are achieved.

3.3 Summary and Conclusions – Part I

In light of the number of extremely high-energy neutrino (EHECν) observatories in operation and under construction with a combined sensitivity ranging up to 10^{17} GeV, the prospects for establishing the existence of EHECν fluxes appear to be very promising. As a next step, the exciting possibility opens up to trace the annihilation of EHECν's and relic anti-neutrinos (and vice versa) into Z bosons by localizing absorption dips in the EHECν spectra at energies set by the neutrino masses. On the one hand, their detection could furnish the most direct evidence for the CνB so far and thereby confirm standard cosmology back to the time of light neutrino decoupling. On the other hand, the shape of the absorption lines could reveal a variation of neutrino masses with time and thus verify the interpretation of the CνB as source of Neutrino Dark Energy.

We therefore considered a viable Mass Varying Neutrino (MaVaN) model with the following features entering our analysis on relic neutrino absorption. By the requirement that the lightest neutrino still has to be moderately relativistic today the neutrino mass scale is set to be low. This leads to very conservative predictions and in the end renders our results for the discovery potential of Neutrino Dark Energy independent of the neutrino mass scale realized in

nature. Furthermore, the evolving neutrino masses $m_{\nu_i}(z)$, which we determined numerically as functions of redshift assuming $m_{\nu_{0,1}} = 10^{-5}$ eV, turned out to be well approximated by simple power laws $(1+z)^{-1}$ and $(1+z)^{-1/2}$ in the low and in the high redshift regime, respectively. Accordingly, as a generically important feature, they are decreasing functions of redshift as in all standard MaVaN scenarios.

In order to provide all technical tools to interpret EHECν absorption dips for a given injection spectrum and to extract valuable information on neutrino physics, cosmology and possibly physics beyond the Standard Model, we proceeded in the following way. We considered in parallel the neutrino masses to be functions of cosmic time as well as to be constants. In our analysis we took into account the full thermal background effects which result from the relic neutrino motion according to their phase space distribution. In order to compare our results to the literature, we included in our discussion common approximations [64, 66, 67] which neglect part or all of the dependence of the damping on the relic neutrino momenta.

On the level of the survival probabilities which govern the EHECν fluxes, we found the following results: For low emission redshifts ($z \sim \mathcal{O}(5)$), the absorption dips produced by the varying neutrino masses $m_{\nu_i}(z)$ for $i = 2, 3$ exhibit narrow absorption minima, which do not suffer a distortion to lower energies as the corresponding dips of constant mass neutrinos. As a consequence, for MaVaNs, the absorption dips of the flavor components ν_μ and ν_τ (which are mostly composed of the heavier two mass eigenstates) are clearly deeper and shifted to higher energies by almost an order of magnitude with respect to the corresponding constant mass minima. For an increased emission redshift $z \gg 5$, these features become somewhat less pronounced but essentially prevail.

A better understanding of the characteristic signatures caused by the mass evolution was obtained by switching off the superposing thermal wash-out caused by the relic neutrino motion. After neglecting the relic neutrino momenta for this purpose, we found that the crucial deviations result from the dependence of the corresponding resonance energies on the neutrino masses $E_i^{\mathrm{res}} \sim 1/m_{\nu_i}$ for $i = 1, 2, 3$. In the case of MaVaNs, the mass variation $m_{\nu_i}(z)$ induces a dependence on the annihilation redshift z according to $E_i^{\mathrm{res}}(z) \sim E_{0,i}^{\mathrm{res}}(1+z)$ for all neutrino species $i = 1, 2, 3$ in the low redshift regime. Accordingly, as a main result, we found this z dependence of the resonance energies to compensate for the energy loss of the EHECν due to cosmic redshift proportional to $(1+z)^{-1}$. This was found to lead to narrow absorption spikes at constant energies $E_i^{\mathrm{res}}(z)/(1+z) = E_{0,i}^{\mathrm{res}}$ (like one would expect for constant neutrino masses in a non-expanding universe). In contrast, for constant neutrino masses $m_{\nu_i} = m_{\nu_{0,i}}$ the absorption dips are broadened, since the redshifted resonance energies to be measured on earth are given by $E_i^{\mathrm{res}}/(1+z) = E_{0,i}^{\mathrm{res}}/(1+z)$, for z taking values between 0 and the EHECν emission redshift.

Thus, since in the standard MaVaN scenario the neutrino masses are decreasing functions of redshift, they generically reduce the effect of cosmic redshift on the EHECν survival probabilities. As a result, they always produce deeper absorption minima, which, in addition, are shifted to higher energies in comparison to the dips caused by constant neutrino masses.

In order to illustrate the discovery potential for absorption dips in the EHECν spectra to be observed at earth and to estimate the prospects of testing scenarios of Neutrino Dark Energy, we considered plausible EHECν fluxes originating from astrophysical acceleration sites or from

topological defect sources. We presented our results both for the energy squared times the flavor summed EHECν flux $E_0^2 F$ with $F = \sum F_{\nu_\alpha} + \sum F_{\bar{\nu}_\alpha}$ and for $E_0^2 F_\tau$ with $F_\tau = F_{\nu_\tau} + F_{\bar{\nu}_\tau}$, where the latter can at best be identified by LOFAR [186]. Despite the adopted low neutrino mass scale, we found both for varying and constant neutrino masses that for topological defect and for astrophysical EHECν sources at $z_{\max} > 5$, LOFAR and ANITA promise a statistically significant evidence for absorption dips (even if the underlying fluxes are well below the cascade limit). Accordingly, the most direct detection of the CνB so far seems to be in reach within the next decade.

Furthermore, the flux dips of varying and constant mass EHECν's expected from astrophysical sources retain the characteristic differences induced by the survival probabilities. Besides being clearly shifted to higher energies, the MaVaN dips are deeper and therefore even facilitate a resolution of absorption features in the EHECν spectra in comparison to constant mass neutrinos both in the case of $E_0^2 F$ and of $E_0^2 F_\tau$. As a main result of our analysis, these deviations of the MaVaN and constant mass absorption curves for astrophysical sources turned out to be statistically significant, yet a decent energy resolution seems necessary for their detection. Given an energy resolution of $\Delta E/E \sim 30\%$ as at best achievable for LOFAR [186], relic neutrino absorption spectroscopy could reveal a variation of neutrino masses and therefore possibly the nature of Dark Energy. Let us note again that this result is representative for the testability of the Mass Varying Neutrino Scenario, since it holds independent of the actual neutrino mass scale realized in nature.

As concerns topological defect sources, the absorption lines in the EHECν fluxes for time dependent and constant neutrino masses altogether are more similar in shape, however, somewhat deeper for constant neutrino masses. Furthermore, they extend to much lower energies than for astrophysical EHECν sources and their minima are considerably deeper. All of these features are a result of the much higher annihilation redshifts $z_s \gg 1$ possible for EHECν's originating from the decomposition of topological defects in comparison to EHECν's from astrophysical acceleration sites. At high redshifts, the EHECν's are absorbed by a hotter bath of relic neutrinos. Consequently, in the energy region spanned by the absorption dips where $m_{\nu_i}/T_\nu \ll 1$, thermal background effects wash out any features produced by the neutrino mass or its possible variation. Since the MaVaN masses are decreasing functions of redshift, they reach this limit for much smaller redshifts than the corresponding constant masses. Only the mass of the heaviest constant mass eigenstate is sufficiently large, $m_{\nu_3}/T_\nu(z) \gg 1$, in the relevant energy region, leading to a deeper absorption curve than the one produced by all of the other MaVaN and constant mass eigenstates. Since ν_τ is mostly composed of the heaviest mass eigenstate, F_τ exhibits deeper constant mass dips than F. Accordingly, for F_τ the signatures of varying neutrino masses can more easily be distinguished from those of constant masses than in the case of F. However, in order to reveal a neutrino mass variation, it seems necessary both to identify the tau neutrino flavor and to have a good energy resolution.

Let us in the following comment on how our results can be generalized to other MaVaN scenarios, whose viability does not rely on a low neutrino mass scale (cf. Sec. 4). As we pointed out, the characteristic absorption signatures of any standard MaVaN scenario (cf. Sec. 3.2.3 and Sec. 3.2.4) are essentially generic apart from details. Yet, a higher neutrino mass scale would even increase the overall dip depth in comparison to our rather conservative predictions and also reduce the importance of the thermal background effects on the absorption

features. Accordingly, we would expect the features produced by a possible mass evolution not to be washed out by the temperature effects for a wider energy range of the dips. Thus the deviations with respect to the corresponding constant mass curves would even be more prominent.

Part II

4 On the Stability of Neutrino Dark Energy

As we have discussed in detail in Sec. 3 and mentioned in the introduction, if neutrinos interact through a new non-standard force mediated by a light scalar field of the dark sector, the combined energy density in the coupled fluid naturally evolves slowly and as a consequence can possibly drive late-time acceleration. However, recently, it has been pointed out by Afshordi, Zaldarriaga and Kohri in Ref. [57] that in the *non-relativistic neutrino regime* this newly proposed attraction felt between neutrinos can provoke the strong growth of hydrodynamic perturbations in the neutrino density and thus can threaten the stability of the scenario. Let us in the following briefly outline how instabilities in general can occur as well as what the possible outcome is. For a better understanding, we will also draw an analogy to the well-known phenomenon of gravitational instabilities on which the theory of galaxy formation is based (see e.g. [86]).

To this end, let us first recall from Secs. 2.1 – 2.4 that the universe at early times on all cosmological scales and today on the very largest scales is remarkably homogeneous. However, according to the standard picture, about this homogeneous background there are small primordial perturbations in the matter densities inherited from inflation [76]. Generally speaking, an attractive force felt between matter causes these small inhomogeneities to produce a force on the surrounding matter. Accordingly, unless they are stabilized in some way, for example by the presence of relativistic pressure support, these initially small fluctuations can grow in amplitude to finally form non-linear structure bound by the attractive force. For instance, identifying the attractive force with gravity, in a nutshell, this is the standard picture of how self-bound structure like galaxies and clusters of galaxies have formed, after the universe was dominated by *non-relativistic* matter with negligible pressure. Note that the universe appears less and less lumpy, the larger the scales one looks at. In numbers, matter perturbations on scales less than about 10 Mpc have grown non-linear (note that galaxies have densities a million times the average density), while large-scale perturbations are still small. This is the regime where linear theory (cf. Sec. 4.2) is the right tool at hand to study the early stages of structure formation.

Coming back to Mass Varying Neutrinos, as a conclusion by analogy, MaVaN instabilities can be stabilized by the pressure support (and the random motions) of a *relativistic* neutrino (cf. the scenario discussed in Sec. 3) [22, 57, 59]. Therefore, only in the *non-relativistic* neutrino regime they can possibly grow by the attractive force mediated by the scalar field.

The stage is now set for the question to be followed up in this chapter: Can mass varying neutrino perturbations be stabilized in some other way *also* in the highly non-relativistic neutrino regime?

In order to motivate the strategy to be pursued to tackle this question, let us summarize the findings of the pioneering work of Afshordi, Zaldarriaga and Kohri in Ref. [57] concerning the issue of stability possibly arising in models of Neutrino Dark Energy.

In the kinetic theory picture, the authors derived an analytical formula for the adiabtic *sound speed squared* of the scalar-neutrino fluid, which was found to take *negative values* in the *non-relativistic regime* of *any* MaVaNs scenario with $m_\phi^2 \gg H^2 > 0$[1]. From this result, the authors concluded that *any* adiabatic MaVaNs scenario becomes unstable to exponentially growing hydrodynamic perturbations as soon as they are not stabilized anymore by the pressure support and the random motions of a relativistic neutrino. Furthermore, based on the assumption of thermal equilibrium, the authors quantitatively confirmed that as an outcome of the instability most of the neutrinos end up in dense 'nuggets' or lumps (cf. also Ref. [58])[2].

Let us remark that in Ref. [60] it has been shown that the generic assertion of a negative sound speed squared can be relaxed, if finite temperature effects are taken into account.

Our approach will be, to revisit the stability issue challenged by Ref. [57] in the appropriate framework provided by linear cosmological perturbation theory in a model-independent way. As it will turn out this naturally leads us to consider the influence of other important cosmic components on the dynamics of the MaVaN perturbations which have not been taken into account in Ref. [57].

In our investigation we will pay particular attention to the question whether a negative adiabatic sound speed squared indeed is a sufficient condition for MaVaN instabilities to occur. In addition, following Ref. [60], in Sec. 4.3 we further pursue the conditions leading to a *positive sound speed squared*. Moreover, in Sec. 4.6.1, we will comment on whether the viability of a MaVaN scenario is necessarily threatened if indeed neutrino lumps should form. The investigation is based on our Ref. [71] and also goes beyond it.

To this end, after setting the stage for a model-independent analysis in the next section, we provide an introduction to linear perturbation theory in Sec. 4.2 and briefly introduce the matter power spectrum for later reference in Sec. 4.2.1. Thereafter, we consider as a simple instructive example gravitational instabilities in Newtonian theory. This will both allow to gain an intuition for the main physical effects leading to instabilities and in addition clarify, under which conditions the sound speed squared can uniquely determine the perturbation dynamics. After discussing the relation between the nature of the sound speed squared and the scales and regimes where possible instabilities can occur, we derive the evolution equations for the MaVaN perturbations in Sec. 4.4 from linearizing Einstein's equations about an expanding background. By applying justified approximations to the analytical results, we will be able to identify an analytical stability condition which will allow to classify the behavior of the perturbations in dependance on the scalar-neutrino coupling function. We will illustrate our results by discussing representative examples both for stable and unstable scenarios in Sec. 4.5 and present our numerical findings from the full evolution equations in Sec. 4.5.2. Based on our results, in Sec. 4.6 and Sec. 4.6.1, we will state to what extent the no-go theorem set up in Ref. [57] for adiabatic models of Neutrino Dark Energy can be relaxed. Finally, in Sec. 4.7,

[1] Note that models of Neutrino Dark Energy which couple a *quintessence* scalar field with mass $\sim H$ to neutrinos [43,44] do not suffer from instabilities even in the highly non-relativistic neutrino regime (cf. Sec. 4.3 for an explanation).

[2] Since the outcome of the instabilities is an inherently non-linear process as such it is difficult to study analytically.

we will summarize our results and provide an outlook.

4.1 Setting the Stage for the Stability Analysis

Let us in this section briefly summarize the ingredients which characterize a general MaVaN model to set the stage for our subsequent model-independent stability analysis. This section is based on our Ref. [71].

First of all, let us note that cosmology is in leading order sensitive to the sum of neutrino masses [43] which we will for simplicity represent by m_ν. Since a MaVaN set-up can only possibly become unstable in the (highly) non-relativistic neutrino regime, we furthermore take a conservative approach in assuming a degenerate neutrino mass spectrum corresponding to three degenerate neutrinos, being highly non-relativistic today (cf. Sec. 3.1 where the stability problem is evaded since a relativistic neutrino is responsible for Dark Energy until today [22, 57, 59, 60]). In Sec. 4.5.2 we will comment on how this conservative assumption influences the stability of a MaVaN scenario.

Accordingly, we will consider the class of MaVaN models whose Lagrangian takes the form,

$$\begin{aligned} \mathcal{L} &\supset \mathcal{L}_\phi + \mathcal{L}_{\nu_{\rm kin}} + \mathcal{L}_{\nu_{\rm mass}}, \text{ where} \\ \mathcal{L}_\phi &= -\left[\frac{1}{2}\partial^\mu\phi\partial_\mu\phi + V_\phi(\phi)\right], \\ \mathcal{L}_{\nu_{\rm mass}} &= -m_\nu(\phi)\bar{\nu}\nu + h.c., \end{aligned} \tag{4.1}$$

besides a standard kinetic term both for the neutrinos and the scalar field it contains a self-interaction potential V_ϕ for ϕ and, importantly, a mass term for the neutrinos. It is generated from the value of the scalar field and thus becomed linked to its dynamics (cf. the discussion in Sec. 3.1). Note that for our purposes it does not matter whether neutrinos are Majorana or Dirac particles. As can be read off Eq. (4.1), a MaVaN model is fully specified by the choice of $V_\phi(\phi)$ as well as by the dependence of the neutrino mass on the VEV of the scalar field, $m_\nu(\phi)$. The latter defines the coupling β between the neutrinos and the scalar field to be [43],

$$\beta \equiv \frac{d\log m_\nu}{d\phi} = \frac{m_\nu'}{m_\nu}, \tag{4.2}$$

where here and in the following primes denote derivatives with respect to ϕ ($' = \partial/\partial\phi$). Furthermore, since we intend to analyze the growth of cosmological perturabtions, the natural choice of the time variable is given by the conformal time τ as introduced in Sec. 2.4. This implies that the Hubble parameter takes the form, $\mathcal{H} = d\log a/d\tau = H/a$, where $H = d\log a/dt$ as introduced in Sec. 2.4.

Let us note that accordingly in the presence of a scalar field the Friedmann equation takes the form,

$$3\mathcal{H}^2 = \frac{a^2}{M_{\rm pl}^2}\left(\frac{\dot{\phi}^2}{2a^2} + V_\phi(\phi) + \rho_m\right), \tag{4.3}$$

with $M_{\rm pl} \equiv (\sqrt{8\pi G})^{-1}$ denoting the reduced Planck mass and the subscript m comprising all matter species.

With these conventions, in the non-relativistic neutrino regime one arrives at the following modified Klein-Gordon equation for the scalar field,

$$\ddot{\phi} + 2\mathcal{H}\dot{\phi} + a^2 V' = 0, \text{ where} \tag{4.4}$$

$$V' = (V_\phi + \rho_\nu)' = V'_\phi + \beta\rho_\nu. \tag{4.5}$$

As argued before, in Sec. 1 and Sec. 3.1, as opposed to a quintessence field the scalar field evolves naturally slow due to the stabilizing influence exerted by the neutrinos and thus we can assume the scalar field mass to be much larger than the expansion rate $\mathcal{H}$,

$$m_\phi^2 = V'' = \rho_\nu \left(\beta' + \beta^2\right) + V''_\phi \gg \mathcal{H}^2. \tag{4.6}$$

Accordingly, we see explicitly from Eq. (4.4) that in this limit the dynamics of the scalar field are determined by the condition,

$$V'(\phi) = 0, \tag{4.7}$$

which means that ϕ adiabatically tracks its effective minimum as described in Sec. 3.1.

Let us in the following discuss which requirements have to be fulfilled by the functions $V_\phi(\phi)$ and $m_\nu(\phi)$ characterizing a MaVaN model in order to accomplish the correct cosmology today. For this purpose, we define $w = p_{\rm DE}/\rho_{\rm DE}$ to be the equation of state of the coupled neutrino-scalar fluid with,

$$p_{\rm DE} \simeq p_\phi = \frac{1}{2a^2}\dot{\phi}^2 - V_\phi(\phi), \tag{4.8}$$

$$\rho_{\rm DE} = \rho_\nu + \rho_\phi \simeq m_\nu n_\nu + \frac{1}{2a^2}\dot{\phi}^2 + V_\phi(\phi), \tag{4.9}$$

where p_ϕ and ρ_ϕ respectively denote the scalar field pressure and energy density as defined in Eq. (4.24) and we have used that $p_\nu \simeq 0$ and $\rho_\nu \simeq m_\nu n_\nu$ in the non-relativistic neutrino regime. We must now demand that the equation of state parameter w of the coupled scalar-neutrino fluid today roughly satisfies $w \sim -1$ as suggested by observations [102]. By noting that for constant w at late times (cf. Sec. 2.4),

$$\rho_{\rm DE} \sim V \propto a^{-3(1+w)}, \tag{4.10}$$

and by requiring energy conservation, one arrives at [21]

$$1 + w = -\frac{1}{3}\frac{\partial \log V}{\partial \log a}. \tag{4.11}$$

In the non-relativistic limit $m_\nu \gg T_\nu$ this is equivalent to,

$$1 + w = -\frac{a}{3V}\left(m_\nu \frac{\partial n_\nu}{\partial a} + n_\nu \frac{\partial m_\nu}{\partial a} + \frac{V'_\phi}{a'}\right) = -\frac{m_\nu V'_\phi}{m'_\nu V}, \tag{4.12}$$

where in the last equality it has been used that $V' = 0$ according to Eq. (4.7). To allow for

an equation of state close to $w \sim -1$ today one can conclude that either the scalar potential V_ϕ has to be fairly flat[3] or the dependence of the neutrino mass on the scalar field has to be quite steep.

Furthermore, the combined present energy density of the scalar field and of the neutrinos has to be identified with the Dark Energy density as measured today (cf. Sec. [201]), $\Omega_{\rm DE} \sim 0.7$.

In the next section we will set the stage for our stability analysis in Sec. 4.2 by introducing the concept of *linear cosmological perturbation theory*.

4.2 Linear Cosmological Perturbation Theory

In section Sec. 2.4 the tools were provided to study the large-scale dynamics of our universe by the help of the idealized Friedmann-Robertson-Walker (FRW) background model which relies on the assumption of homogeneity and isotropy. Let us now model the universe more realistically by allowing for small deviations from the smooth FRW-background, which we call *'perturbations'* (for pioneering work see [81–84] and for comprehensive reviews see [85–91]). This approach will set the stage for our analysis of the coupled neutrino-scalar field perturbations in Sec. 4.4 to investigate the possible growth of MaVaN structure.

In order to describe the evolution of small cosmological perturbations in the framework of linear theory, our task at hand reduces to solving Einstein's equations linearized about an expanding background. Accordingly, small perturbations have to satisfy,

$$\delta G_{\mu\nu} = 8\pi G \delta T_{\mu\nu}, \tag{4.13}$$

where $\delta G_{\mu\nu}$ and $\delta T_{\mu\nu}$ denote the perturbed Einstein tensor and perturbed stress-energy tensor, respectively.

The perturbed quantities $\delta g_{\mu\nu}$ and $\delta T_{\mu\nu}$, which enter the perturbed Einstein equations in Eq. (4.13), expressed in terms of the full metric $g_{\mu\nu}$ and the full stress-energy tensor $T_{\mu\nu}$ as well as their background parts, are given by

$$\delta g_{\mu\nu}(\vec{x},\tau) = g_{\mu\nu}(\vec{x},\tau) - g_{\mu\nu}(\tau), \tag{4.14}$$

$$\delta T^{\mu}_{\nu}(\vec{x},\tau) = T^{\mu}_{\nu}(\vec{x},\tau) - T^{\mu}_{\nu}(\tau). \tag{4.15}$$

Note that the background quantities of the smooth universe introduced in Sec. 2.4 are only functions of conformal time τ. Thus, they can be distinguished from the full quantities (even though they are conventionally labeled by the same symbol), since these as well as the perturbed quantities depend on all comoving coordinates $x^\mu = (\vec{x},\tau)$.

For the purpose of solving the perturbed part of Einstein's equations for the evolution of perturbations, let us successively provide a concrete parameterization for $\delta g_{\mu\nu}$ and δT^{μ}_{ν}.

The form of $\delta g_{\mu\nu}$ depends on the nature of the perturbations (scalar, vector or tensor) under consideration as well as on the choice of the gauge. Since we are interested in the growth of

[3]However, the self-interaction potential does not have to be as flat as in the case of a quintessence scalar field [21].

inhomogeneities, we restrict the following discussion to scalar metric perturbations[4] which are independent from vector and scalar perturbations to linear order. In addition, in this thesis, we choose to work in synchronous gauge[5], in which the publicly available computer code CMBFAST [202], to be used in our numerical studies presented in Sec. 4.5.2, is implemented. By definition, in this gauge the components g_{00} and g_{0i} of the full metric are unperturbed. Accordingly, the perturbed metric $\delta g_{\mu\nu}$ takes the form (see e.g. [86, 89]),

$$\delta g_{\mu\nu} = a^2(\tau)\,\mathrm{diag}(0, h_{ij}), \tag{4.16}$$

where h_{ij} is a small metric perturbation.

For simplicity, in this thesis we will assume the universe to be flat ($\Omega_{\mathcal{K}} = 0$) as predicted by inflation [76] and as supported by observational data (see e.g. [75]). Accordingly, the full line element is given by,

$$ds^2 = g_{\mu\nu}dx^\mu dx^\nu = a^2(\tau)\{-d\tau^2 + (\delta_{ij} + h_{ij})dx^i dx^j\}, \tag{4.17}$$

where Eq. (4.14) has been used in combination with Eq. (4.16) and the FRW-line element of the background stated in Eq. 2.4 in Sec. 2.4. For vanishing curvature $\mathcal{K} = 0$, it is conveniently expressed in terms of Cartesian coordinates for space-like hyper-surfaces rather than polar coordinates.

Since for convenience we will be working in Fourier space in the following, let us define the scalar mode of h_{ij} as Fourier integral by introducing two fields $h(\vec{k}, \tau)$ and $\eta(\vec{k}, \tau)$ in k-space,

$$h_{ij}(\vec{x}, \tau) = \int d^3k e^{i\vec{k}\vec{x}}\{\hat{k}_i\hat{k}_j h(\vec{k}, \tau) + (\hat{k}_i\hat{k}_j - \frac{1}{3}\delta_{ij}6\eta(\vec{k}, \tau))\},\ \vec{k} = k\hat{k}, \tag{4.18}$$

where h denotes the trace of h_{ij} both in real and Fourier space. Let us note for later reference that in terms of h and η the longitudinal traceless space-space parts of the linearized Einstein equations in Eq. (4.13) define the shear σ by the relation,

$$\begin{aligned} \ddot{h} + 6\ddot{\eta} + 2\frac{\dot{a}}{a}(\dot{h} + 6\dot{\eta}) - 2k^2\eta &= -24Ga^2(\rho(\tau) + p(\tau))\sigma, \text{ where} \\ (\rho(\tau) + p(\tau))\sigma &\equiv -(\hat{k}_i\hat{k}_j - \frac{1}{3}\delta_{ij})\Sigma^i_j, \\ \Sigma^i_j &\equiv T^i_j - \frac{\delta^i_j}{3}T^k_k, \end{aligned} \tag{4.19}$$

and the anisotropic stress Σ^i_j denotes the traceless component of T^i_j (cf. Eq. (4.22). Note that here and in the following the pure background quantities can be identified, since we explicitly state their time dependence (cf. the discussion above).

Let us stress that the Fourier decomposition has to be performed with respect to the comoving

[4] For a review including tensor and vector perturbations we refer the interested reader to Ref. [86].

[5] Despite its wide-spread use one has to be aware of the residual gauge freedom in this gauge manifested in the occurrence of spurious gauge modes contained in the solutions to the equations for the density perturbations on super-horizon scales. However, this is not relevant for this thesis which is only concerned with sub-horizon modes.

coordinate system. Accordingly, the *'comoving wavelength* $\lambda_{\rm com}$ is defined as,

$$\lambda_{\rm com} = \frac{2\pi}{k}, \tag{4.20}$$

while the *'physical wavelength'* $\lambda_{\rm phys}$ is given by

$$\lambda_{\rm phys} = a(\tau)\frac{2\pi}{k}. \tag{4.21}$$

Note also that as a nice feature of linear perturbation theory different Fourier modes evolve independently. This is due to the fact that a coupling between them would involve products of perturbations which are of second order and thus negligible in linear theory. Hence, in the evolution equations for the perturbations it will not be necessary to keep the integration over the Fourier modes explicitly as we will make use of later on.

Having defined the perturbed metric entering Eq. (4.13), let us now specify the perturbed stress-energy tensor of the different particle species which compose the total δT^{μ}_{ν}. As we have learned in Sec. 2.5, photons and (ultra-)relativistic neutrinos can only appropriately be described by their full distribution function in phase space and thus in this case the stress-energy tensor involves integrals over momenta and the distribution functions. However, we are interested in the evolution of the universe at late times where photons play a completely subdominant role and their contribution can therefore be neglected as discussed in Sec. 2.4. Furthermore, since it turns out that the neutrino perturbations can only possibly become unstable in the non-relativistic neutrino regime (cf. the discussion in Sec. 4.3), it is convenient to define certain moments of the distributions as *fluid* perturbations, just as for CDM and baryons (cf. Eq. (4.30) and Eq. (4.31)). Therefore, we will in the following discuss the perturbed stress-energy tensor for a general fluid. Finally, we will discuss the case of a scalar field relevant for our investigation of the MaVaN perturbations in Sec. 4.4.

The most general first-order perturbation of the stress-energy tensor in fluid notation can be expressed in terms of four functions all of which depend on the comoving coordinates: the perturbed energy density $\delta\rho$, the perturbed pressure δp, the small coordinate three-velocity of the fluid $u^i \equiv dx^i/d\tau$ (usually assumed to be a first-order perturbation) and the anisotropic stress Σ_{ij} (see also Eq. (4.19)). The perturbed stress-energy tensor has the form (see e.g. [86, 89]),

$$\delta T^{\mu}_{\nu} = \begin{pmatrix} -\delta\rho & (\rho(\tau)+p(\tau))u_i \\ -(\rho(\tau)+p(\tau))u_i & \delta p\,\delta_{ij} + \Sigma_{ij} \end{pmatrix}, \text{ with } \Sigma_{ii=0}, \tag{4.22}$$

where Σ_{ij} is related to σ as stated in Eq. (4.19). Note that δT^{μ}_{ν} denotes the perturbed stress-energy tensor of a *perfect fluid* in case the anisotropic stress in Eq. (4.22) vanishes.

Since we are interested in the evolution of the coupled neutrino and scalar field perturbations, let us in the following specify the components of the perturbed stress-energy tensor for a scalar field,

$$\delta T^0_0 = -\frac{1}{a^2}\dot{\phi}\delta\dot{\phi} - V'_{\phi}(\phi)\delta\phi, \quad \delta T^0_i = \frac{1}{a^2}\dot{\phi}\delta\phi_{,i}, \quad \delta T^i_j = \left[\frac{1}{a^2}\dot{\phi}\delta\dot{\phi} - V'_{\phi}(\phi)\delta\phi\right]\delta^i_j, \tag{4.23}$$

where primes denote derivatives with respect to ϕ ($' \equiv \partial/\partial\phi$), and the comma with space index means differentiation with respect to the corresponding coordinate ($_{,i} \equiv \partial/\partial x^i$). For completeness and for later reference, let us also quote the background part of the stress-energy tensor of the scalar field in terms of conformal time[6],

$$T^0_0(\tau) = \frac{1}{2a^2}\dot{\phi}^2(\tau) + V(\phi(\tau)) = \rho_\phi(\tau), \tag{4.24}$$

$$T^0_i(\tau) = 0, \tag{4.25}$$

$$T^i_j(\tau) = \left[\frac{1}{2a^2}\dot{\phi}^2(\tau) - V(\phi(\tau))\right]\delta^i_j = p_\phi(\tau)\delta^i_j. \tag{4.26}$$

After having the metric and the stress-energy tensor at hand, let us now see how the evolution equations for the matter perturbations can be derived. As we have discussed already in the introductory section, through the Bianchi identities, Einstein's equations implies the conservation of the total stress-energy tensor [89],

$$T^\mu_{\nu;\mu}(\vec{x},\tau) = 0. \tag{4.27}$$

Furthermore, the stress-energy tensor of each individual uncoupled fluid is separately conserved[7]. After plugging in the full stress-energy tensor T^μ_ν in k-space and then linearizing the equations, this implies for the $\nu = 0$ and $\nu = i$ component of the perturbed part of the stress-energy tensor, respectively,

$$\dot{\delta} = -(1+\omega)\left(\theta + \frac{\dot{h}}{2}\right) - 3\frac{\dot{a}}{a}\left(\frac{\delta p}{\delta\rho} - \omega\right)\delta, \tag{4.28}$$

$$\dot{\theta} = -\frac{\dot{a}}{a}(1-3\omega)\theta - \frac{\dot{\omega}}{1+\omega}\theta + \frac{\delta p/\delta\rho}{1+\omega}k^2\delta - k^2\sigma, \tag{4.29}$$

with σ as defined in Eq. (4.19) and Eq. (4.22). Furthermore, δ denotes the *'density contrast'*, which is the fractional departure of the density from the mean,

$$\delta(\vec{x},\tau) \equiv \frac{\rho(\vec{x},\tau) - \rho(\tau)}{\rho(\tau)} = \frac{\delta\rho(\vec{x},\tau)}{\rho(\tau)}, \tag{4.30}$$

and v_i is the *'divergence of the fluid velocity'*

$$\theta \equiv ik^i v_i. \tag{4.31}$$

As we will see in Sec. 4.4, the requirement of energy-momentum conservation between the neutrinos and the scalar field demands a modification of the form of the equations in Eqs. (4.28) – (4.29) which accounts for their interaction.

[6] See also Sec. 2.4, which assumes cosmic time as a time variable.
[7] For the unperturbed part of the stress-energy tensor see Sec. 2.4

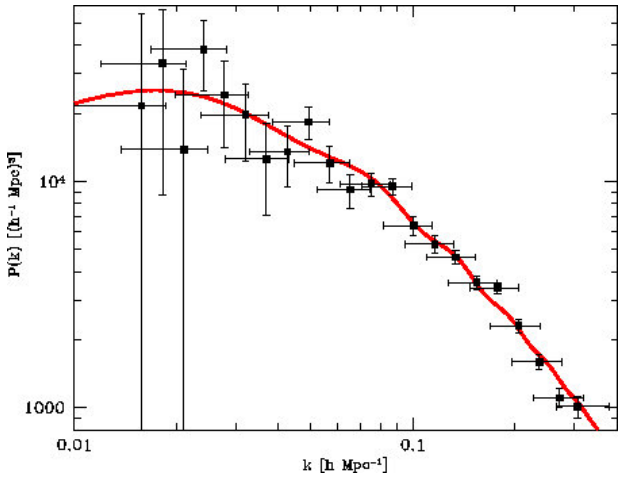

Figure 4.1: The measured power spectrum of $L*$ galaxies. The red curve is the best fit linear concordance model introduced in Sec. 2.4.

4.2.1 The Matter Power Spectrum

After having defined the evolution equation for matter perturbations in the last section, let us in the following briefly introduce the *matter power spectrum* for later reference in Sec. 4.5.2.

The matter power spectrum $P(k)$ is defined as the Fourier transform of the two-point correlation function $\xi(\mathbf{r})$ of non-relativistic matter density fluctuations $\delta = \frac{\delta\rho}{\rho}$,

$$\xi(\mathbf{r}) = \langle \delta(\mathbf{r}' + \mathbf{r}), \delta(\mathbf{r}) \rangle = \int \frac{\mathrm{d}^3 k}{(2\pi)^3} P(k) e^{i(\mathbf{k}/a)\cdot\mathbf{r}}, \tag{4.32}$$

where the average is taken over all $\mathbf{r}'$. This gives a measure for the likelihood of finding a density access at a physical distance $\mathbf{r}$ from a given density access. Accordingly, it is

$$P(k) \propto |\delta(k)|^2. \tag{4.33}$$

The present linear power spectrum is plotted in Fig. 4.1 (the plot is taken from [203]). Observationally, according to a simple analytical model of structure formation the power spectrum can be related to the galaxy-galaxy correlation function (cf. e.g. [5]).

4.2.2 Simple Example in Newtonian Theory

For the purpose of developing an intuition for the main physical effects leading to matter instabilities, let us start in this section by sketching the dynamics of hydrodynamic perturbations in Newtonian theory[8] (for references on this subject see e.g. [25, 98, 204]). In addition, this consideration will help to clarify under which conditions the adiabatic sound speed squared

[8] It should be noted that the validity of the Newtonian description in general is restricted to sub-Hubble scales at late times.

can fully determine the dynamics of hydrodynamic perturbations. In Sec. 4.4 it will turn out that in a more realistic treatment in the framework of General Relativity, along the lines of Sec. 4.2, for MaVaNs these conditions are not generally fulfilled.

Let us in the following assume for a moment the universe to be static, meaning non-expanding, solely filled with a *perfect fluid*, as introduced in Sec. 2.4. This approach will allow us to disentangle the different influences on the dynamics of hydrodynamic fluctuations in a matter species such as of the sound speed, the expansion of the universe and importantly, of other cosmic energy components emerging in the full treatment in Sec. 4.4. Afterwards it will be straightforward to understand the evolution equations for the MaVaN density contrast derived in Sec. 4.4 by linearizing Einstein's equations about an expanding background.

In the following, we describe gravity by the Newtonian gravitational potential Φ and the matter content of the universe by a single perfect fluid. As mentioned in Sec. 2.4, it is characterized by its density ρ, pressure p and velocity $\vec{v}$ (where the latter vanishes in the background). Furthermore, it is described by the continuity equation, Eulers's equations as well as the Possion equation of Newtonian gravity,

$$\begin{aligned} \dot{\rho} + \nabla(\rho\,\vec{v}) &= 0, \\ \dot{\vec{v}} + (\vec{v}\,\nabla)\vec{v} + \frac{1}{\rho}\nabla p + \nabla\Phi &= 0, \\ \nabla\Phi &= 4\pi G\rho. \end{aligned} \tag{4.34}$$

Perturbing the fluid variables about the (static) background ($\rho(\vec{x},t) = \rho(t) + \delta\rho(\vec{x},t)$, $p(\vec{x},t) = p(t) + \delta p(\vec{x},t)$, $\vec{v} = \delta\vec{v}(\vec{x},t)$, $\Phi(\vec{x},t) = \Phi(t) + \delta\Phi(\vec{x},t)$) and linearizing and combining the hydrodynamical equations in Eq. (4.34), for the k^{th} Fourier component of the matter perturbation,

$$\delta(\vec{x},t) = \int \frac{d^3k}{(2\pi)^3} e^{i\vec{k}\vec{x}}\delta_k(t), \tag{4.35}$$

one arrives at the following simple second order differential evolution equation[9],

$$\ddot{\delta}_k + (\underbrace{c_a^2 k^2}_{\text{pressure}} - \underbrace{4\pi G\rho}_{\text{gravity}})\,\delta_k = 0, \quad \text{where } \omega_k = \sqrt{c_a^2 k^2 - 4\pi G\rho}. \tag{4.36}$$

Here, $c_a^2 \equiv \dot{p}/\dot{\rho}$ denotes the adiabatic sound speed squared of the perturbations.

Let us in the following see, which basic conclusions we can draw from Eq. (4.36). Clearly, the evolution of the matter density contrast depends on the competition of the second and third term on the left hand side. Taking a closer look at them, we find that the third term represents the force due to gravity. According to Newton's second law it is,

$$\ddot{\delta\rho}_k \propto G\delta_k, \tag{4.37}$$

since a density excess δ_k, localized at some spacetime point $\vec{x}$, exerts a force $\propto \delta_k$ which attracts the surrounding matter towards $\vec{x}$. Due to the purely attractive nature of gravity, this

[9] As explained in the last section, in linear theory it is not necessary to keep the integration over the Fourier modes explicitly.

corresponds to an instability of flat-space time to the development of density perturbations. However, the second term on the left represents the counteracting force due to the fluid's pressure which in contrast tends to set up acoustic oscillations and inhibits the growth of instabilities. It should be noted that since we are considering a perfect fluid, the sound speed squared c_a^2 and accordingly the perturbations are purely adiabatic and thus $p = p(\rho)$. In the next section, we will extend the discussion to general fluids and will see how their perturbations can possibly be stabilized by non-adiabatic pressure[10].

Restricting our attention again to adiabatic perturbations we find that their evolution according to Eq. (4.36) depends on the sign of ω_k^2. One can define a critical scale, the *Jeans scale* $k_{\text{Jeans}} = \sqrt{4\pi G\rho/c_a^2}$, marking its sign change which depends on the magnitude of the sound speed squared and of the matter density. We can thus discriminate between perturbations with wavenumber

- $k \ll k_{\text{Jeans}}$ ($\omega_k^2 \ll 0$), whose dynamics are governed by gravity, $\delta_k \propto e^{\pm|\omega_k|t}$ with an exponentially growing solution (+)

- $k \gg k_{\text{Jeans}}$ ($\omega_k^2 \gg 0$), where pressure overcomes gravity and the modes oscillate $\delta_k \propto e^{\pm i\omega_k t}$ with $\omega_k \sim c_a k$.

Let us *summarize* what we have learned from the considered example of hydrodynamics matter perturbations of a single fluid in Newtonian theory in a static universe. We have seen that perfect fluids can only exhibit adiabatic perturbations characterized by an adiabatic sound speed squared. Furthermore, for a given background density of the fluid, the perturbation evolution can be directly inferred from the value of the fluid's sound speed squared. The larger it is, the shorter is the time scale, $\tau_{\text{pressure}} \simeq (kc_a)^{-1}$, associated with the response of the fluid's pressure which has to be compared with the dynamical time scale for gravitational collapse $\tau_{\text{grav}} = (\Im(\omega))^{-1} \simeq (4\pi G\rho)^{-1/2}$. Therefore, gravitational instabilities can only occur, if the time scale for gravitational collapse is shorter then the time scale for the 'pressure response'. Accordingly, the fluctuations in a single, non-interacting perfect fluid can only be stabilized against gravitational instability on scales, where the effects of the fluid's pressure can respond to the gravitational attraction and thus restore hydrostatic equilibrium.

In Sec. 4.4 we will perform a more realistic investigation of the evolution of cosmological perturbations by taking into account the effects of the expansion, the gravitational backreaction to metric perturbations and the stabilizing effect of the presence of non-adiabatic pressure. Our ultimate goal is to identify conditions for a stabilization of MaVaN perturbations on all physical scales due to a combination of these additional effects. Of particular relevance will be the gravitational backreaction effect which will turn out to allow other cosmic components to govern (and thus to stabilize) the dynamics of MaVaN perturbations, largely independent of the value of the MaVaN sound speed squared.

[10] Since it turns out that in general the pressure is not a unique function of the energy density, the general fluid's equation of state can exhibit spatial variations (in contrast to the adiabatic fluid).

4.3 The Nature of the Sound Speed Squared

In the last section, we have seen that in the case of an uncoupled perfect fluid the only growth slowing effect is provided by the fluid's pressure. Its relative influence is encoded in the sound speed squared which is thus a good quantity to fully characterize the dynamics of the perturbations.

Let us in this section discuss alternative processes which influence the nature of the sound speed squared and generally tend to inhibit the growth of perturbations. By these means we can already see that the occurrence of MaVaN instabilities depends on the nature of the sound speed squared and in accordance identify scales k and regimes where instabilities are generally precluded. For this purpose, we will proceed by defining the sound speed squared for a general fluid component labeled by i. It takes the following form,

$$c_{si}^2 = \frac{\delta p_i}{\delta \rho_i}, \tag{4.38}$$

where p_i and ρ_i denote the fluid's pressure and energy density, respectively. The sound speed c_{si}^2 can be expressed in terms of the sound speed c_{ai}^2 arising from purely adiabatic perturbations as well as from an additional entropy perturbation Γ_i and the density contrast $\delta_i = \delta\rho_i/\rho_i$ in the rest frame of the perturbations [205–207][11],

$$\begin{aligned} w_i \Gamma_i &= (c_{si}^2 - c_{ai}^2)\, \delta_i, & (4.39)\\ &= \frac{\dot{p}_i}{\rho_i}\left(\frac{\delta p_i}{\dot{p}_i} - \frac{\delta \rho_i}{\dot{\rho}_i}\right). & (4.40) \end{aligned}$$

Here w_i denotes the equation of state parameter and Γ_i is a measure for the relative displacement between hyper-surfaces of uniform pressure and uniform energy density. For most Dark Energy candidates (like quintessence or k-essence) dissipative processes evoke entropy perturbations and thus $\Gamma_i \neq 0$.

However, in contrast to adiabatic perturbations, entropy perturbations do not grow [98]. In general, the presence of dissipative processes stabilizes the perturbations in MaVaN and thus prevents the possible formation of non-linear structure in the neutrino density. Consequently, in the relativistic neutrino regime, on all sub-Hubble scales MaVaN perturbations are stabilized by the combined effects of the (non-adiabatic) pressure in neutrinos and the neutrino free-streaming [101] in the background spacetime arising from the large momentum of (sub-) eV mass neutrinos [208, 209]. However, when neutrinos turn non-relativistic, both the neutrino pressure and the free-streaming scale[12] of neutrinos drops. Accordingly, in this regime, the effective mass of the scalar field $\sim m_\phi \gg \mathcal{H}$ turns out to set the scales where MaVaN perturbations can possibly become unstable. More precisely, on scales $a/k \gtrsim m_\phi^{-1}$ the gradient terms in Eq. (4.39) become unimportant and thus the sound speed becomes adiabatic [57, 210] (for an analytical derivation see [211, 212]).

[11] Note that for $c_{si}^2 > 0$ non-adiabatic pressure support is obtained, which can apparently stabilize the perturbations, since $w_i\Gamma_i \propto \delta_i$ [205].

[12] It corresponds to the typical distance neutrinos can propagate in a Hubble time in the background space-time due to their mean thermal velocity [208, 209].

As an important difference to a quintessence field with finely-tuned mass $\lesssim \mathcal{H}$ and long range $\gtrsim \mathcal{H}^{-1}$, the Compton wavelength of the scalar field m_ϕ^{-1} in the MaVaN scenario is much smaller than the Hubble radius. While this certainly is desirable to make the scalar field more plausibly stable against radiative corrections, as a direct consequence, on sub-Hubble scales $a/k > m_\phi^{-1}$ all dynamical properties of (non-relativistic) MaVaNs are set by the local neutrino energy density [57]. In particular, for small deviations away from the minimum of its effective potential, the scalar field re-adjusts to its new minimum on time scales $\sim m_\phi^{-1}$ small compared to the characteristic cosmological time scale $\mathcal{H}^{-1}$. Accordingly, on these scales $m_\phi^{-1} < a/k < \mathcal{H}^{-1}$, the hydrodynamic perturbations in MaVaNs are adiabatic and can thus possibly grow (cf. the discussion in the last section, the pressure is a unique function of the energy density). Therefore, to analyze the stability of a given model, in the following, we will concentrate on the adiabatic regime of perturbations in the non-relativistic neutrino regime. This implies that the system of non-relativistic neutrinos and the scalar field can be treated as a unified fluid with pressure $p_{DE} = p_\nu + p_\phi$ and energy density $\rho_{DE} = \rho_\nu + \rho_\phi$ without intrinsic entropy, $\Gamma_{DE} = 0$.

As it will turn out later on, the influence of the cosmic expansion in combination with the gravitational drag exerted by CDM on the neutrinos can have a major influence on the stability of a MaVaN model. However, let us inquire in the following whether in the absence of any growth-slowing effects there is still the possibility that the MaVaN scenario does not become unstable in the adiabatic regime of perturbations. Let us for this purpose see how the requirement can be met that the perturbations are characterized by a positive adiabatic sound speed squared,

$$c_a^2 = \frac{\dot{P}_{\rm DE}}{\dot{\rho}_{DE}} = \frac{\dot{w}\rho_{DE} + w\dot{\rho}_{DE}}{\dot{\rho}_{DE}} = w - \frac{\dot{w}}{3\mathcal{H}(1+w)} > 0, \tag{4.41}$$

which follows from the requirement of energy conservation and from Eq. (4.40). In the case $c_a^2 > 0$ the attractive scalar force will be offset by pressure forces and the fluctuations will thus oscillate as sound waves and therefore not grow (cf. the discussion in the last section).

After generalizing the above treatment to include three neutrino generations, it can be shown [60] that the requirement of positive sound speed squared in Eq. (4.41) leads to the following stability condition on the mass evolution for $m_{\nu_i}(a) \gg T_\nu(a)$ with $i = 1, 2, 3$,

$$\sum_{i=1}^{3} \frac{\partial m_{\nu_i}(a)}{\partial a} a^2 \left(\frac{5\alpha T_{\nu_0}^2(a)}{3m_{\nu_i}^2(a)} - 1 \right) + \sum_{i=1}^{3} \frac{25\alpha T_{\nu_0}^2(a)}{3a m_{\nu_i}(a)} > 0, \text{ with}$$

$$\alpha \equiv \frac{\int_0^\infty \frac{dy\, y^4}{e^y+1}}{2\int_0^\infty \frac{dy\, y^2}{e^y+1}} \simeq 6.47. \tag{4.42}$$

We would like to point out that under the assumption of a degenerate neutrino mass spectrum with $m_{\nu_i}(z) \sim m_\nu(z)$, we can solve the resulting first order differential equation in $m_\nu(z)$ for the maximally allowed mass evolution in an adiabatic MaVaN model with positive sound speed squared. In Fig. 4.2 the solution $m_\nu(z)$ is plotted for $m_{\nu_i}(0) \sim m_\nu(0) = 0.312$ eV. We find that

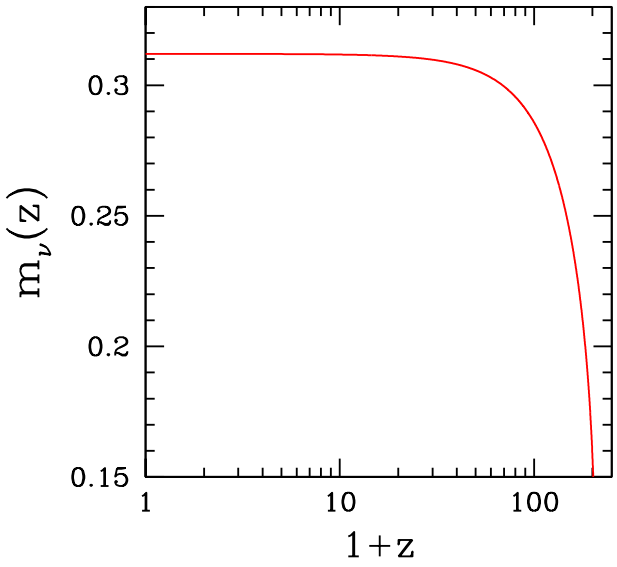

Figure 4.2: Maximally allowed mass evolution in a model with positive sound speed squared for a degenerate neutrino mass spectrum with $m_{\nu_i}(0) \sim m_\nu(0) = 0.312$ eV, where $i = 1, 2, 3$.

in case the perturbations are not stabilized by growth-slowing effects to be discussed later on, the condition of positive sound speed squared severely constrains the allowed neutrino mass variation at late times, where finite temperature effects become less important. This can also be understood from an intuitive argument. Namely, in order to achieve a large neutrino mass variation, the scalar field has to transfer a substantial amount of energy to the neutrinos. However, as a consequence of the increase in the mass of the neutrinos, also the attraction felt between neutrinos rises. This favors the growth of instabilities as reflected by a negative sound speed squared.

In the following we will argue that this result remains valid in the case of a hierarchical neutrino mass spectrum independent of the absolute neutrino mass scale. Therefore, let us consider two different scenarios possibly realized in nature. Either all neutrinos are (highly) non-relativistic today such that Eq. (4.42) is applicable which requires that all the neutrino masses are essentially constant at late times. Or, as allowed by neutrino oscillation experiments, one neutrino mass eigenstate is still relativistic today. It has been shown for a large class of MaVaN models that this case can only be realized if the heaviest, non-relativistic neutrino is stable [59]. Otherwise, the scalar field VEV and thus the neutrino masses are driven to a new scale such that none of the neutrinos remains relativistic until today. This results in a cascaded instability of the system because all components become unstable at nearly the same time.

Possible alternative scenarios are so-called hybrid MaVaN models which involve a second light scalar field [22, 59]. Since they allow for a steeper scalar potential, while accomplishing late-time acceleration, they can be stable even in the presence of an unstable component until the present time. One such stable and thus viable example was discussed in Sec. 3.1, where the lightest neutrino was assumed to be still relativistic today.

Consequently, at least in the class of models possibly subject to a cascaded instability, the stability condition requires the mass of the heaviest, non-relativistic neutrino to be essentially constant at late times. Therefore, in the case that all neutrino masses have the same dependence on the scalar field value and thus on cosmic time, their mass variation is likewise restricted.

Let us note again, for simplicity, in the following stability analysis we will assume a degenerate neutrino mass spectrum corresponding to three highly non-relativistic neutrinos today. However, largely independent of the absolute scale and spectrum of neutrino masses our results can be generalized to apply for all standard MaVaN models possibly subject to a cascaded instability.

4.4 How to Stabilize Mass Varying Neutrino Instabilities

In this section we will analyze the linear MaVaN perturbations in k-space in the synchronous gauge as introduced in Sec. 4.2, which is characterized by a perturbed line element of the form stated in Eq. (4.17) in Sec. 4.2. Let us note, that for simplicity, here and in the following we will suppress the time dependence of ρ and other background quantities (cf. the discussion in Sec. 4.2).

As mentioned in Sec. 2.4 and Sec. 4.2, in contrast to essentially uncoupled cosmic components, the stress-energy tensor T^{μ}_{γ} of neutrinos is not separately conserved in the presence of an interaction with a scalar field [44, 213]. One finds,

$$T^{\mu}_{\gamma;\mu} = \frac{d\log m_\nu}{d\phi}\phi_{,\gamma}\, T^{\mu}_{\mu}, \tag{4.43}$$

where the term on the right hand side takes account of the non-standard interaction with ϕ. Accordingly, the fluid perturbation equations stated in Eqs. (4.28) – (4.29) in Sec. 4.2 are augmented by terms which depend on the scalar field perturbations $\delta\phi$. Namely, from the $\gamma = 0$ component of Eq. (4.43) it follows,

$$\begin{aligned}\dot{\delta}_\nu &= 3\left(\mathcal{H}+\beta\dot{\phi}\right)\left(w_\nu - c_\nu^2\right)\delta_\nu - (1+w_\nu)\left(\theta_\nu + \frac{\dot{h}}{2}\right) \\ &+ \beta\,(1-3w_\nu)\,\delta\dot{\phi} + \beta'\dot{\phi}\delta\phi\,(1-3w_\nu)\,,\end{aligned} \tag{4.44}$$

where $\beta = \frac{d\log m_\nu}{d\phi}$ and $c_\nu = \delta p_\nu/\delta\rho_\nu$ is the neutrino sound speed (cf. Eq. (4.38)). Note that it can directly be calculated from the sound speed of the combined fluid and the scalar field perturbations.

Furthermore, the trace of the metric perturbation, $h \equiv \delta^{ij}h_{ij}$, according to the linearized

Einstein equations satisfies [89],

$$\ddot{h} + \mathcal{H}\dot{h} = \frac{a^2}{M_{\rm pl}^2}[\delta T_0^0 - \delta T_i^i], \text{ where} \tag{4.45}$$

$$\delta T_0^0 = -\frac{1}{a^2}\dot{\phi}\delta\dot{\phi} - V_\phi'(\phi)\delta\phi - \sum_m \rho_m \delta_m, \tag{4.46}$$

$$\delta T_i^i = \frac{3}{a^2}\dot{\phi}\delta\dot{\phi} - 3V_\phi'(\phi)\delta\phi + \sum_r \rho_r\delta_r + 3c_b^2\rho_b\delta_b + 3c_\nu^2\rho_\nu\delta_\nu, \tag{4.47}$$

where the last two equations can be derived by taking Eq. (4.23) in Sec. 4.2 into account. Note that δT_ν^μ denotes the total perturbed stress-energy tensor and the subscripts m and r collect neutrinos, radiation, CDM and baryons (with sound speed c_b) as well as (relativistic) neutrinos and radiation, respectively.

The evolution equation for the neutrino velocity perturbation $\theta_\nu \equiv ik_i v_\nu^i$ with $v_\nu^i \equiv dx^i/d\tau$ reads,

$$\begin{aligned}\dot{\theta}_\nu &= -\mathcal{H}(1-3w_\nu)\theta_\nu - \frac{\dot{w}_\nu}{1+w_\nu}\theta_\nu + \frac{c_\nu^2}{1+w_\nu}k^2\delta_\nu \\ &+ \beta\frac{1-3w_\nu}{1+w_\nu}k^2\delta\phi - \beta(1-3w_\nu)\,\dot{\phi}\,\theta_\nu - k^2\sigma_\nu,\end{aligned} \tag{4.48}$$

where σ_ν denotes the neutrino shear introduced in the last section, which is suppressed in the non-relativistic neutrino regime [89].

Finally, the perturbed Klein-Gordon equation for the coupled scalar field is given by [44]

$$\ddot{\delta\phi} + 2\mathcal{H}\dot{\delta\phi} + \left[k^2 + a^2\left\{V_\phi'' + \beta'(\rho_\nu - 3p_\nu)\right\}\right]\delta\phi + \frac{1}{2}\dot{h}\dot{\phi} = -a^2\beta\delta_\nu\rho_\nu(1-3c_\nu^2). \tag{4.49}$$

We note that instead of proceeding via the fluid equations, Eqs. (4.44) and (4.48), the evolution of the neutrino density contrast can be calculated from the Boltzmann equation [89]. We have verified analytically and numerically that the two methods yield the same results provided that the scalar-neutrino coupling is appropriately taken account of in the Boltzmann hierarchy [214].

As discussed in Sec. 4.3, MaVaNs models can only possibly become unstable on sub-Hubble scales $m_\phi^{-1} < a/k < \mathcal{H}^{-1}$ in the non-relativistic regime of the neutrinos, where the perturbations evolve adiabatically. For our numerical results in the next section we solve the coupled Eqs. (4.44) – (4.49) in the (quasi-)adiabatic regime by neglecting the neutrino shear σ_ν. As we have checked by the help of the Boltzmann treatment mentioned above, this approximation is justified, since the shear is generally suppressed in the non-relativistic neutrino regime, where m_ν is much larger than the mean momentum of the neutrino distribution. In addition, this effect is amplified by the presence of a strong coupling [89].

For the purpose of gaining further analytical insight into the evolution of the neutrino density contrast, it is instructive to apply additional approximations to Eqs. (4.44) – (4.49) to be justified in the following.

Since the minimum of the effective potential tracked by the scalar field evolves only slowly due to changes in the neutrino energy density, we can safely ignore terms proportional to $\dot{\phi}$. Moreover, in the non-relativistic regime of the neutrinos on scales $m_\phi^{-1} < a/k < \mathcal{H}^{-1}$, as a consequence of $p_\nu \sim 0$ it follows that $\sigma_\nu \sim 0$ and $w_\nu \sim 0$ as well as $\rho_r \sim c_b^2 \sim 0$. In addition, in the following we substitute $\delta\phi$ by its average value corresponding to the forcing term on the right hand side of Eq. (4.49) in the above limits,

$$\delta\bar{\phi} = -\frac{\beta\rho_\nu\delta_\nu(1-3c_\nu^2)}{(V_\phi'' + \rho_\nu\beta') + \frac{k^2}{a^2}}, \tag{4.50}$$

which solves the perturbed Klein-Gordon equation reasonably well on all scales [213, 215]. Finally, by combining the derivative of Eq. (4.44) with Eqs. (4.45) – (4.48) and Eq. (4.50) in the non-relativistic limit, we arrive at the equation of motion for the neutrino density contrast valid at late times on length scales $m_\phi^{-1} < a/k < \mathcal{H}^{-1}$ for $c_\nu \ll 1$,

$$\ddot{\delta}_\nu + \mathcal{H}\dot{\delta}_\nu + \left(c_\nu^2 k^2 - \frac{3}{2}\mathcal{H}^2\Omega_\nu\frac{G_{\rm eff}}{G}\right)\delta_\nu = \frac{3}{2}\mathcal{H}^2\left[\ \Omega_{\rm CDM} + \Omega_b\ \right]\delta_{\rm CDM} \tag{4.51}$$

where,

$$G_{\rm eff} = G\left(1 + \frac{2\beta^2 M_{\rm pl}^2}{1 + a^2\{V_\phi'' + \rho_\nu\beta'\}/k^2}\right) \text{ and} \tag{4.52}$$

$$\Omega_i = \frac{a^2\rho_i}{3\mathcal{H}^2 M_{\rm pl}^2}. \tag{4.53}$$

Since deep in the matter dominated regime the baryon density contrast has caught up with that of CDM, we have used $\delta_b = \delta_{\rm CDM}$. Note that this equation is of a similar form as Eq. (4.36) in Sec. 4.2.2 (taking into account that $4\pi G\rho a^2 = 3/2\mathcal{H}^2$), however, it is amended by two terms. Firstly, there is a friction term $\propto \mathcal{H}$ due to cosmic expansion which would moderate an exponential growth of perturbations to take a power law form. Secondly, most importantly, as we will see in the following, an additional source term is present which describes the gravitational effect on the MaVaN perturbations exerted by other important cosmic components, namely CDM and baryons.

Let us also note that since neutrinos not only interact through gravity, but also through the force mediated by the scalar field, they feel an effective Newton's constant $G_{\rm eff}$ as defined in Eq. (4.52). The force depends upon the MaVaN model specific functions β and V_ϕ and takes values between G and $G(1 + 2\beta^2 M_{\rm pl}^2)$ on very large and small length scales, respectively. The scale dependence of $G_{\rm eff}$ is due to the finite interaction range of the scalar field $(V_\phi'' + \rho_\nu\beta')^{-\frac{1}{2}}$. Accordingly, in a MaVaN model both, the scalar potential V_ϕ and the coupling β influence the range of the scalar field force felt by neutrinos, whereas its strength is determined by the coupling β.

Let us now have a closer look at the right hand side of the Eq. (4.51). The forcing term encodes

the effect of the perturbations in other cosmic components on the dynamics of the neutrino density contrast and apparently competes with the scalar field dependent term $\propto \frac{G_{\rm eff}}{G}\Omega_\nu\delta_\nu$ on the left hand side of Eq. (4.51). Correspondingly, apart from the scalar field mediated force the neutrinos feel the gravitational drag exerted by the potential wells formed by CDM. Consequently, as long as the coupling function β does not compensate for the relative smallness of Ω_ν and thus enlarges the influence of the term $\propto \frac{G_{\rm eff}}{G}\Omega_\nu\delta_\nu$, the neutrinos will follow CDM (like baryons) just as in the standard cosmological model, since the influence of the scalar field is subdominant $|-3/2\mathcal{H}^2 G_{\rm eff}/G\Omega_\nu| \ll 3/2\mathcal{H}^2(\Omega_{\rm CDM}+\Omega_b)$.

Accordingly, as the **central result** of this section, the *stability condition* is found to translate into an upper bound on the scalar-neutrino coupling,

$$\beta < \sqrt{\frac{\Omega_{\rm CDM}+\Omega_b-\Omega_\nu}{2M_{\rm pl}^2\Omega_\nu}}. \tag{4.54}$$

Accordingly, we find that as a direct consequence of the relative smallness of the neutrino masses, due to which neutrinos provide a much smaller fraction to the total energy density than CDM and baryons, $\Omega_\nu \ll (\Omega_{\rm CDM}+\Omega_{\rm b})$, in principle the coupling can be much stronger than of gravitational strength $\beta \gg 1/M_{\rm pl}$. More precisely, whereas $\Omega_{\rm CDM}\sim 0.22$ and $\Omega_{\rm b}\sim 0.044$ at present (cf. Sec. 2.4), Ω_ν depends on the so far not known absolute neutrino mass scale realized in nature (cf. the discussion in Sec. 2.6.4). Taking as a lower bound the mass splitting deduced from atmospheric neutrino flavor oscillation experiments (stated in Sec. 2.6.3) and the upper bound derived from tritium beta-decay experiments (as stated in Sec. 2.6.4), we get $7\times 10^{-4} \lesssim \Omega_\nu \lesssim 0.12$ today [13].

Consequently, depending on the actual neutrino mass scale realized in nature, according to current experimental data the scalar-neutrino coupling in principle could take values[14],

$$1M_{\rm pl}^{-1} \lesssim \beta \lesssim 14M_{\rm pl}^{-1}. \tag{4.55}$$

It is important to note that since in the standard MaVaN scenario the neutrino mass is an increasing function of time, at earlier times the ratio $\Omega_\nu/(\Omega_{\rm CDM}+\Omega_{\rm b})$ was even more suppressed than today. In general, it follows that the smaller this ratio is, the larger becomes the relative influence of the forcing term on the right hand side of Eq. (4.51) and therefore its stabilizing effect on the perturbations.

However, let us stress again that independent of the absolute neutrino mass scale realized in nature, we found that the coupling can be at least of gravitational strength $O(1/M_{\rm pl})$. It should be noted for comparison that the evolution of perturbations in cold dark matter (CDM) coupled to a light scalar field in coupled quintessence [215] and chameleon cosmologies [216] is governed by an equation similar to Eq. (4.51). However, we would like to point out that

[13] Note that if the upper limit from the Mainz experiment is saturated, the requirement $\Omega_\nu \ll \Omega_{\rm CDM}$ is formally not satisfied. However, this case should be viewed as very extreme and is most likely excluded based on structure formation arguments.

[14] It should be noted that in case a very low neutrino mass scale is realized in nature, models not possibly subject to a cascaded instability (as defined in Sec. 4.3) can be stabilized by the pressure in a relativistic neutrino and therefore are not required to fulfill the following condition in order to be stable, see Sec. 3.1.

for the same coupling functions the dynamics of the perturbations in neutrinos can be quite different from those in coupled CDM as a direct consequence of the relative smallness of neutrino masses.

Based on the result in Eq. (4.54), in the following we classify the behavior of the neutrino density contrast in models of neutrino Dark Energy subject to all relevant kinds of coupling functions β. In the small-scale limit we distinguish the following three cases

a) For $\beta < \sqrt{\frac{\Omega_{\rm CDM}+\Omega_b-\Omega_\nu}{2M_{\rm pl}^2\Omega_\nu}}$ until the present time, $G_{\rm eff}\Omega_\nu\delta_\nu < G\Omega_{\rm CDM}\delta_{\rm CDM}$, the neutrino density contrast is stabilized by the CDM source term which dominates its dynamics. In this case the influence of the scalar field on the perturbations is subdominant and the density contrast in MaVaNs grows moderately just like gravitational instabilities in standard uncoupled neutrinos.

b) For $\beta \sim$ const. and much larger than all other parameters at late times, $G_{\rm eff} \gg G$, the damping term $\mathcal{H}\dot{\delta}_\nu$ in Eq. (4.51) as well as the terms proportional to $\delta_{\rm CDM}$ can be neglected, leading to exponentially growing solutions.

c) For $\beta \neq$ const. and growing faster than all other parameters at late times, $G_{\rm eff} \gg G$, δ_ν is growing faster than exponentially[15].

In contrast, on scales $(V_\phi'' + \rho_\nu\beta')^{-1/2} \ll a/k < \mathcal{H}^{-1}$ much larger than the range of the ϕ-mediated force,

d) For $\beta \sim$ const. and of moderate strength, $G_{\rm eff} \sim G$ and the perturbations behave effectively like perturbations for uncoupled fluids in General Relativity.

e) For β growing faster than all other quantities at late times, $G_{\rm eff} \gg G$, instabilities develop on all sub-Hubble scales $a/k > (V_\phi'' + \rho_\nu\beta')^{-1/2}$ according to c). However, on large length scales their growth rate is suppressed due to the corresponding small wave number k.

We note that we can directly compare our results with the findings stated in Ref. [57] by recasting Eq. (4.51) for $c_\nu^2 \ll 1$ and $m_\phi^{-1} \lesssim a/k \lesssim \mathcal{H}^{-1}$ into the simple form,

$$\ddot{\delta}_\nu + \mathcal{H}\dot{\delta}_\nu + \left[\frac{c_a^2}{c_a^2+1}k^2 - \frac{3}{2}\mathcal{H}^2\Omega_\nu\right]\delta_\nu = \frac{3}{2}\mathcal{H}^2\left[\ \Omega_{\rm CDM} + \Omega_b\ \right]\delta_{\rm CDM}. \tag{4.56}$$

Apparently, as a consequence, all the effects of the scalar-neutrino coupling on the evolution of δ_ν are encoded in the term governed by the total adiabatic sound speed squared c_a^2 as defined in Eq. (4.41) in the last section and in addition, one recovers an ordinary gravitational term for neutrinos $\propto \delta_\nu$. Clearly, as soon as c_a^2 turns negative (but > -1), the term $\propto k^2$ will change its sign and thus also its nature. Namely, it will amplify the effect of the gravitational

[15] In the limit $\beta(\tau) \to \infty$ for $\tau \to \infty$, Eq. (4.51) takes the form $\ddot{\delta}_\nu - 3\mathcal{H}^2\Omega_\nu\frac{\beta^2(\tau)M_{\rm pl}^2}{1+a^2(V_\phi''+\rho_\nu\beta')/k^2}\delta_\nu = 0$, and it can be shown that $|\frac{\dot{\delta}_\nu}{\delta_\nu}| \to \infty$ for $\tau \to \infty$ [217]. Since this ratio is constant and thus not large enough for an exponentially growing δ_ν, the solution is required to grow faster than exponentially.

term for neutrinos $\propto \delta_\nu$, which tends to drive instabilities to grow (cf. also the discussion in Sec. 4.2.2). However, by approximating $\delta_\nu \sim \delta_{\rm CDM}$, we find that as long as on a scale $k < m_\phi$ at present the following relation holds[16],

$$\frac{|c_a|}{\sqrt{c_a+1}} \lesssim \sqrt{\frac{3}{2}}\frac{\mathcal{H}}{k}\sqrt{\Omega_{\rm CDM}+\Omega_b+\Omega_\nu} \tag{4.57}$$

until today the MaVaN perturbations will be stabilized by CDM which governs the dynamics (cf. *a*)), largely independent of the sign of the sound speed squared. Therefore, *only* in case the stabilizing effect of CDM on the neutrino perturbations becomes negligible, i.e. if Eq. (4.57) does not hold anymore, the negative sign of the sound speed squared can indicate a strong growth of the neutrino density contrast (cf. *b*),*c*)), which was not noted in Ref. [57]. Note also that the stability condition in Eq. (4.57) becomes easier to fulfill, the larger the scale k is. This again demonstrates that if instabilities occur, the phenomenon is of a rather *local* nature (cf. the discussion in Sec. 4.6.1).

4.5 Representative Examples

4.5.1 Significant Potentials and Couplings

In the following, we consider two combinations of scalar potentials $V_\phi(\phi)$ and of scalar-neutrino couplings β which define representative MaVaN models and comply with the requirements discussed in Sec. 4.1. The potentials are chosen to accomplish the correct cosmology and for the time dependence of the couplings we take meaningful limiting cases.

Firstly, we consider a MaVaN model suggested by [21] which we will refer to as the *log-linear model*. The scalar field has a Coleman-Weinberg type [218] logarithmic potential,

$$V_\phi(\phi) = V_0\,\log(1+\kappa\phi), \tag{4.58}$$

where the constants V_0 and κ are chosen appropriately to yield $\Omega_{\rm DE} \sim 0.7$ and $m_\phi \gg \mathcal{H}$ today.

Furthermore, the neutrino mass m_ν is assumed to be inversely proportional to ϕ,

$$m_\nu(\phi) = \frac{\bar{m}^2}{\phi}. \tag{4.59}$$

Such a dependence naturally emerges in the framework of the see-saw mechanism [32–35]. As discussed in Sec. 3.1, in this case the light neutrino mass m_ν arises from integrating out a heavier sterile state, whose mass varies linearly with the value of the scalar field (as employed e.g. in Refs. [21, 57, 59]).

According to Eq. (4.4) in Sec. 4.1 the combined potential V_ϕ, composed of the neutrino density ρ_ν and V_ϕ, determines the evolution of ϕ as plotted in the left panel of Fig. 4.3. It is illustrated

[16] Note that in order for a model to be stable on all scales, the relation has to be satisfied for $k = m_\phi$. Note also that for a given c_a, the following equation expressed as equality defines a sort of Jeans scale $k_{\rm Jeans}$ which separates the stable and unstable regime of perturbations (cf. the discussion in Sec. 4.2.2).

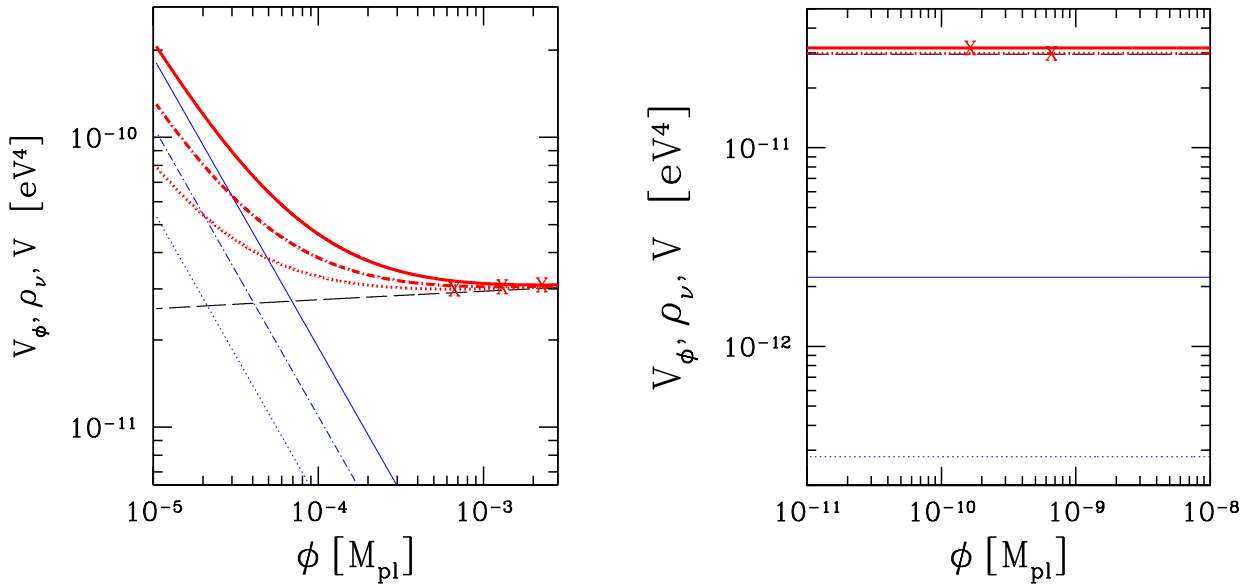

Figure 4.3: The effective potential V (thick lines), composed of the scalar potential V_ϕ (dashed) and the neutrino energy density ρ_ν. *Left*: Logarithmic potential of Eq. (4.58) plotted for three different redshifts, $z = 5$ (solid), $z = 4$ (dashed-dotted), $z = 3$ (dotted). The VEV of ϕ tracks the minimum of V (marked by X) and evolves to smaller values for decreasing redshift. *Right*: Power law potential of stated in Eq. (4.61) plotted for two different redshifts, $z = 1$ (solid), $z = 0$ (dotted), ϕ evolves to larger values for decreasing redshift.

that the competition of the two terms results in a minimum of V at an intermediate value of ϕ, which slowly evolves due to changes in the neutrino energy density. As the universe expands and ρ_ν dilutes, both the minimum and the scalar field are driven to smaller values towards zero.

According to Eq. (4.59) this model is characterized by a field dependent coupling,

$$\beta(\phi) = \frac{1}{m}\frac{\partial m}{\partial \phi} = -\frac{1}{\phi}. \tag{4.60}$$

Since the value of ϕ decreases with time (cf. Fig. 4.3) this means that the rate of energy transfer between the scalar field and the neutrinos and also the attraction felt between neutrinos increases with time. Consequently, both the neutrino mass m_ν in Eq. (4.59) and thus also the energy density in the non-relativistic neutrinos, $\rho_\nu \simeq m_\nu n_\nu$, blow up when ϕ approaches zero. Thus, from these qualitative considerations it can already be expected that the model will run into stability problems in the non-relativistic neutrino regime.

Let us now consider a second set-up proposed in the context of chameleon cosmologies [216, 219], which we will refer to as the *power-model*. The scalar field has an exponential potential which at late times reduces to an inverse power-law potential,

$$V_\phi = M^4 \exp\frac{M^n}{\phi^n} \sim M^4\left(1 + \frac{M^n}{\phi^n}\right), \tag{4.61}$$

since then $\phi \gg M$. Furthermore, the mass parameter M is fixed by the requirements $\Omega_{DE} \sim 0.7$ and $m_\phi \gg \mathcal{H}$. In the right panel of Fig. 4.3 the evolution of ϕ is plotted. In contrast to the first model, the expectation value of ϕ is increasing with time. Note that the scalar potential V_ϕ thus at late times very weakly depends on changes in the VEV of ϕ, since $V_\phi \sim M^4 = \text{const.}$ for $\phi \gg M$.

In this model the dependence of the neutrino mass on the scalar field is taken to be,

$$m_\nu = \bar{m} e^{\beta\phi}, \tag{4.62}$$

which is of a form expected in a special type of scalar-tensor theory, in which the scalar degree of freedom only couples to neutrinos in a conformal way (as e.g.. in [44]). It is important to note that for this model the coupling is constant,

$$\beta = \frac{1}{m_\nu}\frac{\partial m_\nu}{\partial \phi} = \text{const.} \tag{4.63}$$

Since according to Fig. 4.3 $\phi \ll 1$ until the present time, even for $\beta \gg \frac{1}{M_{\rm pl}}$ the exponential function in Eq. (4.63) takes values close to 1. Accordingly, the neutrino mass in Eq. (4.62) depends only weakly on changes in the scalar field VEV and thus hardly evolves with time. In contrast to the log-linear model the effective potential V in Fig. 4.3 only evolves due to the dilution of the neutrino energy density and not additionally due to the mass variation. Furthermore, unlike the log-linear model, the attractive force between neutrinos is essentially time independent in favor of the stability of the scenario.

4.5.2 Stable and Unstable Scenarios – Numerical Results

In this section we present the numerical results of our stability analysis for the two MaVaN models introduced in the last section. They are obtained from modifying the CMBFAST code [202] to include a light scalar field coupled to neutrinos and were checked by altering the CAMB code [220] accordingly. We assume a neutrino energy density of $\Omega_\nu \sim 0.02$, which corresponds to the energy density in three neutrino species with degenerate mass $m_{\nu_i}(z = 0) \sim 0.312\,\text{eV} \gg T_{\nu_0}$ being highly non-relativistic today. It should be noted that this roughly corresponds to the current conservative upper limit on the sum of neutrino masses (~ 1 eV, cf. Sec. 2.6.4) from CMB and Large Scale Structure data [6, 129, 134] [17].

Log-Linear Model

The log-linear model is defined by Eq. (4.58) and Eq. (4.59). By adjusting the parameter V_0 for a fixed value of $\kappa = 10^{20} M_{\rm pl}^{-1}$ in Eq. (4.58), standard cosmology (cf. Sec. 1) at present can be accomplished, where $\Omega_{\rm DE} = \Omega_\nu + \Omega_\phi$. This model will serve to illustrate the occurrence of instabilities.

[17] Note that those constraints were obtained assuming non-interacting neutrino models. Hence this assumption could be relaxed.

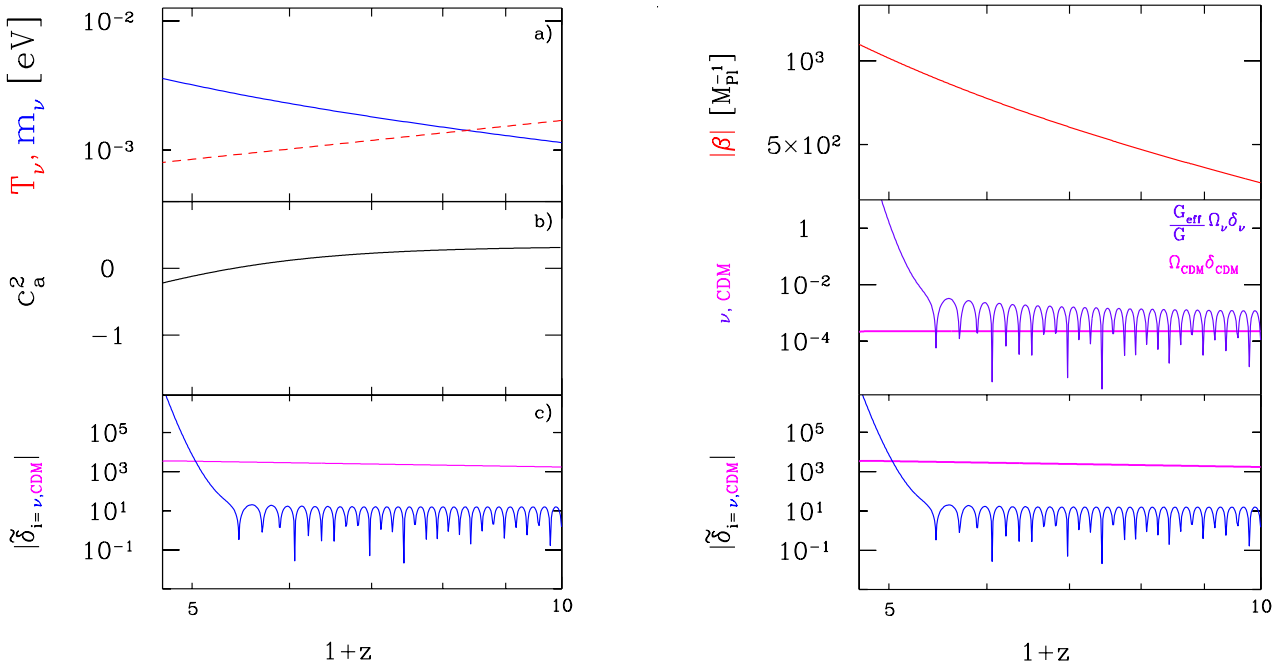

Figure 4.4: *Left: a)* Neutrino mass m_ν (solid) and temperature T_ν (dotted) as a function of redshift. *b)* Adiabatic Dark Energy sound speed squared c_a^2 as a function of redshift. *c)* (Unnormalized) density contrast in neutrinos (solid) $\tilde{\delta}_\nu$ and for comparison in CDM $\tilde{\delta}_{\rm CDM}$ (dash-dotted) as a function of redshift on a scale $k = 0.1\,{\rm Mpc}^{-1}$. *Right: a)* Scalar-neutrino coupling which increases for decreasing redshift. *b)* Comparison of the scalar field dependent term $G_{\rm eff}/G\Omega_\nu\delta_\nu$ and the CDM term $\propto \Omega_{\rm CDM}\delta_{\rm CDM}$ from Eq. (4.51). *c)* (Unnormalized) density contrast in neutrinos (solid) $\tilde{\delta}_\nu$ and in CDM $\tilde{\delta}_{\rm CDM}$ (dash-dotted) (cf. left panel)

The mass of ϕ at present determined from Eq. (4.6) is $m_\phi \gg \mathcal{H}$. Consequently, as discussed in Sec. 4.3, the Compton wavelength of the scalar field, m_ϕ^{-1}, sets the scales on which the perturbations in (non-relativistic) MaVaNs are adiabatic and thus can possibly become unstable at present, $\mathcal{H} \ll k \lesssim 0.1\,{\rm Mpc}^{-1}$ (cf. the discussion in Sec. 4.3). In Fig. 4.4 we present our results for the evolution of the neutrino mass, the adiabatic sound speed squared and the density contrast to be discussed in the following.

a) The evolution of the neutrino mass $m_\nu(z)$ and the neutrino temperature $T_\nu(z) = T_{\nu_0}(1+z)$ is plotted as a function of redshift. As long as $m_\nu(z) \ll T_\nu(z)$, the neutrinos are relativistic, whereas for $m_\nu(z) \gg T_\nu(z)$ they have turned non-relativistic. The transition takes place at roughly $z+1 \sim 7$, i.e. when $m_\nu(z) \simeq T_\nu(z)/3$. One interesting feature is that for $z \to 0$ the neutrino mass grows as $m_\nu(z) \propto a^3$ so that $\rho_\nu \to$ const..

b) A plot of the total adiabatic sound speed squared of the coupled fluid c_a^2. It decreases when the neutrinos approach the non-relativistic regime $m_\nu(z) \gg T_\nu(z)$(cf. *a)*). This is due to the drop in the neutrino pressure from initially $p_\nu \sim 1/3$ to $p_\nu \sim 0$ well after the transition of regimes.

c) A plot of the (unnormalized) density contrast in neutrinos $\tilde{\delta}_\nu$, and for reference in cold dark matter (CDM) $\tilde{\delta}_{\rm CDM}$ on a scale of $k = 0.1$ Mpc^{-1}. As long as the neutrinos are

still relativistic ($m_\nu(z) \ll T_\nu(z)$ cf. a)), the perturbations in the strongly coupled scalar-neutrino fluid oscillate like sound waves. However, after the non-relativistic transition, $m_\nu(z) > T_\nu(z)/3$, the neutrino pressure support drops and cannot offset the attractive force anymore to stabilize the perturbations. At the same time, the neutrino mass rises rapidly, thus as a result of both, the total sound speed squared is quickly driven to negative values as demonstrated in the left panel of Fig. 4.4 b). Finally, after the effective sound speed squared has turned negative, the neutrino density contrast grows at a much faster rate than the density contrast in CDM.

A deeper insight into the perturbation evolution can be gained from considering the evolution of the scalar neutrino coupling β for this model as plotted in a) of the right panel of Fig. 4.4. Since our choice of a large κ corresponds to $\phi \ll M_{\rm pl}$ at late times, β is driven to larger and larger values, while the VEV of ϕ approaches zero (cf. the discussion in the last section). Accordingly the effective Newton's constant $G_{\rm eff}$ felt by neutrinos increases rapidly with time, and the scalar field transfers more and more energy to the neutrinos causing m_ν to increase (cf. a)). Finally, when β is almost three orders of magnitude larger than the gravitational coupling, it clearly over-compensates for the relative smallness of the neutrino energy density and starts to dominate the dynamics. Namely, the scalar field mediated force causes $\tilde{\delta}_\nu$ to grow faster than exponentially (cf. also the discussion in Sec. 4.4) as shown in c) Fig. 4.4 c), since the stabilizing effect on the MaVaN perturbations achieved by the gravitational drag exerted by CDM becomes negligible. To further illustrate this, for comparison we have plotted the relative magnitudes of the scalar-field-induced term $G_{\rm eff}/G\Omega_\nu\delta_\nu$ and the CDM forcing term $\propto \Omega_{\rm CDM}\delta_{\rm CDM}$ from Eq. (4.51), the evolution equation of the neutrino density contrast in Sec. 4.4.

In the following, we will argue that as a result the neutrino density contrast has already turned non-linear in the past. Therefore, we take into account the normalization of the CDM density contrast which gives us a rough estimate for the normalization of $\tilde{\delta}_\nu$. As long as the dimensionless power spectrum $\Delta^2(k) = k^3P(k)/(2\pi^2) < 1$, due to the rough proportional to $\propto \delta^2_{\rm CDM}$, CDM perturbations on a scale k are linear (cf. Sec. 4.2.1 and Fig. 4.1, where we have introduced the power spectrum $P(k)$). Since on the considered scale of $k = 0.1\,{\rm Mpc}^{-1}$ we have $\Delta^2(k) \sim 0.3 - 0.4$ [5] for CDM, we can infer that for neutrinos $\Delta^2(k) \propto \delta^2_\nu > 1$, when $\tilde{\delta}_\nu$ exceeds $\tilde{\delta}_{\rm CDM}$ by more than a factor of $\sqrt{2}$. This is the case at roughly $1 + z \sim 5$, while afterwards linear perturbation theory cannot be trusted anymore. It is thus likely that neutrinos in this model are subject to the formation of non-linear structure in the neutrino energy density [57, 58] before the present time.

Our numerical results presented in Fig. 4.4 demonstrate that the total sound speed squared in the log-linear model is negative at late times and since any growth-slowing effects by CDM are rendered negligible, this corresponds to a fast growth of perturbations. Thus, inevitably, the neutrino density contrast is driven into the non-linear regime and the model becomes unstable with the possible outcome of the formation of neutrino bound states [57].

It should, however, be noted that in case the neutrino mass scale realized in nature is lower than assumed in our analysis, the stabilizing effect of CDM in combination with the pressure support in (quasi)-relativistic neutrinos could prevent a clumping of neutrinos until the present time (cf. Sec. 3 where a relativistic neutrino for the same coupling function prevents the

occurrence of instabilities).

Power-Law Potential

The inverse power-law potential is defined by Eq. (4.61) and Eq. (4.62). We assume $n = 0.3$ in Eq. (4.61) and adjusted the mass parameter M to accomplish the correct cosmology at present. Furthermore, we take $\beta = 1/M_{\rm pl}$ in Eq. (4.62). With these choices of parameters the mass of the scalar field at present is $m_\phi \sim 0.1\,\mathrm{Mpc}^{-1} \gg \mathcal{H}$ and accordingly the MaVaN perturbations are adiabatic on sub-Hubble scales $k \lesssim m_\phi$. This model will serve as an example for a stable model.

We perform our perturbation analysis on a scale $k = 0.1\,\mathrm{Mpc}^{-1}$ where possible instabilities would grow fastest and illustrate our results in Fig. 4.5 to be described in the following.

a) The evolution of the neutrino mass $m_\nu(z)$ and the neutrino temperature $T_\nu(z)$ in the non-relativistic regime $m_\nu(z) \gg T_\nu(z)$ is plotted as a function of redshift. Since the neutrino mass depends only weakly on changes in the scalar field VEV, it hardly evolves with time (cf. Sec. 4.5.1).

b) The evolution of the total sound speed squared c_a^2 of the coupled Dark Energy fluid is plotted as a function of redshift. We observe that c_a^2 takes positive values even in the highly non-relativistic regime of the neutrinos.

c) The evolution of the density contrast in neutrinos $\tilde{\delta}_\nu$, and cold dark matter $\tilde{\delta}_{\rm CDM}$ is plotted as a function of redshift. It is found that the density contrast in MaVaNs grows just as in uncoupled neutrinos in General Relativity. How can this be understood? In contrast to the log-linear model, the coupling between the scalar field and the neutrinos is constant and the neutrino mass very weakly depends on changes in the scalar field VEV. Accordingly, both the energy transfer of the scalar field to the neutrinos as well as the attraction felt between neutrinos hardly increase with time but essentially stay constant. As a result, the effects of the scalar field on the neutrino perturbations is subdominant with respect to the gravitational influence of CDM which thus governs the dynamics just as in the absence of the scalar field. In other words, the analytical stability condition stated in Eq. (4.54) in Sec. 4.4 is fulfilled until the present time.

As a result, the growth of $\tilde{\delta}_\nu$ (as well as of $m_\nu(z)$) with time remains moderate and $\tilde{\delta}_\nu$ turns out to be of comparable size as $\tilde{\delta}_{\rm CDM}$ today (cf. our analytical results in Sec. 4.4).

Accordingly, as argued in Sec. 4.5.2, the CDM perturbations are known to be linear at the considered scale and therefore also the neutrinos perturbations are linear until the present time.

Let us furthermore point out that we checked that the behavior of the neutrino density contrast is retained on the same scale for an increased value of the coupling $\beta = 100/M_{\rm pl}$. It should be noted that in this case the range of the scalar field and thus the scales, where possible instabilities grow fastest, have dropped below the physical scales accessible with CMBFAST/CAMB. We thus ascribe the unaltered behavior of the perturbations to the suppression of the effective Newton's constant $G_{\rm eff}$ felt by neutrinos with increasing

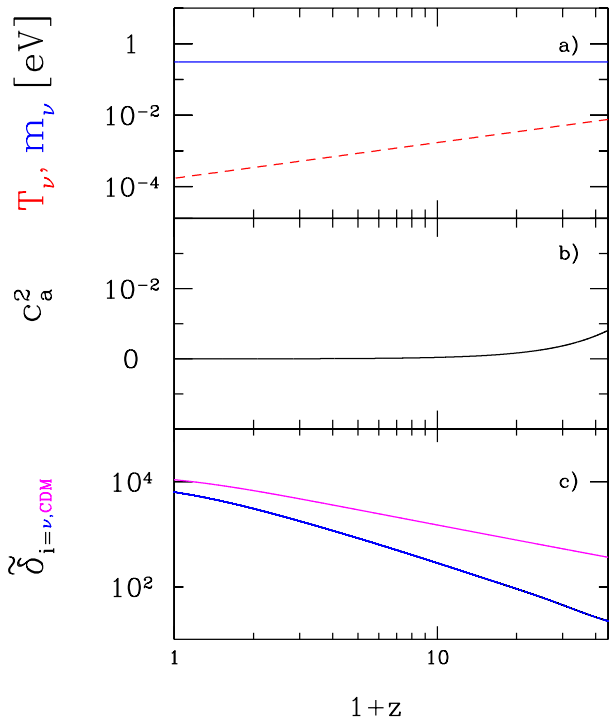

Figure 4.5: *a*) Neutrino mass m_ν (solid) and temperature T_ν (dotted) as a function of redshift. *b*) Adiabatic Dark Energy sound speed squared c_a^2 (solid) as a function of redshift. *c*) (Unnormalized) density contrast in neutrinos (solid) $\tilde{\delta}_\nu$ and in CDM $\tilde{\delta}_{\rm CDM}$ (dash-dotted) as a function of redshift on a scale $k = 0.1\,{\rm Mpc}^{-1}$.

scale a/k (cf. the discussion at the end of Sec. 4.4) in combination with the stabilizing effect achieved by CDM and baryons. This result demonstrates that a possible enhanced growth of MaVaN perturbations can only take place on scales not much larger than the scalar field range, i.e. it is a rather *local* phenomenon. This result is important for our considerations in Sec. 4.6.1.

In conclusion, Fig. 4.5 demonstrates that the adiabatic power-law model is characterized by a positive sound speed squared[18] and the neutrino density contrast on small scales is still in the linear regime today. Accordingly, the model can be viewed as stable until the present time.

We note that the stability traces back to the stabilizing effect on the perturbations achieved by CDM. In addition, it is supported by the behavior of the neutrino mass which hardly evolves with time[19] and thus, as discussed in Sec. 4.3, allows for a positive adiabatic sound speed

[18] We verified that models with larger values for n in Eq. (4.61) are also characterized by a positive total sound speed squared, while reproducing the standard cosmology. Furthermore, m_ϕ increases with n rendering the model more adiabatic. Another interesting result was gained, by subtracting the constant term in the power-law potential in Eq. (4.61). For certain parameter values, models emerged which are stabilized by CDM until today and are characterized by a *negative* sound speed squared.

[19] We would like to point out that in general in order to comply with a positive sound speed squared according to Eq. (4.42) (cf. Fig. 4.2) the restriction on the mass variation in a MaVaN model is alleviated at earlier times when finite temperature effects become more important. In other words, while the neutrino mass is only required to approach an essentially constant value at late times, in the power-model (as a special case) it always stays nearly the same.

squared until today.

We conclude the section by emphasizing that the considered example constitutes a viable MaVaN model that resides permanently in the effective minimum and is characterized by a non-relativistic neutrino phase *and* a positive sound speed squared, a possibility that was not noticed in Ref. [57].

We have thus demonstrated both analytically and numerically that it is crucial to consider the magnitude and the growth rate of the scalar-neutrino coupling and to compare its relative importance to other sources of gravitational attraction. As indicated in Sec. 4.4, the comparison can be made quantitatively through Eq. (4.54).

4.6 Relaxing a No-Go Theorem for Mass Varying Neutrinos

In the following, we will comment on a no-go theorem in Ref. [57] which states that any realistic adiabatic MaVaN model with $m_\phi^2 > 0$ becomes unstable before the present time in the non-relativistic neutrino regime.

For its deduction the authors of Ref. [57] proceeded in the following way. They derived an expression for the total adiabatic sound speed squared c_a^2 in the kinetic theory picture for $p_\nu \ll m_\nu$ assuming the perturbations to be plane waves which grow exponentially. Independent of the choice of the scalar-neutrino coupling and the scalar potential which characterize a MaVaN model, c_a^2 was found to be negative. Accordingly, it was associated with a generic strong growth of MaVaN perturbations, while no reference was made to the relative gravitational importance of other cosmic components like CDM and baryons.

In the present work we have demonstrated analytically and numerically that a detailed analysis of the potential and coupling functions and an assessment of the influence of other important cosmic components, like CDM and baryons, are necessary in order to predict the growth of structure in neutrinos. As our central result, we quantified this statement by deriving an analytical stability condition which translates into a comfortable upper bound on the scalar-neutrino coupling as stated in Eq. (4.54) in Sec. 4.4. We indicate the relative smallness of the neutrino energy density as the reason and stress that accordingly the lower the neutrino mass scale realized in nature turns out to be, the larger scalar-neutrino couplings are allowed by the stability.

In accordance with this finding, in our analytical analysis in Sec. 4.4, we found that the density contrast in neutrinos in the small scale limit only grows exponentially, if the scalar-neutrino coupling is larger than all other relevant parameters and thus leads to negligible growth-slowing effects as provided by cosmic expansion and CDM gravitational drag.

In this case we verified numerically for the log-linear model of Sec. 4.5.2 that the sound speed squared c_a^2 turns negative in agreement with the result of [57]. Let us point out that since the sound speed squared merely encodes the effects of the scalar field on the MaVaN perturbations, its sign *only* indicates the growth of instabilities if the full stability condition in Eq. (4.54) in Sec. 4.4 (cf. also Eq. (4.57)) is not fulfilled i.e. if growth-slowing effects can be neglected.

However, as demonstrated by the result for the power-model, for a moderate constant coupling the evolution of the neutrino density contrast is not modified with respect to the uncoupled case in ordinary General Relativity. Accordingly, also on small scales $\sim m_\phi^{-1}$ the plane-wave solution found in Ref. [57] did not apply and *and* perturbations were driven by a positive sound speed squared. Consequently, the dynamics in stable models are governed by CDM, largely independent of the sign of the sound speed squared, even in the highly non-relativistic regime.

However, let us add that for stable MaVaN models characterized by a positive sound speed squared until the present time the allowed neutrino mass evolution at late times was found to be generically severely constrained (cf. Fig. 4.2 and the discussion in Sec. 4.3).

Based on our analysis, we thus conclude that the no-go theorem stated in Ref. [57] can be substantially relaxed, since a viable and stable class of adiabatic MaVaN models was identified which are characterized by a scalar-neutrino coupling of at least gravitational strength.

In the next subsection we will argue that it might even be *desirable* to achieve a scalar-field induced strong growth of MaVaN instabilities with the likely outcome of the clustering of neutrinos, since under certain circumstances MaVaNs might be promoted to a *dark matter* candidate.

4.6.1 Mass Varying Neutrinos as Dark Energy and Dark Matter?

This section deals with the intriguing question, whether neutrino lumps could play the role of the Dark Matter, while at the same time the observed late-time acceleration is driven by Neutrino Dark Energy.

Let us make a few notes which might help to answer this question. In our stability analysis we have tested the growth of perturbations in the framework of linear perturbation theory valid on large length scales until the present time. Accordingly, we could get a feeling for the relevant physical effects leading to the possible clumping in neutrinos disentangled from any non-trivial non-linear effects inherent in small physical scales.

Furthermore, we integrated the relevant equations using CMBFAST and CAMB which work in the linear regime [202, 220]. Consequently, the mass of the scalar field had to be chosen small enough (however $\gg \mathcal{H}$) to push the scales where possible instabilities could occur into the linear regime. As discussed in Sec. 4.4 and verified by our numerical results for the power-model and $\beta = 100/M_{\rm pl}$, on scales larger than the range of the scalar field the attraction felt by neutrinos becomes considerably suppressed. Thus, the possible enhanced growth in neutrinos was found to be a rather local phenomenon.

By increasing the scalar field mass and thus reducing the range of the scalar field, we would expect a local scalar field induced enhancement of the gravitational clustering of neutrinos in the non-linear regime (on scales, where neutrino free-streaming cannot inhibit the growth of perturbations). Accordingly, resulting neutrino bound states would be interpreted as a contribution to the CDM small scale structure, which however, on average does not affect the equation of state of Neutrino Dark Energy.

Accordingly, if the inverse scalar field mass corresponds to sub-galactic scales, this opens up the intriguing possibility that clustered neutrinos bound by the scalar-field mediated force and by gravity could even be (part of) the *Dark Matter*, while at the same time they could act as source of Neutrino Dark Energy. However, the detailed discussion of such scenarios and their phenomenological implications lies beyond the scope of this work (see Ref. [58] for a later reference on a similar subject).

We note that similarly, in *chameleon cosmologies* such an enhanced small scale growth of the CDM density contrast is predicted [221] due to the coupling of CDM to a light scalar field with range $a/k = 250$ pc today.

Let us remark that the chameleon constitutes another interesting Dark Energy candidate. It is a light scalar field with similar properties as the scalar field in the Mass Varying Neutrino scenario. However, it couples democratically to all matter species in such a way that its mass increases with the local matter density. As a consequence, it can easily escape 'fifth-force' measurements in the laboratory, where the matter density and thus the chameleon mass are comparably high and correspondingly, the chameleon mediated force is sub-millimeter ranged. In our Ref. [222], we proposed an experimental set-up to be implemented in an on-going DESY experiment (ALPS [223]), which allows to indirectly detect the chameleon through an 'afterglow' effect in axion-like particle search experiments. It relies on the possible reconversion of chameleons into photons in an external magnetic field. We demonstrated that according to the current state of technology in principle this method is sensitive to a so far unaccessible region of the parameter space of these theories.

4.7 Summary and Outlook – Part II

Models of neutrinos coupled to a light scalar field have been invoked to naturally explain the observed cosmic acceleration as well as the origin of dynamical neutrino masses. However, the class of MaVaN models characterized by an adiabatic evolution of perturbations in the non-relativistic neutrino regime was claimed to suffer from a strong growth of instabilities and as a result may cease to act as viable realizations of Dark Energy [57]. In this paper we analyzed the stability issue in the appropriate framework of linear perturbation theory. For this purpose we derived the equation of motion of the density contrast in terms of the characteristic MaVaN functions, namely the scalar potential, the scalar-neutrino coupling, and the source terms provided by cold dark matter (CDM) and baryons. Furthermore, we modified both the CMBFAST [202] and CAMB [220] code to include a light scalar field coupled to neutrinos and numerically focused on two significant MaVaN models.

We found that the instabilities in the neutrino density contrast only occur if the influence of the scalar-neutrino coupling on the dynamics of the perturbations dominates over the growth-slowing effects provided by CDM. As long as the coupling is moderate, the neutrinos feel a gravitational drag towards the potential wells formed by CDM which effectively leads to a stabilization of the MaVaN perturbations, largely independent of the sign of the sound speed squared.

As our central result, we derived an analytic stability condition which was shown to translate

into an upper bound on the scalar neutrino coupling which depends on the ratio of the energy densities in cold dark matter and in neutrinos. This ratio can be as large as $O(10^{2\div3})$, depending on the absolute neutrino mass scale realized in nature and therefore in principle allows for couplings much larger than of gravitational strength. We would like to point out that the reason for a possible stabilization of the neutrino density contrast is the relative smallness of the neutrino mass.

However, in turn, if the coupling is strong enough to render any growth-slowing effects negligible, the stability was shown to require the model to exhibit a positive sound speed squared. This condition was found to strongly restrict the allowed neutrino mass variation at late times.

We illustrated these results by considering representative limiting cases for the time dependence of the coupling. At first, we investigated MaVaN models characterized by a strong growth of the coupling and thus of the neutrino masses with time. In this case, at late times any growth-slowing effects on the perturbations provided by the cosmic expansion or the gravitational drag of CDM were found to be negligible. Consequently, independent of the choice of the scalar potential, the analytic equation for the evolution of the neutrino density contrast at late times involved a faster than exponentially growing solution. Our numerical results for such a model with logarithmic scalar potential illustrated that the onset of the instability is around the time when the neutrinos turn non-relativistic. In this case, the instability could be seen as the effect of the adiabatic sound speed squared becoming negative, since growth-slowing effects where negligible. Since the attraction between neutrinos increases rapidly, the sound speed changes sign as soon as the counterbalancing pressure forces in neutrinos have dropped sufficiently. As a result, the non-relativistic neutrino density contrast is inevitably driven into the non-linear regime with the likely outcome of the formation of non-linear structure in the neutrino density [57, 58].

However, we demonstrated that this result does not hold true if the scalar-neutrino coupling in a MaVaN model is not strong enough to overcompensate for the growth-slowing effects provided by other cosmic components. Our numerical results for the choice of a moderate constant coupling and an inverse power law scalar potential showed that the neutrino density contrast behaves as in the uncoupled case of standard cosmology, since the scalar-field-induced effects are subdominant. Accordingly, the dynamics are governed by CDM as in the uncoupled case. As a consequence, the neutrino density contrast was found to be still in the linear regime up to the present time, even on scales where possible instabilities would grow fastest. Accordingly, we have identified an example for an adiabatic MaVaN model which is stable until the present time. Based on our results, in a later reference [47] another example of a stable MaVaN model has been presented.

To summarize, our analysis allowed to identified a stable class of adiabatic MaVaN models characterized by a comfortable strength of the scalar-neutrino coupling at least as large as that of gravity, even for the largest absolute neutrino mass scale allowed by terrestrial upper bounds (as given in Sec. 2.6.4).

Outlook

We would like to comment on another intriguing class of models, which might at the same time explain *Dark Energy* and (part of the) *Dark Matter* by the help of Mass Varying neutrinos.

This might be accomplished if the scalar field range (i.e. its inverse mass) corresponds to sub-galactic scales and if in addition the scalar-neutrino coupling is *large* enough to initiate the strong growth of MaVaN instabilities. Since we demonstrated that on scales much larger than the range of the scalar field the attraction felt by neutrinos becomes considerably suppressed, the likely outcome is the formation of bound neutrino structure – however, *only* on sub-galactic scales. Accordingly, under these circumstances on small scales MaVaNs could be (part of the) Dark Matter, while averaged over all scales, the equation of state of Neutrino Dark Energy would not be affected and could thus still drive late-time acceleration.

The quantitative discussion of these interesting scenarios lies, however, beyond the scope of this work. While this possibility was so far not noticed in the MaVaN literature (see Ref. [58] for a later reference on a similar subject), a similar reasoning can be found in models of chameleon cosmologies [221], see e.g. our Ref. [222] for a proposed laboratory based test for these theories to be implemented in an on-going DESY experiment (ALPS [223]).

5 Final Conclusions and Outlook

In this thesis we explored various theoretical aspects and phenomenological implications resulting from non-standard neutrino interactions with a light scalar field attributed to the sector responsible for *Dark Energy*. All in all, we conclude that such connections are rich and attractive from the theoretical point of view and as a further merit allow to be verified within the near future. Considering that at the current experimental stage it is not even possible to state whether the observed late-time acceleration arises from a constant or a dynamical source of energy or even from a modification of gravity on the largest scales, it would really be exciting if neutrino physics turned out to open a window into the dark sector.

In the following we will summarize the central results gained in the first and second main part of this thesis.

1) Signatures of Mass Varying Neutrinos in the Sky?

In light of the possible realization of Neutrino Dark Energy in nature, we explored a more direct way of probing the cosmic neutrino background (CνB) by means of neutrino observatories [61–68]. They open up the exciting possibility to trace the annihilation of extremely high-energy neutrinos (EHECν's) and relic anti-neutrinos of the CνB (and vice versa) into Z bosons by localizing absorption dips in the EHECν spectra at energies set by the neutrino masses. For various EHECν sources we illustrated the discovery potential for the CνB by means of relic neutrino absorption spectroscopy and estimated the prospects for probing its interpretation as source of Neutrino Dark Energy largely following our Refs. [69, 70].

To this end, we provided all state-of-the-art technical tools to interpret EHECν absorption dips for a given injection spectrum, both for constant and for varying neutrinos masses, including all thermal background effects caused by the relic neutrino motion.

We demonstrated that within the MaVaN framework proposed in Ref. [22], remarkably, the redshift distortion of the absorption dips caused by cosmic expansion is essentially compensated by the time evolution of the neutrino masses, leading to features as in a static universe for constant neutrino masses. This could be seen most clearly analytically by switching off the thermal effects. Correspondingly, a reduction of the effects of the expansion on the absorption features is generically achieved, if the neutrino mass is a decreasing function of redshift as in the standard Mass Varying Neutrino scenario.

Therefore, as a main result, we found that compared to constant mass neutrinos, mass varying neutrinos from astrophysical sources produce much sharper absorption dips clearly shifted to higher energies at a statistically significant level. Even though the impact of the thermal washout on these characteristics turned out to grow for decreasing neutrino mass, this nice

and clear-cut feature was found to prevail also for the lowest possible neutrino mass scale realized in nature.

Accordingly, if the radio-telescope LOFAR [158] achieves the projected energy resolution of $\Delta E/E \sim 30\%$ [186], we demonstrated in a largely model-independent way that it seems feasible to trace a time variation of neutrino masses and thus to possibly reveal the nature of Dark Energy within the next decade.

2) On the stability of Neutrino Dark Energy

Recently the authors of Ref. [57] argued that any adiabatic Mass Varying Neutrino Scenario in the non-relativistic neutrino regime is threatened by a severe stability problem. Their claim was based on the following line of arguments. Firstly, every realization of such a scenario is characterized by a negative adiabatic sound speed squared. Secondly, a negative sound speed squared generically implies the strong growth of instabilities.

Based on our Ref. [71], we reconsidered the stability issue in the appropriate framework of linear cosmological perturbation theory in a model-independent way. We found that this no-go theorem can be considerably relaxed, since both of these arguments do not generally hold.

To this end, we derived the equation of motion of the density contrast in neutrinos from the linearized Einstein equations in terms of the characteristic MaVaN model dependent functions, namely the scalar potential, the scalar-neutrino coupling as well as the source terms provided by cold dark matter (CDM) and baryons. Let us note that the gravitational effect of these other important cosmic components, most notably of CDM, was not considered in Ref. [57], since the adiabatic sound speed squared merely encodes the influence of the scalar field on the neutrino perturbations.

Based on our analytical results, we found that the gravitational drag felt by neutrinos towards the potential wells formed by CDM can effectively lead to a stabilization of the MaVaN perturbations, largely independent of the sign of the sound speed squared. Moreover, importantly, the equation of motion of the neutrino density contrast allowed to directly infer a model-independent, analytic stability condition.

As our central finding, the stability condition turned out to translate into an upper bound on the scalar-neutrino coupling $\beta \lesssim \sqrt{\frac{\Omega_{\rm CDM}}{2\Omega_\nu}}\frac{1}{M_{\rm pl}}$, which is determined by the ratio of the energy densities in cold dark matter $\Omega_{\rm CDM}$ and in neutrinos Ω_ν. Since according to experimental data this ratio can range up to $O(10^{2\div 3})$, the coupling in principle is allowed to be much stronger than gravity, depending on the absolute neutrino mass scale realized in nature.

This result directly relates to the fact that the strength of the two competing forces felt by neutrinos does not only depend on the coupling, but also on the masses which attract each other. Accordingly, in physical terms the stability condition simply states that the gravitational drag exerted by the CDM source term dominates the dynamics of the perturbations, if the scalar-neutrino coupling does not overcompensate for the relative smallness of neutrino masses. In accordance with this finding, we showed that if the stability condition is satisfied, the density contrast in MaVaNs grows only moderately on all scales just as in the absence of the scalar-neutrino coupling in General Relativity. As a result, it stays in the linear and thus

stable regime until the present time.

If, however, the scalar-neutrino coupling is sufficiently strong to render the growth-slowing effects of CDM negligible, the stability of the model was found to require a positive sound speed squared. We demonstrated that models of Neutrino Dark Energy in general can comply with this condition (cf. also [60]), however, as a consequence, the allowed neutrino mass variation was found to be strongly restricted at late times.

We illustrated our results by considering representative examples both for stable and unstable scenarios.

To summarize, independent of the neutrino mass scale realized in nature, a class of viable, stable Mass Varying Neutrino scenarios could be identified, which is characterized by a scalar-neutrino coupling of at least gravitational strength.

Outlook

As an outlook we would like to remark on another intriguing class of scenarios which *are* characterized by a scalar-neutrino coupling strong enough to initiate the rapid growth of MaVaN instabilities (cf. our Ref. [71]). The likely outcome is the formation of bound neutrino lumps held together by the scalar-field mediated force and by gravity [57, 58]. However, as we demonstrated analytically, not only the force mediated by the scalar field but also the scalar-field induced growth of instabilities becomes strongly suppressed on scales much larger than its Compton wavelength or correspondingly its inverse mass. Accordingly, the possible occurrence of bound neutrino structure is a local phenomenon restricted to scales which decrease with increasing scalar field mass. Accordingly, while on average the equation of state associated with Neutrino Dark Energy is not expected to be affected by this local phenomenon, for an inverse scalar field mass corresponding to sub-galactic scales, the clustering neutrinos could even play the role of (part of) the *Dark Matter* (for a later reference see [58] on a similar subject)[1].

[1] A similar reasoning can be found in models of chameleon cosmologies [221] (see e.g. our Ref. [222] for a proposed laboratory based test for these theories to be implemented in an on-going DESY experiment (ALPS [223])).

Bibliography

[1] **SDSS** Collaboration, S. Dodelson *et al.*, "The three-dimensional power spectrum from angular clustering of galaxies in early SDSS data," *Astrophys. J.* **572** (2001) 140–156, astro-ph/0107421.

[2] **SDSS** Collaboration, A. S. Szalay *et al.*, "KL estimation of the power spectrum parameters from the angular distribution of galaxies in early SDSS data," *Astrophys. J.* **591** (2003) 1–11, astro-ph/0107419.

[3] **Supernova Search Team** Collaboration, A. G. Riess *et al.*, "Type Ia Supernova Discoveries at $z > 1$ From the Hubble Space Telescope: Evidence for Past Deceleration and Constraints on Dark Energy Evolution," *Astrophys. J.* **607** (2004) 665–687, astro-ph/0402512.

[4] P. S. Corasaniti, M. Kunz, D. Parkinson, E. J. Copeland, and B. A. Bassett, "The foundations of observing dark energy dynamics with the Wilkinson Microwave Anisotropy Probe," *Phys. Rev.* **D70** (2004) 083006, astro-ph/0406608.

[5] W. J. Percival *et al.*, "The shape of the SDSS DR5 galaxy power spectrum," *Astrophys. J.* **657** (2007) 645–663, astro-ph/0608636.

[6] D. N. Spergel *et al.*, "Wilkinson Microwave Anisotropy Probe (WMAP) three year results: Implications for cosmology," astro-ph/0603449.

[7] G. Dvali and M. S. Turner, "Dark energy as a modification of the Friedmann equation," astro-ph/0301510.

[8] S. M. Carroll, V. Duvvuri, M. Trodden, and M. S. Turner, "Is cosmic speed-up due to new gravitational physics?," *Phys. Rev.* **D70** (2004) 043528, astro-ph/0306438.

[9] S. Weinberg, "The cosmological constant problem," *Rev. Mod. Phys.* **61** (1989) 1–23.

[10] C. Wetterich, "Cosmology and the Fate of Dilatation Symmetry," *Nucl. Phys.* **B302** (1988) 668.

[11] P. J. E. Peebles and B. Ratra, "Cosmology with a Time Variable Cosmological Constant," *Astrophys. J.* **325** (1988) L17.

[12] R. R. Caldwell, R. Dave, and P. J. Steinhardt, "Cosmological Imprint of an Energy Component with General Equation-of-State," *Phys. Rev. Lett.* **80** (1998) 1582–1585, astro-ph/9708069.

[13] I. Zlatev, L.-M. Wang, and P. J. Steinhardt, "Quintessence, Cosmic Coincidence, and the Cosmological Constant," *Phys. Rev. Lett.* **82** (1999) 896–899, astro-ph/9807002.

[14] C. Armendariz-Picon, V. F. Mukhanov, and P. J. Steinhardt, "Essentials of k-essence," *Phys. Rev.* **D63** (2001) 103510, astro-ph/0006373.

[15] T. Padmanabhan, "Accelerated expansion of the universe driven by tachyonic matter," *Phys. Rev.* **D66** (2002) 021301, hep-th/0204150.

[16] V. Gorini, A. Kamenshchik, and U. Moschella, "Can the Chaplygin gas be a plausible model for dark energy?," *Phys. Rev.* **D67** (2003) 063509, astro-ph/0209395.

[17] N. Bilic, G. B. Tupper, and R. D. Viollier, "Unification of dark matter and dark energy: The inhomogeneous Chaplygin gas," *Phys. Lett.* **B535** (2002) 17–21, astro-ph/0111325.

[18] E. G. Adelberger, B. R. Heckel, and A. E. Nelson, "Tests of the gravitational inverse-square law," *Ann. Rev. Nucl. Part. Sci.* **53** (2003) 77–121, hep-ph/0307284.

[19] C. M. Will, "The confrontation between general relativity and experiment," *Living Rev. Rel.* **4** (2001) 4, gr-qc/0103036.

[20] S. M. Carroll, "Quintessence and the rest of the world," *Phys. Rev. Lett.* **81** (1998) 3067–3070, astro-ph/9806099.

[21] R. Fardon, A. E. Nelson, and N. Weiner, "Dark energy from mass varying neutrinos," *JCAP* **0410** (2004) 005, astro-ph/0309800.

[22] R. Fardon, A. E. Nelson, and N. Weiner, "Supersymmetric theories of neutrino dark energy," *JHEP* **03** (2006) 042, hep-ph/0507235.

[23] L. Amendola, M. Baldi, and C. Wetterich, "Growing Matter," arXiv:0706.3064 [astro-ph].

[24] C. Wetterich, "Growing neutrinos and cosmological selection," *Phys. Lett.* **B655** (2007) 201–208, arXiv:0706.4427 [hep-ph].

[25] E. W. Kolb and M. S. Turner, "The Early universe," *Front. Phys.* **69** (1990) 1–547.

[26] M. Kawasaki, H. Murayama, and T. Yanagida, "Neutrino dark matter with a galactic range new force," *Mod. Phys. Lett.* **A7** (1992) 563–570.

[27] A. Singh, "A Small nonvanishing cosmological constant from vacuum energy: Physically and observationally desirable," *Phys. Rev.* **D52** (1995) 6700–6707, hep-ph/9412240.

[28] J. Stephenson, G. J., T. Goldman, and B. H. J. McKellar, "Neutrino Clouds," *Int. J. Mod. Phys.* **A13** (1998) 2765–2790, hep-ph/9603392.

[29] J. Stephenson, G. J., T. Goldman, and B. H. J. McKellar, "MSW-like enhancements without matter," *Mod. Phys. Lett.* **A12** (1997) 2391–2398, hep-ph/9610317.

[30] P. Q. Hung, "Sterile neutrino and accelerating universe," `hep-ph/0010126`.

[31] P. Gu, X. Wang, and X. Zhang, "Dark energy and neutrino mass limits from baryogenesis," *Phys. Rev.* **D68** (2003) 087301, `hep-ph/0307148`.

[32] R. S. M. Gell-Mann, P. Ramond in *Supergravity*, F. van Nieuwenhuizen and D.Freedmann, eds., p. 315. North Holland, Amsterdam, 1979.

[33] T. Yanagida in *Proc. of the Workshop on Unified Theory and the Baryon Number of the Universe*. KEK, Japan, 1979.

[34] P. Minkowski in *In Proceedings of Cargese Summer Institute on Quarks and Leptons*. Plenum Press, New York, 1980. *Phys. Lett.* **B 67**, *(1977), 687-713*.

[35] R. N. Mohapatra and G. Senjanovic, "Neutrino mass and spontaneous parity nonconservation," *Phys. Rev. Lett.* **44** (1980) 912.

[36] A. Strumia and F. Vissani, "Neutrino masses and mixings and.," `hep-ph/0606054`.

[37] C. F. Kolda and D. H. Lyth, "Quintessential difficulties," *Phys. Lett.* **B458** (1999) 197–201, `hep-ph/9811375`.

[38] R. D. Peccei, "Light scalars in cosmology," `hep-ph/0009030`.

[39] M. Doran and J. Jaeckel, "Loop corrections to scalar quintessence potentials," *Phys. Rev.* **D66** (2002) 043519, `astro-ph/0203018`.

[40] M. Garny, "Quantum corrections in quintessence models," *Phys. Rev.* **D74** (2006) 043009, `hep-ph/0606120`.

[41] J. A. Frieman, C. T. Hill, and R. Watkins, "Late time cosmological phase transitions. 1. Particle physics models and cosmic evolution," *Phys. Rev.* **D46** (1992) 1226–1238.

[42] J. A. Frieman, C. T. Hill, A. Stebbins, and I. Waga, "Cosmology with ultralight pseudo Nambu-Goldstone bosons," *Phys. Rev. Lett.* **75** (1995) 2077–2080, `astro-ph/9505060`.

[43] A. W. Brookfield, C. van de Bruck, D. F. Mota, and D. Tocchini-Valentini, "Cosmology with massive neutrinos coupled to dark energy," *Phys. Rev. Lett.* **96** (2006) 061301, `astro-ph/0503349`.

[44] A. W. Brookfield, C. van de Bruck, D. F. Mota, and D. Tocchini-Valentini, "Cosmology of mass-varying neutrinos driven by quintessence: Theory and observations," *Phys. Rev.* **D73** (2006) 083515, `astro-ph/0512367`.

[45] P. Q. Hung and H. Pas, "Cosmo MSW effect for mass varying neutrinos," *Mod. Phys. Lett.* **A20** (2005) 1209–1216, `astro-ph/0311131`.

[46] A. Friedland, K. M. Zurek, and S. Bashinsky, "Constraining Models of Neutrino Mass and Neutrino Interactions with the Planck Satellite," `arXiv:0704.3271 [astro-ph]`.

[47] L. Anchordoqui, V. Barger, H. Goldberg, and D. Marfatia, "Phase transition in the fine structure constant," `arXiv:0711.4055 [hep-ph]`.

[48] H. Li, Z.-g. Dai, and X.-m. Zhang, "Testing mass varying neutrino with short gamma ray burst," *Phys. Rev.* **D71** (2005) 113003, hep-ph/0411228.

[49] D. B. Kaplan, A. E. Nelson, and N. Weiner, "Neutrino oscillations as a probe of dark energy," *Phys. Rev. Lett.* **93** (2004) 091801, hep-ph/0401099.

[50] N. Weiner and K. Zurek, "New matter effects and BBN constraints for mass varying neutrinos," hep-ph/0509201.

[51] K. M. Zurek, "New matter effects in neutrino oscillation experiments," *JHEP* **10** (2004) 058, hep-ph/0405141.

[52] M. Cirelli, M. C. Gonzalez-Garcia, and C. Pena-Garay, "Mass varying neutrinos in the sun," *Nucl. Phys.* **B719** (2005) 219–233, hep-ph/0503028.

[53] M. C. Gonzalez-Garcia, P. C. de Holanda, and R. Zukanovich Funchal, "Effects of environment dependence of neutrino mass versus solar and reactor neutrino data," *Phys. Rev.* **D73** (2006) 033008, hep-ph/0511093.

[54] V. Barger, P. Huber, and D. Marfatia, "Solar mass-varying neutrino oscillations," *Phys. Rev. Lett.* **95** (2005) 211802, hep-ph/0502196.

[55] T. Schwetz and W. Winter, "Testing mass-varying neutrinos with reactor experiments," *Phys. Lett.* **B633** (2006) 557–562, hep-ph/0511177.

[56] P.-H. Gu, X.-J. Bi, B. Feng, B.-L. Young, and X. Zhang, "Detecting dark energy in long baseline neutrino oscillations," hep-ph/0512076.

[57] N. Afshordi, M. Zaldarriaga, and K. Kohri, "On the stability of dark energy with mass-varying neutrinos," *Phys. Rev.* **D72** (2005) 065024, astro-ph/0506663.

[58] N. Brouzakis, N. Tetradis, and C. Wetterich, "Neutrino Lumps in Quintessence Cosmology," arXiv:0711.2226 [astro-ph].

[59] C. Spitzer, "Stability in MaVaN Models," astro-ph/0606034.

[60] R. Takahashi and M. Tanimoto, "Speed of sound in the mass varying neutrinos scenario," *JHEP* **05** (2006) 021, astro-ph/0601119.

[61] T. J. Weiler, "Resonant absorption of cosmic ray neutrinos by the relic neutrino background," *Phys. Rev. Lett.* **49** (1982) 234.

[62] T. J. Weiler, "Big Bang Cosmology, relic neutrinos, and absorption of neutrino cosmic rays," *Astrophys. J.* **285** (1984) 495.

[63] P. Gondolo, G. Gelmini, and S. Sarkar, "Cosmic neutrinos from unstable relic particles," *Nucl. Phys.* **B392** (1993) 111–136, hep-ph/9209236.

[64] E. Roulet, "Ultrahigh-energy neutrino absorption by neutrino dark matter," *Phys. Rev.* **D47** (1993) 5247–5252.

[65] S. Yoshida, H.-y. Dai, C. C. H. Jui, and P. Sommers, "Extremely high energy neutrinos and their detection," *Astrophys. J.* **479** (1997) 547–559, astro-ph/9608186.

[66] B. Eberle, A. Ringwald, L. Song, and T. J. Weiler, "Relic neutrino absorption spectroscopy," *Phys. Rev.* **D70** (2004) 023007, hep-ph/0401203.

[67] G. Barenboim, O. Mena Requejo, and C. Quigg, "Diagnostic potential of cosmic-neutrino absorption spectroscopy," *Phys. Rev.* **D71** (2005) 083002, hep-ph/0412122.

[68] J. C. D'Olivo, L. Nellen, S. Sahu, and V. Van Elewyck, "UHE neutrino damping in a thermal gas of relic neutrinos," *Astropart. Phys.* **25** (2006) 47–56, astro-ph/0507333.

[69] A. Ringwald and L. Schrempp, "Probing neutrino dark energy with extremely high-energy cosmic neutrinos," *JCAP* **0610** (2006) 012, astro-ph/0606316.

[70] L. Schrempp, "Probing the variation of relic neutrino masses with extremely high-energy cosmic neutrinos," in *Proc. of the First Workshop on Exotic Physics with Neutrino Telescopes*, C. de los Heros, ed., pp. 111–115. 2007. astro-ph/0611912.

[71] O. E. Bjaelde, A. W. Brookfield, C. van de Bruck, S. Hannestad, D. F. Mota, L. Schrempp, and D. Tocchini-Valentini, "Neutrino Dark Energy – Revisiting the Stability Issue," *JCAP* **0801** (2008) 026, arXiv:0705.2018 [astro-ph].

[72] **Supernova Search Team** Collaboration, A. G. Riess *et al.*, "Observational Evidence from Supernovae for an Accelerating Universe and a Cosmological Constant," *Astron. J.* **116** (1998) 1009–1038, astro-ph/9805201.

[73] **Supernova Cosmology Project** Collaboration, S. Perlmutter *et al.*, "Measurements of Omega and Lambda from 42 High-Redshift Supernovae," *Astrophys. J.* **517** (1999) 565–586, astro-ph/9812133.

[74] U. Seljak, A. Slosar, and P. McDonald, "Cosmological parameters from combining the Lyman-alpha forest with CMB, galaxy clustering and SN constraints," *JCAP* **0610** (2006) 014, astro-ph/0604335.

[75] **Boomerang** Collaboration, P. de Bernardis *et al.*, "A Flat Universe from High-Resolution Maps of the Cosmic Microwave Background Radiation," *Nature* **404** (2000) 955–959, astro-ph/0004404.

[76] A. H. Guth, "The Inflationary Universe: A Possible Solution to the Horizon and Flatness Problems," *Phys. Rev.* **D23** (1981) 347–356.

[77] K. Sato, "First Order Phase Transition of a Vacuum and Expansion of the Universe," *Mon. Not. Roy. Astron. Soc.* **195** (1981) 467–479.

[78] R. Brout, F. Englert, and E. Gunzig, "THE CREATION OF THE UNIVERSE AS A QUANTUM PHENOMENON," *Ann. Phys.* **115** (1978) 78.

[79] A. A. Starobinsky, "A new type of isotropic cosmological models without singularity," *Phys. Lett.* **B91** (1980) 99–102.

[80] V. F. Mukhanov and G. V. Chibisov, "Quantum Fluctuation and Nonsingular Universe. (In Russian)," *JETP Lett.* **33** (1981) 532–535.

[81] E. Lifshitz, "On the Gravitational stability of the expanding universe," *J. Phys. (USSR)* **10** (1946) 116.

[82] E. M. Lifshitz and I. M. Khalatnikov, "Investigations in relativistic cosmology," *Adv. Phys.* **12** (1963) 185–249.

[83] W. H. Press and E. T. Vishniac, "Tenacious myths about cosmological perturbations larger than the horizon size," *Astrophys. J.* **239** (1980) 1–11.

[84] J. M. Bardeen, "Gauge Invariant Cosmological Perturbations," *Phys. Rev.* **D22** (1980) 1882–1905.

[85] H. Kodama and M. Sasaki, "Cosmological Perturbation Theory," *Prog. Theor. Phys. Suppl.* **78** (1984) 1–166.

[86] V. F. Mukhanov, H. A. Feldman, and R. H. Brandenberger, "Theory of cosmological perturbations. Part 1. Classical perturbations. Part 2. Quantum theory of perturbations. Part 3. Extensions," *Phys. Rept.* **215** (1992) 203–333.

[87] M. Bruni, G. F. R. Ellis, and P. K. S. Dunsby, "Gauge invariant perturbations in a scalar field dominated universe," *Class. Quant. Grav.* **9** (1992) 921–946.

[88] J.-c. Hwang, "Evolution of ideal fluid cosmological perturbations," *Astrophys. J.* **415** (1993) 486–504.

[89] C.-P. Ma and E. Bertschinger, "Cosmological perturbation theory in the synchronous and conformal Newtonian gauges," *Astrophys. J.* **455** (1995) 7–25, `astro-ph/9506072`.

[90] R. Durrer, "Anisotropies in the cosmic microwave background: Theoretical foundations," *Helv. Phys. Acta* **69** (1996) 417–433, `astro-ph/9610234`.

[91] R. H. Brandenberger, "Lectures on the theory of cosmological perturbations," *Lect. Notes Phys.* **646** (2004) 127–167, `hep-th/0306071`.

[92] R. Durrer, "The theory of CMB anisotropies," *J. Phys. Stud.* **5** (2001) 177–215, `astro-ph/0109522`.

[93] S. M. Carroll, "The cosmological constant," *Living Rev. Rel.* **4** (2001) 1, `astro-ph/0004075`.

[94] E. Hubble, "A relation between distance and radial velocity among extra–galactic nebulae," *Proc. Nat. Acad. Sci.* **15** (1929) 168–173.

[95] S. M. Carroll, "TASI lectures: Cosmology for string theorists," `hep-th/0011110`.

[96] M. Trodden and S. M. Carroll, "TASI lectures: Introduction to cosmology," `astro-ph/0401547`.

[97] E. J. Copeland, M. Sami, and S. Tsujikawa, "Dynamics of dark energy," *Int. J. Mod. Phys.* **D15** (2006) 1753–1936, `hep-th/0603057`.

[98] R. Brandenberger, "Topics in cosmology," *PoS* **P2GC** (2006) 007, `hep-th/0701157`.

[99] C. P. Burgess, "Lectures on Cosmic Inflation and its Potential Stringy Realizations," *PoS* **P2GC** (2006) 008, `arXiv:0708.2865 [hep-th]`.

[100] S. Dodelson, "Modern cosmology,". Amsterdam, Netherlands: Academic Pr. (2003) 440 p.

[101] J. Lesgourgues and S. Pastor, "Massive neutrinos and cosmology," *Phys. Rept.* **429** (2006) 307–379, `astro-ph/0603494`.

[102] P. Serra, A. Heavens, and A. Melchiorri, "Bayesian Evidence for a Cosmological Constant using new High-Redshift Supernovae Data," *Mon. Not. Roy. Astron. Soc.* **379** (2007) 169–175, `astro-ph/0701338`.

[103] A. Melchiorri, L. Pagano, and S. Pandolfi, "When Did Cosmic Acceleration Start ?," *Phys. Rev.* **D76** (2007) 041301, `arXiv:0706.1314 [astro-ph]`.

[104] R. D. Peccei, "Neutrino models of dark energy," *Phys. Rev.* **D71** (2005) 023527, `hep-ph/0411137`.

[105] D. J. Fixsen *et al.*, "The Cosmic Microwave Background Spectrum from the Full COBE/FIRAS Data Set," *Astrophys. J.* **473** (1996) 576, `astro-ph/9605054`.

[106] S. Singh and C.-P. Ma, "Neutrino clustering in cold dark matter halos: Implications for ultra high energy cosmic rays," *Phys. Rev.* **D67** (2003) 023506, `astro-ph/0208419`.

[107] A. Ringwald and Y. Y. Y. Wong, "Gravitational clustering of relic neutrinos and implications for their detection," *JCAP* **0412** (2004) 005, `hep-ph/0408241`.

[108] W. Hollik, "Electroweak theory," *J. Phys. Conf. Ser.* **53** (2006) 7–43.

[109] W. Buchmuller, R. D. Peccei, and T. Yanagida, "Leptogenesis as the origin of matter," *Ann. Rev. Nucl. Part. Sci.* **55** (2005) 311–355, `hep-ph/0502169`.

[110] Z. Maki, M. Nakagawa, and S. Sakata, "Remarks on the unified model of elementary particles," *Prog. Theor. Phys.* **28** (1962) 870.

[111] G. L. Fogli, E. Lisi, A. Marrone, A. Palazzo, and A. M. Rotunno, "Neutrino mass and mixing parameters: A short review," `hep-ph/0506307`.

[112] **LSND** Collaboration, C. Athanassopoulos *et al.*, "Candidate events in a search for anti-muon-neutrino → anti-electron-neutrino oscillations," *Phys. Rev. Lett.* **75** (1995) 2650–2653, `nucl-ex/9504002`.

[113] **LSND** Collaboration, A. Aguilar *et al.*, "Evidence for neutrino oscillations from the observation of anti-nu/e appearance in a anti-nu/mu beam," *Phys. Rev.* **D64** (2001) 112007, `hep-ex/0104049`.

[114] **The MiniBooNE** Collaboration, A. A. Aguilar-Arevalo *et al.*, "A Search for Electron Neutrino Appearance at the Delta m**2 1 eV**2 Scale," *Phys. Rev. Lett.* **98** (2007) 231801, arXiv:0704.1500 [hep-ex].

[115] V. M. Lobashev *et al.*, "Direct search for neutrino mass and anomaly in the tritium beta-spectrum: Status of 'Troitsk neutrino mass' experiment," *Nucl. Phys. Proc. Suppl.* **91** (2001) 280–286.

[116] C. Kraus *et al.*, "Final results from phase II of the Mainz neutrino mass search in tritium beta decay," *Eur. Phys. J.* **C40** (2005) 447–468, hep-ex/0412056.

[117] **Particle Data Group** Collaboration, W. M. Yao *et al.*, "Review of particle physics," *J. Phys.* **G33** (2006) 1–1232.

[118] **KATRIN** Collaboration, A. Osipowicz *et al.*, "KATRIN: A next generation tritium beta decay experiment with sub-eV sensitivity for the electron neutrino mass," hep-ex/0109033.

[119] **KATRIN** Collaboration, J. Angrik *et al.*, "KATRIN design report 2004,". FZKA-7090.

[120] **KATRIN** Collaboration, R. G. H. Robertson, "KATRIN: an experiment to measure the neutrino mass," arXiv:0712.3893 [nucl-ex].

[121] A. Staudt, T. T. S. Kuo, and H. V. Klapdor-Kleingrothaus, "beta beta decay of Te-128, Te-130, and Ge-76 with renormalized effective interactions derived from Paris and Bonn potentials," *Phys. Rev.* **C46** (1992) 871–883.

[122] E. Caurier, F. Nowacki, A. Poves, and J. Retamosa, "Shell Model Studies of the Double Beta Decays of ^{76}Ge, ^{82}Se, and ^{136}Xe," *Phys. Rev. Lett.* **77** (Sep, 1996) 1954–1957.

[123] H. V. Klapdor-Kleingrothaus *et al.*, "Latest results from the Heidelberg-Moscow double-beta- decay experiment," *Eur. Phys. J.* **A12** (2001) 147–154, hep-ph/0103062.

[124] **IGEX** Collaboration, C. E. Aalseth *et al.*, "The IGEX Ge-76 neutrinoless double-beta decay experiment: Prospects for next generation experiments," *Phys. Rev.* **D65** (2002) 092007, hep-ex/0202026.

[125] V. A. Rodin, A. Faessler, F. Simkovic, and P. Vogel, "On the uncertainty in the 0nu beta beta decay nuclear matrix elements," *Phys. Rev.* **C68** (2003) 044302, nucl-th/0305005.

[126] M. Pedretti *et al.*, "Results from CUORICINO experiment and prospects for CUORE,". Prepared for 9th ICATPP Conference on Astroparticle, Particle, Space Physics, Detectors and Medical Physics Applications, Villa Erba, Como, Italy, 17-21 Oct 2005.

[127] H. V. Klapdor-Kleingrothaus, I. V. Krivosheina, A. Dietz, and O. Chkvorets, "Search for neutrinoless double beta decay with enriched Ge- 76 in Gran Sasso 1990-2003," *Phys. Lett.* **B586** (2004) 198–212, hep-ph/0404088.

[128] **GERDA** Collaboration, S. Schonert *et al.*, "Status of the Germanium Detector Array (GERDA) in the search of neutrinoless beta beta decays of Ge-76 at LNGS," *Phys. Atom. Nucl.* **69** (2006) 2101–2108.

[129] A. Goobar, S. Hannestad, E. Mortsell, and H. Tu, "A new bound on the neutrino mass from the SDSS baryon acoustic peak," *JCAP* **0606** (2006) 019, astro-ph/0602155.

[130] B. Feng, J.-Q. Xia, J. Yokoyama, X. Zhang, and G.-B. Zhao, "Weighing neutrinos in the presence of a running primordial spectral index," *JCAP* **0612** (2006) 011, astro-ph/0605742.

[131] M. Cirelli and A. Strumia, "Cosmology of neutrinos and extra light particles after WMAP3," *JCAP* **0612** (2006) 013, astro-ph/0607086.

[132] S. Hannestad and G. G. Raffelt, "Neutrino masses and cosmic radiation density: Combined analysis," *JCAP* **0611** (2006) 016, astro-ph/0607101.

[133] G. L. Fogli *et al.*, "Observables sensitive to absolute neutrino masses: A reappraisal after WMAP-3y and first MINOS results," *Phys. Rev.* **D75** (2007) 053001, hep-ph/0608060.

[134] M. Tegmark *et al.*, "Cosmological Constraints from the SDSS Luminous Red Galaxies," *Phys. Rev.* **D74** (2006) 123507, astro-ph/0608632.

[135] C. Zunckel and P. G. Ferreira, "Conservative estimates of the mass of the neutrino from cosmology," *JCAP* **0708** (2007) 004, astro-ph/0610597.

[136] J. R. Kristiansen, O. Elgaroy, and H. Dahle, "Using the cluster mass function from weak lensing to constrain neutrino masses," astro-ph/0611761.

[137] F. Bauer and L. Schrempp, "Relaxing neutrino mass bounds by a running cosmological constant," arXiv:0711.0744 [astro-ph].

[138] J. F. Beacom, N. F. Bell, and S. Dodelson, "Neutrinoless universe," *Phys. Rev. Lett.* **93** (2004) 121302, astro-ph/0404585.

[139] C. Hagmann, "Cosmic neutrinos and their detection," astro-ph/9905258.

[140] A. Ringwald and Y. Y. Y. Wong, "Relic neutrino clustering and implications for their detection," hep-ph/0412256.

[141] G. B. Gelmini, "Prospect for relic neutrino searches," *Phys. Scripta* **T121** (2005) 131–136, hep-ph/0412305.

[142] A. Ringwald, "How to detect big bang relic neutrinos?," hep-ph/0505024.

[143] S. Hannestad, "Neutrinos in cosmology," *New J. Phys.* **6** (2004) 108, hep-ph/0404239.

[144] http://lhc.web.cern.ch/lhc/.

[145] D. F. Torres and L. A. Anchordoqui, "Astrophysical origins of ultrahigh energy cosmic rays," *Rept. Prog. Phys.* **67** (2004) 1663–1730, astro-ph/0402371.

[146] P. Bhattacharjee and G. Sigl, "Origin and propagation of extremely high energy cosmic rays," *Phys. Rept.* **327** (2000) 109–247, astro-ph/9811011.

[147] A. D. Linde, "Hybrid inflation," *Phys. Rev.* **D49** (1994) 748–754, astro-ph/9307002.

[148] J. Wess and J. Bagger, "Supersymmetry and supergravity,". Princeton, USA: Univ. Pr. (1992) 259 p.

[149] M. Ackermann *et al.*, "Flux limits on ultra high energy neutrinos with AMANDA-B10," *Astropart. Phys.* **22** (2005) 339–353.

[150] F. Halzen and D. Hooper, "AMANDA observations constrain the ultra-high energy neutrino flux," astro-ph/0605103.

[151] **IceCube** Collaboration, A. Silvestri, "Results from the AMANDA experiment," *Mod. Phys. Lett.* **A22** (2007) 1769–1778.

[152] **ANITA** Collaboration, S. W. Barwick *et al.*, "Constraints on cosmic neutrino fluxes from the ANITA experiment," *Phys. Rev. Lett.* **96** (2006) 171101, astro-ph/0512265.

[153] N. G. Lehtinen, P. W. Gorham, A. R. Jacobson, and R. A. Roussel-Dupre, "FORTE satellite constraints on ultra-high energy cosmic particle fluxes," *Phys. Rev.* **D69** (2004) 013008, astro-ph/0309656.

[154] P. W. Gorham *et al.*, "Experimental limit on the cosmic diffuse ultrahigh-energy neutrino flux," *Phys. Rev. Lett.* **93** (2004) 041101, astro-ph/0310232.

[155] I. Kravchenko *et al.*, "Recent results from the RICE experiment at the South Pole," astro-ph/0306408.

[156] **EUSO** Collaboration, S. Bottai and S. E. C. Giurgola, "Downward neutrino induced EAS with EUSO detector,". Prepared for 28th International Cosmic Ray Conferences (ICRC 2003), Tsukuba, Japan, 31 Jul - 7 Aug 2003.

[157] **The IceCube** Collaboration, J. Ahrens *et al.*, "IceCube: The next generation neutrino telescope at the South Pole," *Nucl. Phys. Proc. Suppl.* **118** (2003) 388–395, astro-ph/0209556.

[158] O. Scholten *et al.*, "Optimal radio window for the detection of ultra-high-energy cosmic rays and neutrinos off the moon," astro-ph/0508580.

[159] F. W. Stecker *et al.*, "Observing the ultrahigh energy universe with OWL eyes," *Nucl. Phys. Proc. Suppl.* **136C** (2004) 433–438, astro-ph/0408162. J.F. Krizmanic, private communications.

[160] X. Bertou, P. Billoir, O. Deligny, C. Lachaud, and A. Letessier-Selvon, "Tau neutrinos in the Auger observatory: A new window to UHECR sources," *Astropart. Phys.* **17** (2002) 183–193, astro-ph/0104452.

[161] P. Gorham *et al.*, "Measurements of the suitability of large rock salt formations for radio detection of high energy neutrinos," *Nucl. Instrum. Meth.* **A490** (2002) 476–491, hep-ex/0108027. private communication.

[162] M. Ahlers *et al.*, "Neutrinos as a diagnostic of cosmic ray galactic / extra- galactic transition," *Phys. Rev.* **D72** (2005) 023001, astro-ph/0503229.

[163] Z. Fodor, S. D. Katz, A. Ringwald, and H. Tu, "Bounds on the cosmogenic neutrino flux," *JCAP* **0311** (2003) 015, hep-ph/0309171.

[164] Z. Fodor, S. Katz, A. Ringwald, T. J. Weiler, and Y. Y. Wong. unpublished.

[165] **Baikal** Collaboration, R. Wischnewski *et al.*, "The Baikal neutrino telescope: Results and plans," *Int. J. Mod. Phys.* **A20** (2005) 6932–6936, astro-ph/0507698.

[166] K. Greisen, "End to the cosmic ray spectrum?," *Phys. Rev. Lett.* **16** (1966) 748–750.

[167] G. T. Zatsepin and V. A. Kuzmin, "Upper limit of the spectrum of cosmic rays," *JETP Lett.* **4** (1966) 78–80.

[168] D. Fargion, B. Mele, and A. Salis, "Ultrahigh energy neutrino scattering onto relic light neutrinos in galactic halo as a possible source of highest energy extragalactic cosmic rays," *Astrophys. J.* **517** (1999) 725–733, astro-ph/9710029.

[169] T. J. Weiler, "Cosmic ray neutrino annihilation on relic neutrinos revisited: A mechanism for generating air showers above the Greisen-Zatsepin-Kuzmin cut-off," *Astropart. Phys.* **11** (1999) 303–316, hep-ph/9710431.

[170] S. Yoshida, G. Sigl, and S.-j. Lee, "Extremely high energy neutrinos, neutrino hot dark matter, and the highest energy cosmic rays," *Phys. Rev. Lett.* **81** (1998) 5505–5508, hep-ph/9808324.

[171] Z. Fodor, S. D. Katz, and A. Ringwald, "Determination of absolute neutrino masses from Z-bursts," *Phys. Rev. Lett.* **88** (2002) 171101, hep-ph/0105064.

[172] Z. Fodor, S. D. Katz, and A. Ringwald, "Relic neutrino masses and the highest energy cosmic rays," *JHEP* **06** (2002) 046, hep-ph/0203198.

[173] G. Gelmini, G. Varieschi, and T. J. Weiler, "Bounds on relic neutrino masses in the Z-burst model," *Phys. Rev.* **D70** (2004) 113005, hep-ph/0404272.

[174] **Pierre Auger Observatory** Collaboration, T. P. a. Collaboration, "Correlation of the highest-energy cosmic rays with the positions of nearby active galactic nuclei," arXiv:0712.2843 [astro-ph].

[175] **Particle Data Group** Collaboration, S. Eidelman *et al.*, "Review of particle physics," *Phys. Lett.* **B592** (2004) 1.

[176] D. Y. Bardin, A. Leike, T. Riemann, and M. Sachwitz, "Energy dependent width effects in e^+e^- annihilation near the Z pole," *Phys. Lett.* **B206** (1988) 539–542.

[177] D. Y. Bardin *et al.*, "Z line shape,". Presented at the 2nd General Meeting of the LEP Physics Workshop 89, Geneva, Switzerland, May 8-9, 1989.

[178] R. J. Protheroe, "Effect of energy losses and interactions during diffusive shock acceleration: Applications to SNR, AGN and UHE cosmic rays," *Astropart. Phys.* **21** (2004) 415–431, astro-ph/0401523.

[179] P. Chen, T. Tajima, and Y. Takahashi, "Plasma wakefield acceleration for ultra high energy cosmic rays," *Phys. Rev. Lett.* **89** (2002) 161101, astro-ph/0205287.

[180] H. Li, S. A. Colgate, M. Kusunose, and R. V. E. Lovelace, "On the Particle Heating and Acceleration in Black Hole Accretion Systems," astro-ph/9812418.

[181] P. P. Kronberg, Q. W. Dufton, H. Li, and S. A. Colgate, "Magnetic Energy of the Intergalactic Medium from Galactic Black Holes," astro-ph/0106281.

[182] M. Sakellariadou, "The revival of cosmic strings," *Annalen Phys.* **15** (2006) 264–276, hep-th/0510227.

[183] M. Sakellariadou, "Cosmic strings," hep-th/0602276.

[184] P. Bhattacharjee, C. T. Hill, and D. N. Schramm, "Grand unified theories, topological defects and ultrahigh- energy cosmic rays," *Phys. Rev. Lett.* **69** (1992) 567–570.

[185] A. Ringwald, "Extremely energetic cosmic neutrinos: Opportunities for astrophysics, particle physics, and cosmology," hep-ph/0510341.

[186] J. Bacelar. Private Communications.

[187] V. S. Berezinsky and A. Vilenkin, "Ultra high energy neutrinos from hidden-sector topological defects," *Phys. Rev.* **D62** (2000) 083512, hep-ph/9908257.

[188] V. Berezinsky, M. Narayan, and F. Vissani, "Mirror model for sterile neutrinos," *Nucl. Phys.* **B658** (2003) 254–280, hep-ph/0210204.

[189] O. E. Kalashev, V. A. Kuzmin, D. V. Semikoz, and G. Sigl, "Ultra-high energy neutrino fluxes and their constraints," *Phys. Rev.* **D66** (2002) 063004, hep-ph/0205050.

[190] D. V. Semikoz and G. Sigl, "Ultra-high energy neutrino fluxes: New constraints and implications," *JCAP* **0404** (2004) 003, hep-ph/0309328.

[191] O. Stal, J. Bergman, B. Thide, L. Ahlen, and G. Ingelman, "Lunar satellite detection of ultra-high energy neutrinos with the use of radio methods," astro-ph/0509210.

[192] O. Stal, J. Bergman, B. Thide, L. K. S. Daldorff, and G. Ingelman, "Satellite detection of radio pulses from ultrahigh energy neutrinos interacting with the moon," astro-ph/0604199.

[193] V. Berezinsky and A. Y. Smirnov, "Cosmic neutrinos of ultra-high energies and detection possibility," *Astrophysics and Space Science* **32** (1975) 461.

[194] K. Mannheim, R. J. Protheroe, and J. P. Rachen, "On the cosmic ray bound for models of extragalactic neutrino production," *Phys. Rev.* **D63** (2001) 023003, astro-ph/9812398.

[195] V. Berezinsky, M. Kachelriess, and S. Ostapchenko, "Electroweak jet cascading in the decay of superheavy particles," *Phys. Rev. Lett.* **89** (2002) 171802, hep-ph/0205218.

[196] M. Birkel and S. Sarkar, "Extremely high energy cosmic rays from relic particle decays," *Astropart. Phys.* **9** (1998) 297–309, hep-ph/9804285.

[197] V. Berezinsky and M. Kachelriess, "Monte Carlo simulation for jet fragmentation in SUSY-QCD," *Phys. Rev.* **D63** (2001) 034007, hep-ph/0009053.

[198] Z. Fodor and S. D. Katz, "Grand unification signal from ultrahigh-energy cosmic rays?," *Phys. Rev. Lett.* **86** (2001) 3224–3227, hep-ph/0008204.

[199] S. Sarkar and R. Toldra, "The high energy cosmic ray spectrum from massive particle decay," *Nucl. Phys.* **B621** (2002) 495–520, hep-ph/0108098.

[200] C. Barbot and M. Drees, "Detailed analysis of the decay spectrum of a super-heavy X particle," *Astropart. Phys.* **20** (2003) 5–44, hep-ph/0211406.

[201] **The SNLS** Collaboration, P. Astier *et al.*, "The Supernova Legacy Survey: Measurement of Omega_m, Omega_Lambda and w from the First Year Data Set," *Astron. Astrophys.* **447** (2006) 31–48, astro-ph/0510447.

[202] U. Seljak and M. Zaldarriaga, "A Line of Sight Approach to Cosmic Microwave Background Anisotropies," *Astrophys. J.* **469** (1996) 437–444, astro-ph/9603033.

[203] **SDSS** Collaboration, M. Tegmark *et al.*, "The 3D power spectrum of galaxies from the SDSS," *Astrophys. J.* **606** (2004) 702–740, astro-ph/0310725.

[204] A. R. Liddle and D. H. Lyth, "Cosmological inflation and large-scale structure,". Cambridge, UK: Univ. Pr. (2000) 400 p.

[205] W. Hu, "Structure Formation with Generalized Dark Matter," *Astrophys. J.* **506** (1998) 485–494, astro-ph/9801234.

[206] R. Bean and O. Dore, "Probing dark energy perturbations: the dark energy equation of state and speed of sound as measured by WMAP," *Phys. Rev.* **D69** (2004) 083503, astro-ph/0307100.

[207] S. Hannestad, "Constraints on the sound speed of dark energy," *Phys. Rev.* **D71** (2005) 103519, astro-ph/0504017.

[208] W. Hu and D. J. Eisenstein, "Small scale perturbations in a general MDM cosmology," *Astrophys. J.* **498** (1998) 497, astro-ph/9710216.

[209] W. Hu, D. J. Eisenstein, and M. Tegmark, "Weighing neutrinos with galaxy surveys," *Phys. Rev. Lett.* **80** (1998) 5255–5258, astro-ph/9712057.

[210] M. Kaplinghat and A. Rajaraman, "Stable Models of superacceleration," *Phys. Rev.* **D75** (2007) 103504, astro-ph/0601517.

[211] R. Bean, E. E. Flanagan, and M. Trodden, "Adiabatic instability in coupled dark energy-dark matter models," arXiv:0709.1128 [astro-ph].

[212] R. Bean, E. E. Flanagan, and M. Trodden, "The Adiabatic Instability on Cosmology's Dark Side," `arXiv:0709.1124 [astro-ph]`.

[213] T. Koivisto, "Growth of perturbations in dark matter coupled with quintessence," *Phys. Rev.* **D72** (2005) 043516, `astro-ph/0504571`.

[214] K. Ichiki and Y.-Y. Keum, "Primordial Neutrinos, Cosmological Perturbations in Interacting Dark-Energy Model: CMB and LSS," `arXiv:0705.2134 [astro-ph]`.

[215] L. Amendola and D. Tocchini-Valentini, "Baryon bias and structure formation in an accelerating universe," *Phys. Rev.* **D66** (2002) 043528, `astro-ph/0111535`.

[216] P. Brax, C. van de Bruck, A.-C. Davis, J. Khoury, and A. Weltman, "Detecting dark energy in orbit: The cosmological chameleon," *Phys. Rev.* **D70** (2004) 123518, `astro-ph/0408415`.

[217] E. Kamke, "Differentialgleichungen, Gewoehnliche Differentialgleichungen," *Teubner Verlag* **1** (2002).

[218] S. R. Coleman and E. Weinberg, "Radiative Corrections as the Origin of Spontaneous Symmetry Breaking," *Phys. Rev.* **D7** (1973) 1888–1910.

[219] J. Khoury and A. Weltman, "Chameleon fields: Awaiting surprises for tests of gravity in space," *Phys. Rev. Lett.* **93** (2004) 171104, `astro-ph/0309300`.

[220] A. Lewis and S. Bridle, "Cosmological parameters from CMB and other data: a Monte-Carlo approach," *Phys. Rev.* **D66** (2002) 103511, `astro-ph/0205436`.

[221] P. Brax, C. van de Bruck, A.-C. Davis, and A. M. Green, "Small Scale Structure Formation in Chameleon Cosmology," *Phys. Lett.* **B633** (2006) 441–446, `astro-ph/0509878`.

[222] M. Ahlers, A. Lindner, A. Ringwald, L. Schrempp, and C. Weniger, "Alpenglow - A Signature for Chameleons in Axion-Like Particle Search Experiments," *Phys. Lett.* **D77** (2008) 015018, `arXiv:0710.1555 [hep-ph]`.

[223] K. Ehret *et al.*, "Production and detection of axion-like particles in a HERA dipole magnet: Letter-of-intent for the ALPS experiment," `hep-ex/0702023`.

Acknowledgments

First of all, I am very grateful to my supervisor Andreas Ringwald for introducing me to the rich and exciting topic of Neutrino Dark Energy, for stimulating discussions, for his good advice and continuous and valuable support. I also highly appreciate the very good personal and scientific atmosphere in his working group and in the DESY Theory group. It has been a great time!

Furthermore, I would like to thank Jan Louis and Jochen Bartels for acting as co-referees for this thesis and the disputation.

My special thanks go to Steen Hannestad for many fruitful discussions and valuable support which I highly appreciate.

It is a pleasure to thank my collaborators Markus Ahlers, Florian Bauer, Ole Eggers Bjaelde, Anthony W. Brookfield, Steen Hannestad, David F. Mota, Andreas Ringwald, Domenico Tocchini-Valentini, Carsten van de Bruck and Christoph Weniger for sharing their knowledge with me, for very inspiring teamwork and for a good time.

I am also indebted to Luca Amendola, Alessandro Melchiorri, David F. Mota, Carsten van de Bruck and Christof Wetterich for very interesting discussions and valuable support.

Thanks also to Jose Bacelar, Laura Covi, Dan Hooper, Olaf Scholten and Yvonne Y. Y. Wong for helpful discussions and support as well as to Dirk Brömmel for helping with computer problems.

I would also like to thank Markus Ahlers, Daniela Amrath, Florian Bauer, Markus Diehl, Jan Möller, Jonas Schmidt and Mattias Wohlfahrt and many others for an enjoyable time and many interesting lunch-break conversations.

Many thanks also to the secretaries of the DESY Theory group, Julia Herrmann and Nora Van Looveren, for always being so friendly and ready to help.

I am most grateful to my parents and Daniel for continuous support and for backing me all the way.